

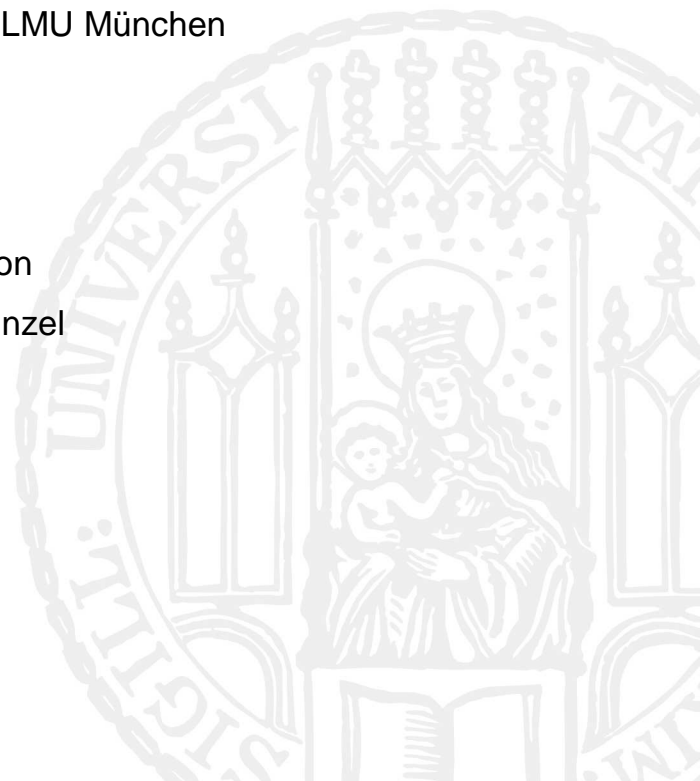
**Targeting the Heat Shock Protein 90 with the
Novel Small-Molecule Inhibitor NW457
Sensitizes Tumor Cells to Ionizing Radiation**

Dissertation der Fakultät für Biologie der
Ludwig-Maximilians-Universität München

Angefertigt an der Klinik und Poliklinik für Strahlentherapie
und Radioonkologie der LMU München

2013

Vorgelegt von
Linda Anne Kinzel



Erstgutachterin: PD Dr. Anna A. Friedl
Zweitgutachter: Prof. Dr. Heinrich Leonhardt

Tag der Abgabe: 19.09.2013
Tag der mündlichen Prüfung: 25.02.2014

Table of contents

| | |
|--|-----------|
| Abbreviations | 7 |
| 1 Abstract | 11 |
| 2 Introduction | 13 |
| 2.1 Hallmarks of cancer | 14 |
| 2.2 Radiotherapy in cancer treatment..... | 18 |
| 2.3 Molecularly targeted therapies..... | 19 |
| 2.4 Heat shock protein 90 and its role in cancer | 21 |
| 2.5 Pharmacological inhibitors of HSP90..... | 26 |
| 3 Purpose | 30 |
| 4 Material | 31 |
| 4.1 Directory of manufacturers and suppliers..... | 31 |
| 4.2 Cell lines..... | 32 |
| 4.3 Antibodies..... | 33 |
| 4.3.1 Primary antibodies | 33 |
| 4.3.2 Secondary antibodies | 35 |
| 4.4 Primers | 36 |
| 5 Methods | 38 |
| 5.1 Cell biology methods | 38 |
| 5.1.1 Cell culture | 38 |
| 5.1.2 <i>In vitro</i> drug treatment and irradiation | 41 |
| 5.1.3 Microscopic quantification of apoptotic cells | 41 |
| 5.1.4 Cell viability assay | 42 |
| 5.1.5 Wound healing assay | 42 |
| 5.1.6 Transmigration assay | 43 |
| 5.1.7 Immunofluorescence staining and microscopy..... | 44 |
| 5.1.8 Flow cytometry | 45 |
| 5.1.9 Detection of HSP70 release into cell culture supernatants..... | 46 |
| 5.1.10 Clonogenic survival assay | 46 |
| 5.2 Biochemical methods..... | 47 |
| 5.2.1 Preparation of whole cell protein lysates..... | 47 |
| 5.2.2 Bradford assay | 48 |
| 5.2.3 SDS-PAGE | 48 |
| 5.2.4 Western blotting and immunodetection | 50 |
| 5.2.5 Caspase activity assay | 50 |
| 5.3 Molecular biological methods..... | 51 |

| | | |
|----------|---|-----------|
| 5.3.1 | RNA extraction | 51 |
| 5.3.2 | Quantitation of RNA..... | 52 |
| 5.3.3 | Reverse transcription..... | 52 |
| 5.3.4 | Quantitative real-time PCR | 53 |
| 5.4 | <i>In vivo</i> experiments..... | 54 |
| 5.4.1 | Tumor implantation..... | 54 |
| 5.4.2 | <i>In vivo</i> drug administration, irradiation, and measurement of tumor volumes | 55 |
| 5.5 | Statistical methods..... | 55 |
| 5.5.1 | Statistics | 55 |
| 5.5.2 | Combination index..... | 55 |
| 6 | Results | 56 |
| 6.1 | Targeting HSP90 with the novel small-molecule inhibitor NW457 sensitizes colorectal cancer cells to ionizing radiation | 56 |
| 6.1.1 | Inhibition of HSP90 by NW457 induces the degradation of HSP90 client proteins and mediates the upregulation of HSP70 expression, cell surface exposure, and release | 56 |
| 6.1.2 | NW457 induces apoptosis and sensitizes colorectal cancer cells to ionizing radiation..... | 59 |
| 6.1.3 | Interaction of NW457 stimulation and ionizing radiation occurs in a synergistic mode..... | 61 |
| 6.1.4 | The radiosensitizing effects of NW457 involve the activation of the caspase cascade with subsequent caspase substrate cleavage..... | 63 |
| 6.1.5 | NW457-mediated apoptosis induction and radiosensitization do not require functional p53 | 66 |
| 6.1.6 | NW457 augments radiation-induced clonogenic cell death of colorectal cancer cells | 69 |
| 6.1.7 | Colorectal cancer cells are sensitive to HSP90 inhibition irrespective of their KRAS status | 72 |
| 6.1.8 | NW457 reveals very little hepatocytotoxicity | 75 |
| 6.1.9 | NW457 shows potent antitumor efficacy in combination with radio- therapy <i>in vivo</i> | 77 |
| 6.2 | The novel HSP90 inhibitor NW457 abrogates the radioresistance of human glioblastoma cells and impairs their migratory potential | 80 |
| 6.2.1 | NW457 abolishes the intrinsic radioresistance of human glioblastoma cells | 80 |

| | | |
|-----------|---|------------|
| 6.2.2 | NW457 dose-dependently induces apoptosis in glioblastoma cells as characterized by caspase activation and subsequent caspase substrate cleavage | 84 |
| 6.2.3 | NW457 enhances radiation-induced clonogenic cell death of glioblastoma cell lines and affects critical regulators of the DNA damage response..... | 86 |
| 6.2.4 | Inhibition of HSP90 by NW457 decreases the migratory potential of LN229 glioblastoma cells..... | 89 |
| 6.2.5 | Irradiation-induced hypermigration of glioblastoma cells is inhibited by NW457 | 90 |
| 6.2.6 | Analysis of potential mechanisms associated with LN229 migration patterns in response to HSP90 inhibition and irradiation | 93 |
| 7 | Discussion | 99 |
| 7.1 | HSP90 - an unlikely but promising drug target for anticancer therapies | 99 |
| 7.2 | Potential benefits of NW457 in the therapy of colorectal carcinomas and glioblastomas..... | 100 |
| 7.3 | HSP90 inhibitor-induced apoptosis and the dispensability of p53 | 102 |
| 7.4 | Potential mechanisms underlying clonogenic cell death upon HSP90 inhibition | 104 |
| 7.5 | Tolerability of HSP90 inhibitors by hepatocytes | 106 |
| 7.6 | Targeting HSP90 for affecting tumor cell migration..... | 107 |
| 7.7 | <i>In vivo</i> potency of HSP90 inhibitors | 110 |
| 7.8 | Conclusion and outlook | 111 |
| 8 | References..... | 112 |
| 9 | List of figures and tables | 132 |
| 10 | Appendix..... | 134 |
| | Eidesstattliche Erklärung..... | 136 |
| | Acknowledgments | 137 |

Abbreviations

| | |
|-------------|---|
| μ | Micro (10 ⁻⁶) |
| 17-AAG | 17-Allylamino-17-demethoxygeldanamycin, tanespimycin |
| 17-DMAG | 17-Dimethylaminoethylamino-17-demethoxygeldanamycin, alvespimycin |
| 5-FU | 5-Fluorouracil |
| Ac-DEVD-AMC | N-acetyl-Asp-Glu-Val-Asp-7-amino-4-methylcoumarin |
| ADP | Adenosine diphosphate |
| AHA1 | Activator of HSP90 ATPase homolog 1 |
| AKT | Protein kinase B |
| ALT | Alanine transaminase, also referred to as glutamic-pyruvic transaminase (GPT) |
| AMC | 7-Amino-4-methylcoumarin |
| APAF-1 | Apoptotic protease activating factor 1 |
| APE1 | Apurinic/apyrimidinic endonuclease 1 |
| APS | Ammonium peroxodisulfate |
| AST | Aspartate transaminase, also referred to as glutamic-oxaloacetic aminotransferase (GOT) |
| ATCC | American Type Culture Collection |
| ATM | Ataxia telangiectasia mutated protein |
| ATP | Adenosine triphosphate |
| ATR | Ataxia telangiectasia and RAD3-related protein |
| BAK | BCL-2 homologous antagonist/killer |
| BAX | BCL-2-associated X protein |
| BCL-2 | B-cell lymphoma 2 protein |
| BCL-xL | B-cell lymphoma-extra large protein |
| BER | Base excision repair |
| BIM | BCL-2-like protein 11 |
| bp | Base pairs |
| BRAF | V-RAF murine sarcoma viral oncogene homolog B1 |
| BRCA1/2 | Breast cancer type 1/2 susceptibility protein |
| BSA | Bovine serum albumin |
| Casp | Caspase |
| CDC | Cell division cycle |
| CDK | Cyclin-dependent kinase |
| CHAPS | 3-[(3-Cholamidopropyl)dimethylammonio]-1-propanesulfonate |

Abbreviations

| | |
|----------|---|
| CHIP | Carboxyl terminus of HSC70-interacting protein |
| CHK1/2 | Checkpoint kinase 1/2 |
| CT | Computed tomography |
| Ctrl | Control |
| DAPI | 4',6-Diamidino-2-phenylindole |
| DDR | DNA damage response |
| DMEM | Dulbecco's Modified Eagle Medium |
| DMSO | Dimethyl sulfoxide |
| DNA | Deoxyribonucleic acid |
| DNA-PKcs | DNA-dependent protein kinase, catalytic subunit |
| dNTP | Deoxyribonucleotide triphosphate |
| DSB | DNA double-strand break |
| e.g. | For example |
| ECM | Extracellular matrix |
| EDTA | Ethylendiamintetraacetat |
| EGF | Epidermal growth factor |
| EGF-R | Epidermal growth factor receptor |
| EGTA | Ethylene glycol-bis(2-aminoethylether)-N,N,N',N'-tetraacetic acid |
| ELISA | Enzyme-linked immunosorbent assay |
| EMT | Epithelial-mesenchymal transition |
| EphA2 | Ephrin receptor A2 |
| ERK | Extracellular signal-regulated kinase |
| FACS | Fluorescence activated cell sorting |
| FAK | Focal adhesion kinase |
| FANCA | Fanconi anemia complementation group A |
| FCS | Fetal calf serum |
| FGF | Fibroblast growth factor family |
| FI | Fluorescence intensity |
| FITC | Fluorescein isothiocyanate |
| FOX | Forkhead box family proteins |
| FSC | Forward scatter |
| FU | Fluorescence units |
| GA | Geldanamycin |
| GBM | Glioblastoma multiforme |
| GIST | Gastrointestinal stroma tumor |
| GRP94 | Glucose-regulated protein 94 |
| h | Hour |

Abbreviations

| | |
|----------------|---|
| HDAC | Histone deacetylase |
| HEPES | 4-(2-Hydroxyethyl)-1-piperazineethanesulfonic acid |
| HER-2 | Human epidermal growth factor receptor 2, also referred to as ERBB2 |
| HGF | Hepatocyte growth factor |
| HIF-1 α | Hypoxia-inducible factor-1 α |
| HIP | HSC70 interacting protein |
| HNSCC | Head and neck squamous cell carcinoma |
| HOP | HSP70/HSP90 organizing protein |
| HRP | Horseradish peroxidase |
| HSC70 | Constitutively expressed isoform of HSP70 |
| HSP | Heat shock protein |
| hTERT | Human telomerase reverse transcriptase |
| IF | Immunofluorescence |
| IGF-1R | Insulin-like growth factor-1 receptor |
| IR | Ionizing radiation |
| kDa | Kilodalton |
| KRAS | Kirsten rat sarcoma viral oncogene homolog |
| m | Milli (10^{-3}) |
| M | Molar |
| MAPK | Mitogen-activated protein kinases |
| MGMT | O-6-Methylguanine-DNA methyltransferase |
| min | Minute |
| MMP | Matrix metalloproteinase |
| mTOR | Mammalian target of rapamycin |
| MV | Megavolts |
| n | Nano (10^{-9}) |
| NF- κ B | Nuclear factor kappa-light-chain-enhancer of activated B-cells |
| NHEJ | Non-homologous end joining |
| nM | Nanomolar |
| NSCLC | Non small cell lung cancer |
| PARP | Poly(ADP-ribose)polymerase |
| PBS | Phosphate buffered saline |
| PCR | Polymerase chain reaction |
| PDGF | Platelet-derived growth factor |
| PDGF-R | Platelet-derived growth factor receptor |
| PE | Phycoerythrin |
| PFA | Paraformaldehyde |

Abbreviations

| | |
|--------------|---|
| PI | Propidium iodide |
| PI3K | Phosphatidylinositol 3-kinase |
| PKC | Protein kinase C |
| PLC | Phosphoinositide phospholipase C |
| Pol- β | DNA polymerase beta |
| PUMA | p53-upregulated modulator of apoptosis |
| qPCR | Quantitative real-time PCR |
| RAF-1 | V-RAF-1 murine leukemia viral oncogene homolog 1, also referred to as C-RAF |
| RB | Retinoblastoma protein |
| RNA | Ribonucleic acid |
| ROS | Reactive oxygen species |
| RPMI | Roswell Park Memorial Institute Medium |
| RT | Radiotherapy |
| RTK | Receptor tyrosine kinase |
| s | Second |
| SD | Standard deviation |
| SDS | Sodium dodecyl sulfate |
| SDS-PAGE | Sodium dodecyl sulfate polyacrylamide gel electrophoresis |
| SEM | Standard error of the mean |
| SFM | Serum-free medium |
| SSB | DNA single-strand break |
| SSC | Sideward scatter |
| STK33 | Serine/threonine kinase 33 |
| TBS | Tris-buffered saline |
| TEMED | N,N,N',N'-tetramethylethylenediamine |
| TGF- β | Transforming growth factor beta |
| TMZ | Temozolomide |
| TRAP1 | Tumor necrosis factor receptor-associated protein 1 |
| Tris | Tris(hydroxymethyl)aminomethane |
| u | Unit |
| VEGF | Vascular endothelial growth factor |
| VEGF-R | Vascular endothelial growth factor receptor |
| Vinc | Vinculin |
| vol | Volume |
| vs. | Versus |

1 Abstract

Tumor cells strongly rely on the chaperoning function of the heat shock protein 90 (HSP90) in order to compensate for high levels of proteotoxic stress to which they are exposed due to genetic aberrations and deregulated oncogenic signaling pathways. HSP90 is responsible for maintaining the conformational stability and function of a large number of client proteins, many of which play key roles in tumorigenesis, proliferation, angiogenesis, survival, invasion, and metastasis. Therefore, HSP90 has emerged as a promising target for anticancer therapies and different small-molecule inhibitors are currently being evaluated in preclinical studies. The pochoxime NW457 is one of these promising compounds and its antitumor potential is characterized here for the first time in combination with ionizing radiation (IR) in preclinical models of colorectal cancer and glioblastoma multiforme (referred to as glioblastoma in the following).

In vitro, NW457 was found to potently sensitize human HCT116 colorectal carcinoma cells to ionizing radiation through caspase-mediated apoptosis induction via the mitochondrial pathway and enhancement of irradiation-induced clonogenic cell death. Interestingly, the antitumor activities of NW457 were virtually independent of the cellular p53 and KRAS status, suggesting that inhibition of HSP90 by NW457 might provide a novel, promising therapeutic option also for tumor subtypes which are deficient for functional p53 or driven by activating KRAS mutations. In contrast to the first-generation HSP90 inhibitor geldanamycin, NW457 revealed very little hepatocytotoxicity as exposure of primary murine hepatocytes to NW457 practically did not affect the cellular viability or perturb the typical hepatocellular morphology. Based on the encouraging *in vitro* results regarding NW457-mediated radiosensitization and its good tolerability by primary hepatocytes, the antitumor efficacy of NW457 was investigated in combination with radiotherapy in an *in vivo* model of colorectal cancer. Indeed, combined treatment with 4x 100 mg/kg NW457 plus radiotherapy potently delayed tumor growth and prolonged the survival of immunocompetent Balb/c mice, thus identifying NW457 as a promising candidate compound for future clinical studies.

In the second part of the present thesis, the antitumor activity of NW457 was investigated in human glioblastoma models. Glioblastomas are clinically associated with pronounced radioresistance and high invasiveness - two characteristics that might be addressed by the novel pochoxime HSP90 inhibitor NW457. Indeed, NW457 was found to interfere with the radioresistant phenotype of human glioblastoma cells as it potently induced apoptosis and sensitized LN229 and T98G cells towards IR-induced clonogenic cell death. Mechanistically, NW457 provoked the destabilization of critical regulators of the DNA damage response as it time-dependently induced the depletion of ATM, ATR, CHK1, and

CHK2. In addition to its radiosensitizing effects, NW457 demonstrated potent anti-invasive activities as it decreased the inherent migration of LN229 cells and also inhibited irradiation-induced hypermigration.

Collectively, the data of the present work prove HSP90 as a clinically relevant target for novel therapy concepts for colorectal carcinomas and glioblastomas and they identify NW457 as a promising candidate compound for the entry of pochoxime HSP90 inhibitors into the clinic.

2 Introduction

Cancer is a malignant neoplasm which represents the third most common cause of death worldwide behind cardiovascular and infectious/parasitic diseases (World Health Organization, 2008). It is estimated that in 2008 about 12.7 million new cancer cases were diagnosed and 7.6 million cancer deaths occurred worldwide, accounting for approximately 13% of all human deaths worldwide. These global statistics were published by the International Agency for Research on Cancer (IARC) as part of the GLOBOCAN project in 2008 which provides estimated incidence, mortality and prevalence of cancer worldwide (<http://globocan.iarc.fr>; Jemal et al., 2011). Lung cancer in males and breast cancer in females are the most frequently diagnosed tumor entities and the leading causes of cancer death worldwide, followed by prostate, colorectal, and stomach cancer in males and colorectal, cervical, and lung cancer in females (<http://globocan.iarc.fr>, measured by incidence rates).

So far, economically developed countries display incidence rates for all cancers combined about twice as high as developing countries. In the future, global cancer rates will further increase both in developed and developing countries because of aging societies and changing lifestyle factors in the developing world.

The importance of lifestyle factors for the development of cancer is reflected by the percentage contribution of genetic and environmental factors associated with cancer risk, estimated as 5-10% and 90-95%, respectively (Anand et al., 2008). Thus, the majority of cancers are not caused by inherited genetic defects, but attributed to various environmental factors, such as dietary habits, smoking, infections by certain viruses and bacteria (e.g. human papillomavirus, Epstein Barr virus, Kaposi's sarcoma-associated herpes virus, *Helicobacter pylori*), as well as chronic alcohol consumption, obesity, radiation, and exposure to certain chemicals. The individual sensitivity towards these environmental factors, however, is presumably affected by genetic factors.

Tumors arise from normal tissues and are initiated by the malignant transformation of a normal cell into a cancer cell. During tumor progression individual cells can spread from the primary tumor to distant sites and develop metastases. The majority of human cancers originate from epithelial tissues (Weinberg, 2007). These tumors are responsible for more than 80% of the cancer-related deaths per year. Epithelial tumors are termed carcinomas and classified into two major categories – adenocarcinomas and squamous cell carcinomas. The first comprises tumors originated e.g. from the lung, colon, breast, pancreas, prostate, and ovaries, whereas the second group involves tumors derived e.g. from the skin, oropharynx, esophagus, larynx, and cervix (Weinberg, 2007).

The minority of human cancers are spawned by nonepithelial tissues and classified into three major types – (i) sarcomas (e.g. osteosarcoma, liposarcoma, fibrosarcoma), (ii) hematopoietic malignancies including leukemias and lymphomas, and (iii) neuroectodermal tumors (e.g. glioblastomas) (Weinberg, 2007).

Some tumors, however, do not match into any of these groups, as tumor cells are able to transdifferentiate from one lineage into another. Such a reprogramming process appears for instance during the epithelial-mesenchymal transition (EMT) in which epithelial cells lose their typical characteristics, such as polarization and cell-cell adhesion, and acquire properties of mesenchymal cells. The EMT is associated with profound phenotypic changes and involves crucial alterations in gene expression. By adopting a multifaceted process which normally takes place during embryonic development and wound healing, cancer cells acquire multiple abilities that enable cancer progression, invasion, and metastasis (De Craene and Berx, 2013; Sanchez-Tillo et al., 2012). The biological properties required for the malignant transformation of a normal into a cancer cell are described in the following section.

2.1 Hallmarks of cancer

The hallmarks of cancer originally proposed by Hanahan and Weinberg in the year 2000 define six functional capabilities that are required for the malignant transformation of a normal cell into a cancer cell (Hanahan and Weinberg, 2000). Recently, their original wording has been restated due to progress in cancer research during the past decade. The revised hallmarks were published in 2011 (Hanahan and Weinberg, 2011) and comprise the following six characteristics: (i) sustaining proliferative signaling (formerly: self-sufficiency in growth signals), (ii) evading growth suppressors (formerly: insensitivity to anti-growth signals), (iii) resisting cell death (formerly: evading apoptosis), (iv) enabling replicative immortality (formerly: limitless replicative potential), (v) inducing angiogenesis (formerly: sustained angiogenesis), and (vi) activating invasion and metastasis (formerly: tissue invasion and metastasis). These hallmarks define biological capabilities that allow cancer cells to survive, proliferate, and disseminate into distant sites. They describe functions which are acquired in different tumor types via distinct mechanisms and at various times during the multistep development of tumors, thereby providing a solid concept and logical framework for understanding the remarkable biology and diversity of cancer (Hanahan and Weinberg, 2011).

Conceptual progress in cancer research in the last decade has led to new mechanistic findings underlying the hallmark capabilities, and to the definition of two newly emerging hallmarks (Hanahan and Weinberg, 2011). One of them comprises the capability to

reprogram cellular metabolism in order to provoke cell growth and division. The second one involves active evasion of malignant cells from immunological destruction, primarily by B and T lymphocytes, macrophages, and natural killer cells.

Additionally, Hanahan and Weinberg described two enabling characteristics that represent the basic prerequisite for the acquisition of both core and emerging hallmarks: The first one is that genomic instability and mutations provide tumor cells with genetic alterations that are needed to orchestrate tumor progression. Since certain mutations may confer selective advantage and dominance in a local tissue environment, tumor cells often enhance their mutation rates, e.g. by impeding the cellular surveillance systems that normally detect and resolve defects in the DNA.

The second enabling characteristic highlights the important role of immune cells, particularly of the innate immune system, on neoplastic progression. Inflammatory cells can facilitate multiple hallmark capabilities by providing the tumor environment with tumor-stimulatory molecules, such as growth factors that maintain proliferative signaling or prosurvival factors that limit cell death induction (Hanahan and Weinberg, 2011). Core hallmark capabilities, emerging hallmarks, and enabling characteristics are illustrated in Figure 1, and the core hallmarks are described in detail in the next section as most of them are functionally associated with the heat shock protein 90 - the main object of this work.

Sustaining proliferative signaling

One of the most fundamental traits of cancer cells is their ability to sustain proliferation. Whereas non-malignant cells carefully control the production and release of growth-promoting signals, tumor cells deregulate their mitogenic signaling in order to become self-sufficient. One strategy of tumor cells is their autocrine stimulation of growth factor receptors as they can produce growth factor ligands themselves and respond via the expression of cognate receptors (Hanahan and Weinberg, 2011). Alternatively, cancer cells can proliferate in a ligand independent manner by expressing structurally altered receptor molecules which can be activated by autophosphorylation. In addition, growth factor independence can be initiated by the constitutive activation of components that are acting downstream of these receptors (Hanahan and Weinberg, 2011). Crucial players can be found e.g. in the PI3K/AKT (phosphatidylinositol 3-kinase/protein kinase B) pathway and the MAPK (mitogen-activated protein kinase) cascade (Jiang and Liu, 2009; Yuan and Cantley, 2008), which are involved in pursuing growth signals downstream of the epidermal growth factor receptor (EGF-R), platelet-derived growth factor receptor (PDGF-R), and vascular endothelial growth factor receptor (VEGF-R).

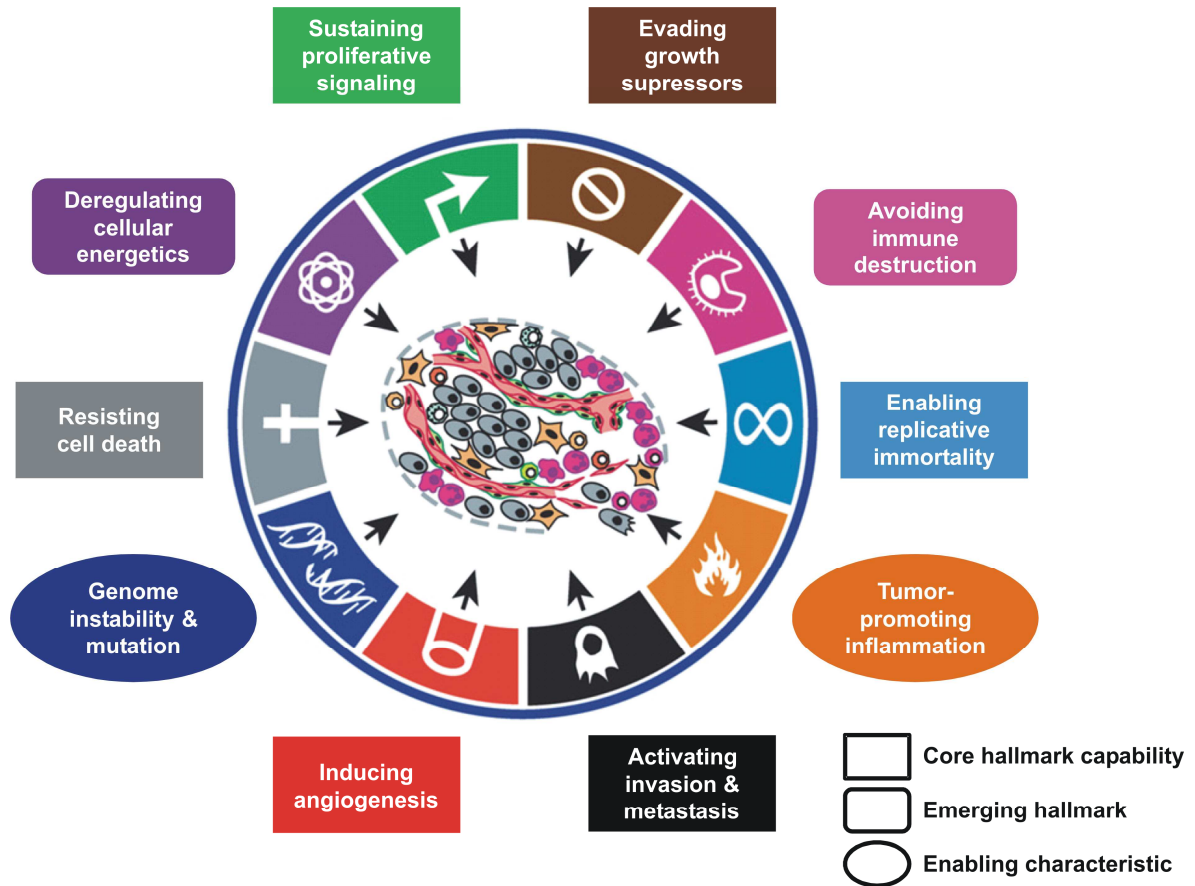


Figure 1. The hallmarks of cancer.

The illustration comprises the six core hallmark capabilities originally proposed by Hanahan and Weinberg in the year 2000 as well as two emerging hallmarks and two enabling characteristics defined by Hanahan and Weinberg in their recently published work (2011). The hallmarks describe crucial functions acquired during tumorigenesis that allow cancer cells to survive, proliferate, and disseminate. Thereby, they provide a solid concept for understanding the biology and diversity of cancer. Acquisition of both core and emerging hallmarks is facilitated by two enabling characteristics - development of genomic instability, and inflammation by innate immune cells. The figure was modified from Hanahan and Weinberg, 2011.

Evading growth suppressors

In order to maintain their proliferative phenotype, tumor cells do not only rely on positively acting growth-stimulatory signals, but additionally evade antiproliferative signals mediated by growth suppressors. Therefore, cancer cells may render themselves insensitive to tumor suppressors, such as p53, the retinoblastoma protein (RB), and its related proteins p107 and p130. p53 and RB transduce extracellular and intracellular growth-inhibitory signals in response to genomic damage and other cellular stressors, and are able to stop cell-cycle progression until the optimal conditions are readjusted (Burkhardt and Sage, 2008; Levine et al., 1991; Mirza et al., 2003; Sherr and McCormick, 2002; Vogelstein et al., 2000). Tumor cells with defects in p53 or RB pathway function are thus losing critical gatekeeper functions and may proceed through their growth and division cycle.

Resisting cell death

Resistance to apoptosis or other forms of cell death is a hallmark capability acquired by most or perhaps all types of cancer. Tumor cells evolve multiple strategies in order to circumvent cell death. Apoptosis can be avoided for instance by increasing the expression of anti-apoptotic regulators, such as the B-cell lymphoma 2 protein (BCL-2) and the B-cell lymphoma-extra large protein (BCL-xL), while, at the same time, downregulating pro-apoptotic factors, such as the BCL-2-associated X protein (BAX), the BCL-2 homologous antagonist/killer (BAK), the p53 upregulated modulator of apoptosis (PUMA), and the BCL-2-like protein 11 (BIM) (Adams and Cory, 2001; Reed et al., 1998; Willis and Adams, 2005). Furthermore, activation of the PI3K/AKT pathway acting downstream of the EGF-R and PDGF-R is responsible for desensitizing cancer cells to apoptotic stimuli. The serine/threonine kinase AKT promotes cell survival by inhibiting pro-apoptotic transcription factors, such as members of the Forkhead box family (FOX), while activating prosurvival transcription factors, such as the nuclear factor kappa-light-chain-enhancer of activated B-cells (NF- κ B) (Brunet et al., 1999; Romashkova and Makarov, 1999).

Enabling replicative immortality

Limitless replicative potential is an acquired hallmark of cancer cells that is facilitated by upregulated telomerase levels. Whereas the continuous multiplication of normal, non-malignant cells is self-limited by telomere shortening to 60-70 doublings, tumor cells can evade this fate and become immortal. Telomeres are noncoding regions at the ends of chromosomes and composed of multiple tandem hexanucleotide repeats (de Lange et al., 1990; Moyzis et al., 1988). In non-malignant cells, the telomeres shorten progressively during each replication cycle by losing 50 to 100 bp of their length, since the DNA polymerase is unable to completely replicate the 3' ends of chromosomal DNA. This process involves impaired chromosome stability and is associated with an increased frequency of dicentric chromosomes (Counter et al., 1992). However, cancer cells are able to counteract this life-limiting process by upregulating the expression of telomerase, which adds novel hexanucleotide repeats to the end of shortened chromosomes. Indeed, approximately 80% of human cancers exhibit elevated telomerase activity, thus enabling replicative immortality (Shay and Bacchetti, 1997).

Inducing angiogenesis

Induction of neovascularization and maintenance of angiogenesis are essential processes during tumorigenesis. In the adult, angiogenesis is normally turned off, and the normal vasculature becomes quiescent, aside from physiological processes, such as wound healing. In contrast, angiogenesis can be reinduced during tumor development via the

“angiogenic switch” (Bergers and Benjamin, 2003; Ribatti et al., 2007). This fundamental event stimulates normally quiescent vasculature to sprout new vessels, and seems to be an early process during tumor development (Folkman, 1995; Hanahan and Folkman, 1996). Tumor cells induce the angiogenic switch by deregulating the balance of endogenous angiogenic inducers and inhibitors (Hanahan and Folkman, 1996), e.g. by upregulating the expression of vascular endothelial growth factors (VEGFs), platelet-derived growth factors (PDGFs) or members of the fibroblast growth factor family (FGF) (Baeriswyl and Christofori, 2009; Carmeliet, 2005).

Activating invasion and metastasis

Invasion into adjacent tissues and metastasis to distant sites are important prerequisites for the infiltrative and destructive growth pattern of many tumors including glioblastomas. Active invasion requires the interaction of multiple cellular processes involving (i) detachment from the original site, (ii) attachment to the extracellular matrix (ECM), (iii) degradation of the ECM, and (iv) migration to distant sites (Nakada et al., 2007). These processes are triggered by cell surface receptors including receptor tyrosine kinases (e.g. EGF-R, PDGF-R, MET, ephrin receptors), TGF- β (transforming growth factor beta) receptors, matrix metalloproteinases (e.g. MMP-2, MMP-8, MMP-9), cytokine receptors, and integrins, most of which are overexpressed in cancers (Nakada et al., 2007; Teodorczyk and Martin-Villalba, 2010).

In summary, the malignant transformation from normal to tumor cells is enabled by different hallmark capabilities that facilitate the development of typical tumor-associated properties which in turn further tumor progression and maintain tumor survival.

2.2 Radiotherapy in cancer treatment

Radiotherapy (RT), also referred to as radiation therapy, is the medical application of ionizing radiation as an important component of cancer treatment concepts. Depending on tumor type, localization, stage, and dissemination, radiotherapy is commonly applied in combination with surgery, chemotherapy, and molecularly targeted therapies, whereby it may operate in a curative or palliative manner. Notably, more than half of all cancer patients will receive radiotherapy during their treatment (Delaney et al., 2005).

Like chemotherapy and molecularly targeted therapies (section 2.3), radiotherapy achieves its therapeutic effects by inducing different forms of cell death, such as apoptosis, necrosis/necroptosis, autophagy or mitotic catastrophe (Eriksson and Stigbrand, 2010; Gewirtz et al., 2009). Using these mechanisms, one of the major aims of radiotherapy is the abrogation of clonogenic tumor cell survival (Dunne et al., 2003; Held,

1997; Williams et al., 2008) in order to prevent tumor proliferation, dissemination/metastasis, and disease progression.

The main impact of radiotherapy on the molecular level is the induction of DNA lesions which can occur either directly or indirectly through the creation of reactive oxygen species (ROS) (Hall and Giaccia, 2011). Ionizing radiation can induce different types of DNA damage, such as double-strand breaks (DSB), single-strand breaks (SSB), and base modifications (e.g. oxidation, deamination, and alkylation). Depending on the lesion type, cells activate different signal transduction pathways in order to arrest their cell cycle, to allow effective DNA repair, or alternatively to induce programmed cell death. Collectively, these cellular mechanisms are known as the DNA damage response (DDR) (Jackson and Bartek, 2009; Rouse and Jackson, 2002; Zhou and Elledge, 2000).

Radiotherapy concepts for the treatment of cancer comprise different application forms of irradiation which are selected according to the cancer type, size, and progression state. External-beam RT delivers photon beams (X-rays, gamma rays), protons or heavy ions from an external device, whereas internal RT, also referred to as brachytherapy, utilizes a radiation source placed inside the body or into a surgical cavity.

In the past years, novel radiation concepts have been developed and enabled the mitigation of RT-associated side effects, a better protection of the normal tissue, and a general advancement in the clinical outcome. However, there is still room for improvements in anticancer therapies, as many tumors develop gene mutations and exhibit resistance to radiotherapy or chemotherapeutic agents. One possible approach to further ameliorate the therapeutic outcome of RT patients would be the modulation of the cellular response towards radiotherapy by targeting specific pathways that are involved in crucial processes, such as tumor cell survival, proliferation, motility, and DNA repair, or which are known to be deregulated in specific cancer types.

In this regard, the application of targeted agents that specifically sensitize tumor cells to the cytotoxic effects of irradiation represents a promising strategy to enhance the therapeutic efficacy. The following section provides an overview of molecularly targeted therapies and combinatorial antitumor treatment strategies.

2.3 Molecularly targeted therapies

Over the past decade, therapeutic cancer research has increasingly focused on molecularly targeted therapies. Compared to conventional chemotherapies which generally interfere with all rapidly proliferating cells, molecularly targeted drugs specifically target a certain signaling protein that is known to be critically involved in cancer pathogenesis. Hence, molecularly targeted therapies are expected to provide a novel

treatment modality that is more effective and less toxic than conventional chemotherapeutics (Thaker and Pollack, 2009).

The development of targeted therapies has mainly focused on the inhibition of hormone receptors (e.g. estrogen receptor), growth factor receptors (e.g. EGF-R, PDGF-R, and VEGF-R), and downstream signal transducers (Argyriou and Kalofonos, 2009; Klener and Klener, 2012; Kwak et al., 2007).

One of the major targets for drug development is the EGF-R, a transmembrane tyrosine kinase belonging to the HER/ErbB receptor family that functions as a key driver in carcinogenesis. Enhanced EGF-R expression and activity mediate intracellular signaling events that contribute to tumor development and progression, migration and invasion (Bianco et al., 2007; Engebraaten et al., 1993; Mendelsohn, 2001). The EGF-R is overexpressed in a broad range of tumor entities including head and neck squamous cell carcinoma (HNSCC), colon carcinoma, and malignant glioma (Ekstrand et al., 1991; Grandis and Tweardy, 1993). Clinically, EGF-R overexpression commonly correlates with reduced recurrence-free and overall survival rates (Nicholson et al., 2001).

Several therapeutic approaches have been undertaken to target the EGF-R, including small molecule tyrosine kinase inhibitors and blocking antibodies. The most successful compound to date is cetuximab (Erbix[®], Merck Serono), a monoclonal antibody directed against the extracellular domain of EGF-R (Baselga, 2001). It was the first compound undergoing clinical evaluation, and has been tested in numerous clinical trials, mainly in combinatorial regimes with irradiation and/or conventional chemotherapy (for an overview see <http://clinicaltrials.gov>). Thus, for instance, the combination of cetuximab with radiotherapy in a Phase III trial significantly increased the locoregional control and overall survival of HNSCC patients as compared to radiotherapy alone (Bonner et al., 2006; Bonner et al., 2010).

Cancer cells exhibit multiple strategies and pathways in order to regulate fundamental processes such as tumor growth, proliferation, and survival. As they use parallel and converging signaling pathways, they may be able to circumvent specific signaling nodes that are deregulated, for instance due to pharmacological intervention. Therefore, antitumor drugs that address only one molecular target may be inefficient and elicit therapy resistance. One possible strategy to overcome these limitations and to improve the efficacy of molecular targeted anticancer therapies may be represented by drugs which inhibit the molecular chaperone heat shock protein 90 (HSP90). Since HSP90 is critically involved in the regulation of a multitude of different cellular signaling pathways that are important for cancer pathogenesis, pharmacological inhibition of the chaperone itself has emerged as a unique anticancer drug target in the past decade (Goetz et al., 2003; Maloney and Workman, 2002; Neckers and Ivy, 2003; Neckers and Neckers, 2002;

Neckers and Workman, 2012; Whitesell et al., 2003). The biological role of HSP90 in the context of cancer and the potential of pharmacological HSP90 inhibitors are described in the following two sections.

2.4 Heat shock protein 90 and its role in cancer

HSP90 is an ATP-dependent molecular chaperone with a molecular mass of 90 kDa which assists to maintain the intracellular protein homeostasis (Taipale et al., 2010). During protein synthesis, HSP90 is involved in the *de novo* protein folding and the late-stage maturation of conformationally destabilized proteins (Freeman and Morimoto, 1996; Picard, 2002). Moreover, the chaperone regulates the activation, stability, and translocation of a broad range of so-called client proteins (Young et al., 2004). These are defined as proteins which temporarily bind to and interact with HSP90 in order to maintain their function and stability. In addition, HSP90 regulates the normal protein turnover, since it directs misfolded and damaged proteins towards CHIP (carboxyl terminus of HSC70-interacting protein)-dependent ubiquitination and subsequent proteasomal degradation (Connell et al., 2001; Xu et al., 2002).

HSP90 is ubiquitously expressed in eukaryotic cells and represents 1-2% of total cytosolic proteins already under constitutive, non-stressed conditions (Welch and Feramisco, 1982). There are five isoforms of HSP90 in humans that differ in their cellular localization: the cytoplasmic isoforms HSP90 α , HSP90 β , and HSP90N, the mitochondrial isoform TRAP1 (tumor necrosis factor receptor-associated protein 1), and the endoplasmic reticulum isoform GRP94 (glucose-regulated protein 94) (Argon and Simen, 1999; Csermely et al., 1998; Felts et al., 2000; Grammatikakis et al., 2002). Except the HSP90N isoform, HSP90 consists of three structural domains – a highly conserved N-terminal domain with ATPase activity, a middle domain that plays a key role in client protein binding and stabilization, and a C-terminal domain that possesses an alternative ATP-binding site and is implicated in HSP90 dimerization (Prodromou and Pearl, 2003). HSP90N lacks the N-terminal domain and possesses a hydrophobic 30 amino acid sequence instead (Grammatikakis et al., 2002).

HSP90 forms homodimers and is functionally organized in multiprotein complexes including HSP40, HSP70, and co-chaperones such as AHA1 (activator of HSP90 ATPase homolog 1), HOP (HSP70/HSP90 organizing protein), HIP (HSC70 interacting protein), p23, and CDC37 (cell division cycle 37 homolog) (Frydman and Hohfeld, 1997; Hernandez et al., 2002; Isaacs et al., 2003; Johnson et al., 1998; Johnson and Toft, 1994; Panaretou et al., 2002; Powers and Workman, 2007; Stepanova et al., 1996). Cycling of this chaperone complex is driven by ATP hydrolysis (Obermann et al., 1998; Panaretou et

al., 1998) which induces a conformational change of HSP90 (Csermely et al., 1993). A simplified model of the HSP90—client protein cycle is illustrated in Figure 2. In the initial step of the cycle, a client protein is loaded on the HSP90 homodimer. Upon ATP binding to the N-terminal site and its hydrolysis, HSP90 changes from the so-called open to the closed conformation (Csermely et al., 1993; Trepel et al., 2010). During the process of client protein folding and maturation different co-chaperones (see above) associate with and dissociate from the multiprotein complex, finally leading to the release of the mature client protein.

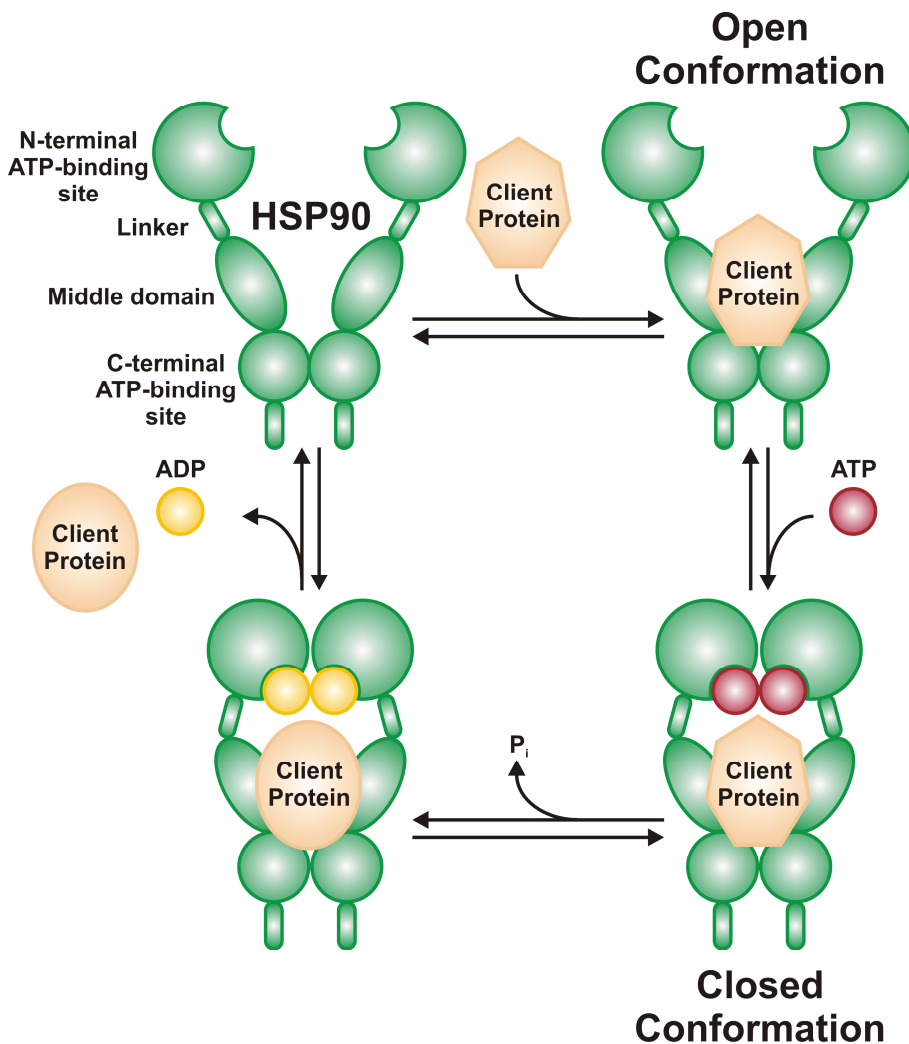


Figure 2. Schematic model of the HSP90—client protein cycle.

A misfolded or otherwise damaged client protein binds to the middle domain of an HSP90 homodimer that is functionally associated in a multiprotein complex with other heat shock proteins and co-chaperones (not shown here). Following N-terminal ATP binding and hydrolysis, HSP90 undergoes a conformational change from an open to a closed conformation. HSP90 catalyzes the stability and maturation of its client protein that is finally released from the chaperone complex. This schematic model was modified from Trepel et al., 2010.

So far, more than 200 HSP90 client proteins have been identified – an updated list of HSP90 interactors can be found on the web page of Prof. Didier Picard's laboratory (<http://picard.ch/downloads>). Intriguingly, the set of known HSP90 client proteins comprises many oncogenic kinases, transcription factors, and other crucial proteins which are functionally associated with the hallmarks of cancer and thus regulate critical processes, such as tumor growth (e.g. CDK4, CDK6, CyclinD), proliferation (e.g. EGF-R, HER-2/ERBB2), angiogenesis (e.g. VEGF-R, MET, HIF-1 α), migration (e.g. EphA2, MET, FAK), and survival (e.g. AKT, IGF-1R) (Aligue et al., 1994; Annamalai et al., 2009; Basso et al., 2002; Eustace et al., 2004; Fortugno et al., 2003; Kim et al., 2008b; Park et al., 2008; Stepanova et al., 1996). Based on the current body of literature which identified and described novel HSP90 client proteins, the illustration of the hallmarks of cancer was complemented with functionally relevant HSP90 clients (Figure 3).

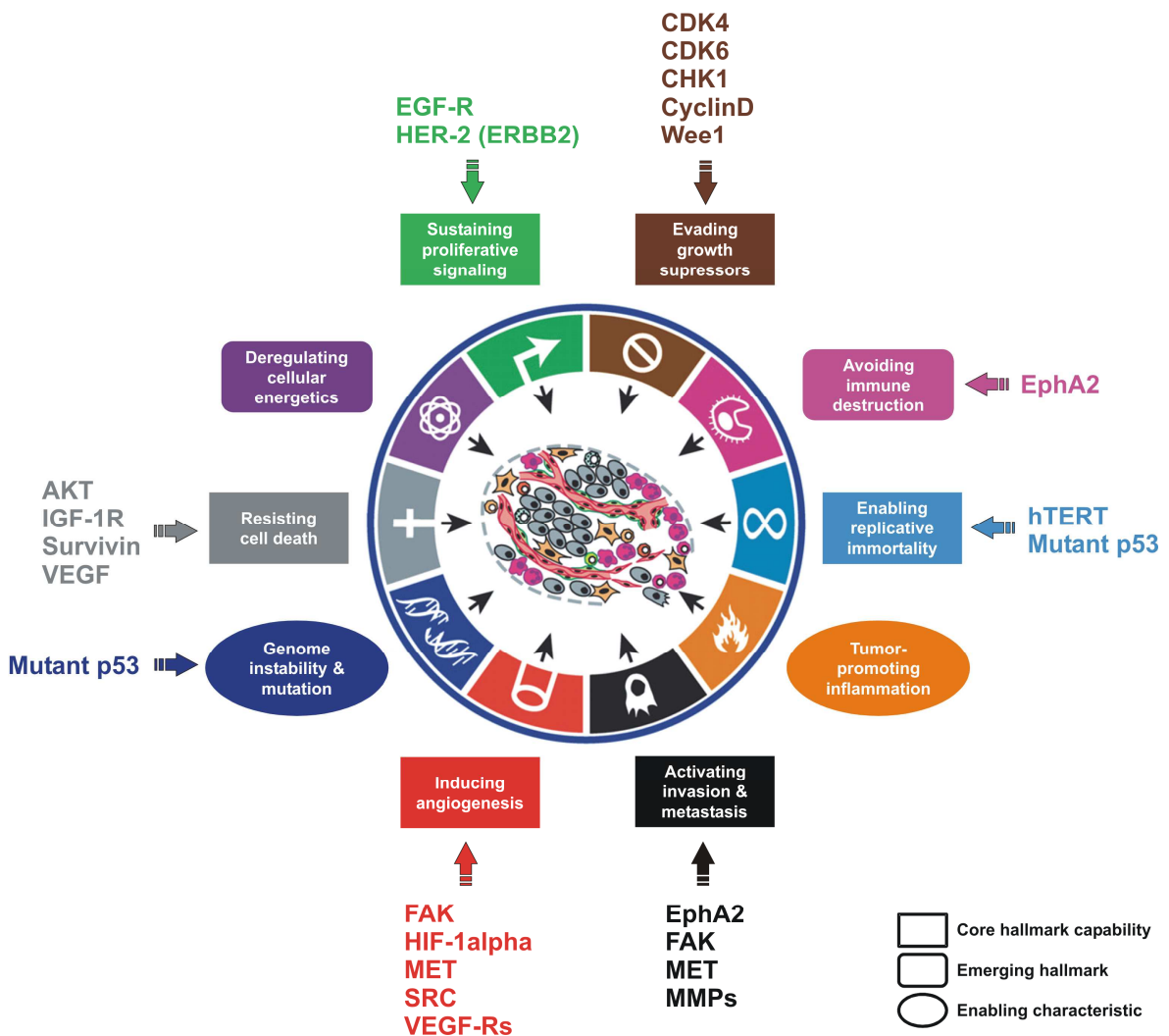


Figure 3. Association of crucial HSP90 client proteins with the hallmarks of cancer. Multiple HSP90 client proteins are functionally associated with different hallmark capabilities of cancer cells and therefore play critical roles in the transformation of a normal cell into a cancer cell. The list of known HSP90 client proteins comprises signaling

molecules that are involved in genome instability, enabling replicative immortality, evading growth suppressors, sustaining proliferation, inducing angiogenesis, resisting cell death, and activating motility. AKT: protein kinase B; CDK 4/6: cyclin-dependent kinase 4/6; CHK1: checkpoint kinase 1; EGF-R: epidermal growth factor receptor; EphA2: ephrin receptor A2; FAK: focal adhesion kinase; HER-2/ERBB2: human epidermal growth factor receptor 2; HIF-1 α : hypoxia-inducible factor-1 α ; hTERT: human telomerase reverse transcriptase; IGF-1R: insulin-like growth factor-1 receptor; MMP: matrix metalloproteinase; VEGF-R: vascular endothelial growth factor receptor. The illustration was modified from Hanahan and Weinberg (Hanahan and Weinberg, 2011) and complemented with relevant HSP90 client proteins.

Importantly, cancer cells are permanently exposed to high levels of proteotoxic stress in consequence of their malignant “lifestyle” (Neckers and Workman, 2012). Compared to non-malignant cells, tumor cells are characterized by an increased proliferation rate that is accompanied by a higher overall protein turnover and elevated expression of mutant oncoproteins, many of which are less stable than their wild-type counterparts (Whitesell and Lindquist, 2005). Therefore, cancer cells strongly rely on a compensatory cellular stress response and have an increased dependence on proteins that assist regulating their protein homeostasis (Whitesell and Lindquist, 2005). One important chaperone for maintaining proper folding of conformationally destabilized proteins is HSP90 and notably, it has been found to be 2- to 10-fold overexpressed in tumor cells compared to normal cells (Ferrarini et al., 1992; Isaacs et al., 2003; Koga et al., 2009). Moreover, HSP90 in tumor cells is being present in an activated form with higher affinity for ATP binding, whereas HSP90 in normal tissues appears in an inactive, uncomplexed form with lower ATP binding affinity (Kamal et al., 2003). Independent studies revealed that high expression of HSP90 in tumor biopsies is associated with tumor aggressiveness, invasion, lymph node metastasis, and decreased survival in different types of cancer (Gallegos Ruiz et al., 2008; Pick et al., 2007; Wang et al., 2013).

Given the fact that tumor cells are more dependent on the chaperoning function of HSP90 than non-malignant cells and that tumor cell HSP90 shows a higher ATP binding affinity (Kamal et al., 2003), the chaperone has emerged to a promising target for anticancer drugs that prevent ATP binding and thereby inhibit the chaperoning function of HSP90 (Roe et al., 1999). Pharmacological HSP90 inhibitors, such as the novel compound NW457 that is studied in the present work, mainly focus on cytoplasmic HSP90 α and β , as the other isoforms do not appear to be critically associated with cancer-related client proteins and oncogenic signaling pathways (Argon and Simen, 1999; Felts et al., 2000; Johnson et al., 2010). Most of the HSP90 inhibitors that have been developed interfere with the N-terminal ATP-binding pocket (Johnson et al., 2010), thereby impeding the chaperoning activity and the maturation of HSP90 client proteins. Hence, immature client proteins including critical oncogenic signaling proteins are released from the chaperoning cycle and subjected to proteasomal degradation (Figure 4). Therefore, pharmacological

inhibition of HSP90 has considerable consequences for cancer cells as it targets a broad range of fundamental oncogenic signaling pathways.

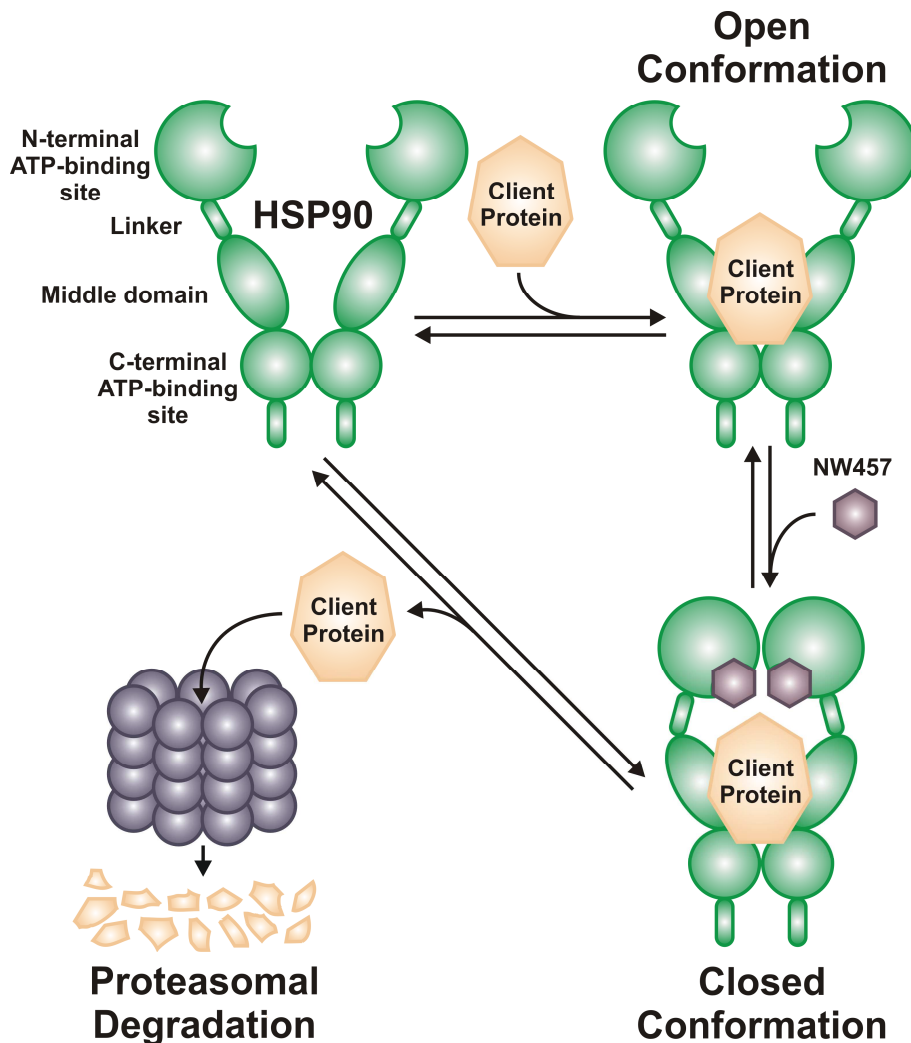


Figure 4. Modulation of the HSP90—client protein cycle in the presence of the pharmacological HSP90 inhibitor NW457 (schematic model).

A destabilized client protein binds to the middle domain of an HSP90 homodimer that is functionally associated in a multiprotein complex with other heat shock proteins and co-chaperones (not shown here). As pharmacological HSP90 inhibitors, such as NW457, bind to the N-terminal ATP binding site of HSP90, they prevent ATP-binding and suppress chaperoning activity, thereby impeding the maturation of the client protein. Hence, the HSP90 client protein is released in an unstable conformation and finally subjected to proteasomal degradation. This schematic model was modified from Trepel et al., 2010.

Taken together, HSP90 provides an attractive anticancer drug target as (i) the chaperone is specifically overexpressed in tumor cells due to elevated proteotoxic stress, (ii) many HSP90 client proteins are mutated or overexpressed oncoproteins with tumor-promoting capabilities, (iii) tumor cells are highly dependent on HSP90's chaperoning activity, and (iv) pharmacological inhibition of HSP90 results in the degradation of crucial client proteins (Isaacs et al., 2003; Neckers and Workman, 2012).

2.5 Pharmacological inhibitors of HSP90

The mechanisms of cancer cells to overcome growth control and resist cell death are multifaceted, thus restricting the antitumor activity of small-molecule inhibitors that target only one of many oncogenic signaling pathways. Hence, targeting multiple pathways simultaneously is assumed to provide a more effective therapeutic strategy in cancer. Targeting HSP90 represents a prime example for such an extensive treatment approach. Due to its pivotal role in the regulation of multiple oncogenic signaling pathways, HSP90 has emerged as an attractive anticancer drug target over the past decade (Johnson et al., 2010; Kim et al., 2009; Neckers and Workman, 2012). Since many of its client proteins contribute to the hallmarks of cancer (see Figure 3), HSP90 inhibition provides a potent strategy to simultaneously interrupt multiple pathways associated with tumorigenesis.

Geldanamycin is the natural parent compound of the first class of HSP90 inhibitors having demonstrated antitumor activity. It is a benzoquinone ansamycin produced by *Streptomyces hygroscopicus* var. *geldanus* and was isolated for its antibiotic activity in 1970 (DeBoer et al., 1970). However, it took some time until geldanamycin was demonstrated to specifically bind to HSP90 (Whitesell et al., 1994) and to exert potent antitumor activity *in vitro* and *in vivo* (Supko et al., 1995). The discovery of geldanamycin revealed the significance of HSP90 for tumor cells, elucidated how the HSP90 multichaperone machinery functions, and facilitated the identification of many HSP90 client proteins (Fukuyo et al., 2010; Grenert et al., 1997; Stebbins et al., 1997). However, translation of this natural compound into the clinic was hampered due to unacceptable hepatotoxicity at the doses required for therapeutic efficacy (Supko et al., 1995). This led to the development of the semi-synthetic derivatives 17-allylamino-17-demethoxygeldanamycin (17-AAG or tanespimycin) and 17-dimethylaminoethylamino-17-demethoxygeldanamycin (17-DMAG or alvespimycin). 17-AAG was the first HSP90 inhibitor entering the clinic in 1999, and has been tested since then in more than 30 Phase I and II trials, either as single agent or in combination with other approved anticancer therapeutics (Kim et al., 2009). Despite its promising antitumor activity, poor aqueous solubility and difficulties in formulation precluded further clinical testing of 17-AAG. The second semi-synthetic derivative of geldanamycin, 17-DMAG, also demonstrated clinical activity, but again, unacceptable toxicity abandoned further clinical development of this compound in 2008. However, this was not the end of HSP90 as anticancer drug target - rather, strong efforts have been carried out in the last years in developing novel, fully synthetic HSP90 inhibitors which overcome the pharmacokinetic limitations of the first generation compounds.

Numerous novel second generation HSP90 inhibitors based on different non-ansamycin chemical scaffolds have been developed and are now undergoing clinical evaluation. One of the first synthetic candidates entering clinical trials was BIIB021 (Biogen), which is based on the purine scaffold (Kasibhatla et al., 2007; Lundgren et al., 2009) and has previously been shown to potently radiosensitize head and neck squamous cell carcinoma (HNSCC) both *in vitro* and *in vivo* (Yin et al., 2010). BIIB021 has been evaluated in seven Phase I/II trials in patients with breast cancer, gastrointestinal stroma tumors (GIST), and advanced solid tumors (<http://clinicaltrials.gov>; Dickson et al., 2013). The second generation HSP90 inhibitors currently most intensely studied include STA-9090 (ganetespib, Synta Pharmaceuticals) and AUY922 (NVP-AUY922, Novartis). Due to their promising activity as single agents and in combined regimes in different preclinical tumor models (Eccles et al., 2008; Gaspar et al., 2010; Jensen et al., 2008; Lin et al., 2008; Moser et al., 2012; Okui et al., 2012; Shimamura et al., 2012; Stingl et al., 2010; Zaidi et al., 2012), these inhibitors have each entered over 20 clinical trials so far (see <http://clinicaltrials.gov> for the status quo).

Another natural macrocyclic HSP90 inhibitor is radicicol (also referred to as monorden), which was originally isolated from the fungus *Monosporium bonorden* (Delmotte and Delmotte-Plaque, 1953; Kwon et al., 1992), and interferes with the N-terminal ATP-binding site of HSP90 (Schulte et al., 1998). The binding mode of radicicol differs from that of geldanamycin (Johnson et al., 2010). In contrast to geldanamycin, radicicol lacks the toxic hydroquinone moiety, thus making it significantly less hepatotoxic (Johnson et al., 2010). Despite promising antitumor activity *in vitro*, radicicol demonstrated metabolic instability *in vivo* which furthered the development of synthetic oxime derivatives with improved pharmacodynamic and pharmacokinetic properties (Agatsuma et al., 2002; Winssinger et al., 2009; Yang et al., 2004). The laboratory of Prof. Nicolas Winssinger (Department of Organic Chemistry, University of Geneva, Switzerland) played a pivotal role in this process and generated an extended library of pochoxime HSP90 inhibitors that are characterized by cellular efficacies in the nanomolar range (Barluenga et al., 2009; Barluenga et al., 2008; Wang et al., 2009). This library identified several pochoxime analogues with enhanced cellular efficacies compared to radicicol. The introduction of a hydroxyl group at carbon 6 on the macrocycle, e.g. in 6-hydroxy-pochoxime C, further improved their potency. The structures of radicicol and its synthetic pochoxime derivatives are shown in Figure 5. The comparison of the cocrystal structure of radicicol and pochoxime A with human HSP90 α reveals that the synthetic oxime derivative binds to a different conformation of HSP90 than its natural parent compound (Figure 5B), thus possibly ameliorating the binding affinity and enhancing the biological activity (Barluenga et al., 2009; Barluenga et al., 2008; Wang et al., 2009). The derivative 6-hydroxy-

pochoxime C (hereinafter referred to as NW457) is the compound that is studied in the present work.

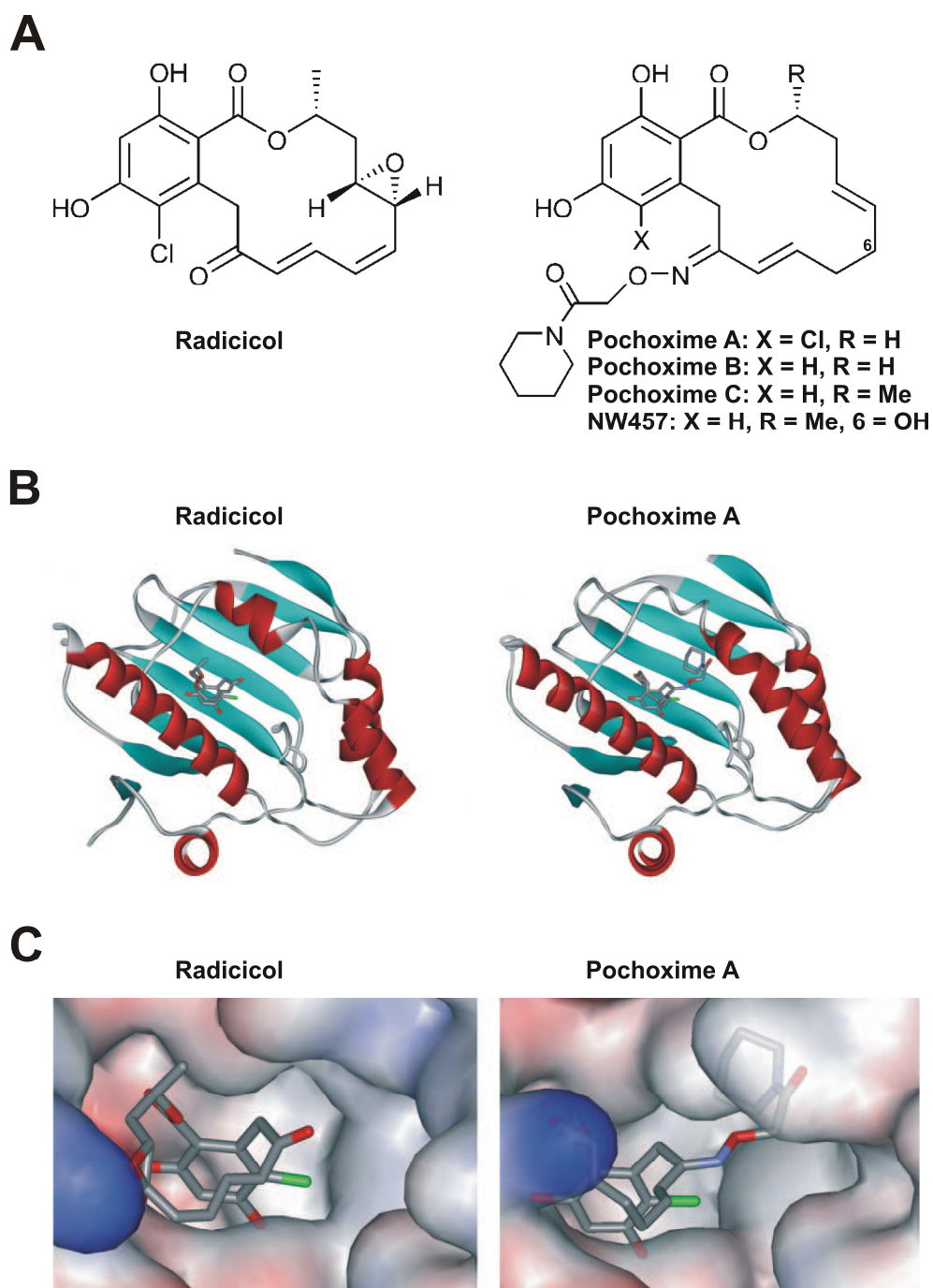


Figure 5. Chemical and cocrystal structures of pochoxime HSP90 inhibitors and their interference with the N-terminal ATP-binding pocket of HSP90.

(A) Structures of radicol and its synthetic pochoxime derivatives including NW457. (B) Structure of the N-terminal domain of human HSP90 α in complex with radicol (left) and pochoxime A (right). HSP90 α -helices=red, β -sheets=green, loops=grey. (C) Crystallographic structure of the N-terminal ATP-binding pocket of human HSP90 α in complex with radicol (left) and pochoxime A (right). HSP90: negatively charged regions = red, positively charged regions=blue; HSP90 inhibitor: carbon=grey, oxygen=red, nitrogen=purple, chloride=green. The figures were modified from Barluenga et al. (Barluenga et al., 2009).

The novel pochoxime series was screened *in vitro* for HSP90 affinity, HSP90 client protein depletion (HER-2/ERBB2), and cytotoxicity to two human breast cancer cell lines (SKBr3 and HCC1954). Thereby, pochoximes A, B, and C were identified as the most potent compounds as they exhibited biological activity in the nanomolar range (Barluenga et al., 2008). The efficacy of pochoxime A was further investigated in a BT-474 (human breast cancer cell line) xenograft mouse model, in which a dose-dependent inhibition of tumor growth accompanied by massive apoptosis induction could be observed (Barluenga et al., 2008). Moreover, pochoxime A (also referred to as NXD30001, patented by NexGenix Pharmaceuticals) was studied *in vitro* in primary murine and human glioblastoma multiforme cells (GBM), as well as in a genetically engineered mouse model of GBM (Zhu et al., 2010). The authors could show that intravenously administered pochoxime A was able to penetrate the blood brain barrier and finally accumulated in brain tissue. Furthermore, the compound potently inhibited the proliferation of primary GBM cells, but not of non-malignant astrocytes. Growth inhibition was accompanied by the degradation of HSP90 client proteins EGF-R, AKT, CDK4, and CyclinD1, and finally resulted in apoptosis. *In vivo*, NXD30001 treatment induced tumor regression and significantly increased survival of EGF-R-driven GBM bearing mice.

In summary, the novel pochoxime series seems to exhibit superior pharmacodynamics and promising anticancer activities both *in vitro* and *in vivo* compared to former HSP90 inhibitors. As the introduction of a hydroxyl group at carbon 6 on the pochoxime macrocycle was reported to improve aqueous solubility and to further enhance cellular efficacy, 6-hydroxy-pochoxime C (hereinafter referred to as NW457) was chosen for the present work. As a first approach here, the antitumor potency of NW457 is studied with specific regard to its radiosensitizing capacity and cell death induction, both in a colorectal cancer system and in a model of glioblastoma multiforme.

3 Purpose

Due to multiple genetic aberrations and a general upregulation of oncogenic proteins, cancer cells are commonly exposed to high levels of proteotoxic stress and thus critically rely on compensatory mechanisms in order to sustain their protein homeostasis. Therefore, tumor cells are highly dependent on the assistance of molecular chaperones, such as the heat shock protein 90 (HSP90). Since HSP90 maintains the conformational stability and function of numerous oncogenic proteins, it has emerged as an interesting anticancer drug target, and several small-molecule inhibitors with different chemical scaffolds have been developed in the recent years.

One of these compounds is NW457 (6-hydroxy-pochoxime C), whose antitumor potential was characterized here in combination with ionizing radiation for the first time. The aim of the present work was to investigate whether and by which molecular mechanisms NW457 sensitizes tumor cells to ionizing radiation. Therefore, in the first part of the thesis, the impact of NW457 on tumor cell radiosensitization was examined in colorectal cancer models with specific regard to the mechanisms of cell death induction and the relevance of the KRAS, p53, and BAX status. Furthermore, the tolerability of the novel HSP90 inhibitor by primary hepatocytes and its efficacy in combination with radiotherapy *in vivo* were analyzed. The second part of the thesis investigated the radiosensitizing potential of NW457 in human glioblastoma cell lines and evaluated whether its combined application with irradiation might be a promising approach to interfere with the radioresistant and invasive phenotypes which are commonly associated with the pathology of glioblastomas and assumed to account for the unfavorable outcome of this disease.

4 Material

4.1 Directory of manufacturers and suppliers

Table 1. Manufacturers and suppliers

| Manufacturer | City, Country |
|---|------------------------------|
| Abbott | Wiesbaden, Germany |
| AbD Serotec | Puchheim, Germany |
| B. Braun | Melsungen, Germany |
| Bachem | Bubendorf, Switzerland |
| BD Biosciences | Heidelberg, Germany |
| BD Pharmingen, distributed by BD Biosciences | Heidelberg, Germany |
| Biochrom | Berlin, Germany |
| BioRad | Munich, Germany |
| BioTek | Bad Friedrichshall, Germany |
| BioVision | Milpitas, CA, USA |
| Cell Signaling Technology, distributed by New England Biolabs | Frankfurt (Main), Germany |
| Fermentas | St. Leon-Rot, Germany |
| Ibidi | Martinsried, Germany |
| Invitrogen Life Technologies | Darmstadt, Germany |
| Janvier Labs | Le Genest Saint Isle, France |
| LI-COR Biosciences | Bad Homburg, Germany |
| Lonza | Cologne, Germany |
| Macherey-Nagel | Düren, Germany |
| Merck Millipore | Darmstadt, Germany |
| Multimmune | Munich, Germany |
| PAA | Cölbe, Germany |
| Philips Healthcare | Hamburg, Germany |
| Promega | Mannheim, Germany |
| R&D Systems | Wiesbaden, Germany |
| Roche | Penzberg, Germany |
| Siemens | Munich, Germany |
| Sigma-Aldrich | Seelze, Germany |
| Thermo Scientific | Karlsruhe, Germany |
| Zeiss | Oberkochen, Germany |

4.2 Cell lines

Table 2. Cell lines

| Cell line | Origin | Source / Reference | Medium | CO ₂ |
|----------------|---|--|-----------------------------|-----------------|
| HCT116 | Human colorectal carcinoma; expressing wild-type p53 and mutant KRAS | Kindly provided by P. Daniel, Max-Delbrück-Center for Molecular Medicine, Berlin, Germany | Mc Coy's 5A medium +10% FCS | 7.5% |
| HCT116 BAX -/- | Human colorectal carcinoma; BAX-deficient subclone of HCT116 cell line | Kindly provided by P. Daniel, Max-Delbrück-Center for Molecular Medicine, Berlin, Germany (Zhang et al., 2000) | Mc Coy's 5A medium +10% FCS | 7.5% |
| HCT116 p53 -/- | Human colorectal carcinoma; p53-deficient subclone of HCT116 cell line | Kindly provided by P. Daniel, Max-Delbrück-Center for Molecular Medicine, Berlin, Germany (Bunz et al., 1998) | Mc Coy's 5A medium +10% FCS | 7.5% |
| Hke3 | Human colorectal carcinoma; subclone of HCT116 cells expressing wild-type KRAS | Kindly provided by S. Shirasawa, Fukuoka University, Japan (Shirasawa et al., 1993) | Mc Coy's 5A medium +10% FCS | 7.5% |
| LN229 | Human glioblastoma | American Type Culture Collection | DMEM +10% FCS | 7.5% |
| T98G | Human glioblastoma | American Type Culture Collection | DMEM +10% FCS | 7.5% |
| CT26 | Murine colorectal carcinoma; derived from an undifferentiated adenocarcinoma induced by N-nitroso-N-methylurethane of Balb/c mice; carrying wild-type p53 and mutant KRAS | American Type Culture Collection | RPMI 1640 medium +10% FCS | 5.0% |

4.3 Antibodies

4.3.1 Primary antibodies

Table 3. Primary antibodies

| Antibody | Source | Manufacturer | Catalog number | Dilution | Application |
|--|--------|---------------------------|----------------|----------|----------------|
| Anti-ATM | rabbit | Merck Millipore | #07-1286 | 1:500 | Western blot |
| Anti-ATR | rabbit | Merck Millipore | #09-070 | 1:1000 | Western blot |
| Anti-BAK | rabbit | Cell Signaling Technology | #3814 | 1:1000 | Western blot |
| Anti-BAX | rabbit | Cell Signaling Technology | #2774 | 1:1000 | Western blot |
| Anti-BCL-xL (54H6) | rabbit | Cell Signaling Technology | #2764 | 1:1000 | Western blot |
| Anti-BRAF | mouse | BD Biosciences | #612374 | 1:250 | Western blot |
| Anti-Caspase-3 | mouse | BD Biosciences | #610323 | 1:250 | Western blot |
| Anti-Caspase-9 | mouse | R&D Systems | #MAB8301 | 1:1000 | Western blot |
| Anti-CHK1 | mouse | Sigma-Aldrich | #C9358 | 1:1000 | Western blot |
| Anti-CHK2 | mouse | BD Biosciences | #611570 | 1:1000 | Western blot |
| Anti-Cleaved Caspase-3 (Asp175) (5A1E) | rabbit | Cell Signaling Technology | #9664 | 1:1000 | Western blot |
| Anti-EGF-R-PE | mouse | BD Biosciences | #555997 | 1:25 | Flow cytometry |
| Anti-EphA1-PE | goat | R&D Systems | #FAB638P | 1:25 | Flow cytometry |
| Anti-EphA2-Alexa Fluor® 488 | mouse | R&D Systems | #FAB3035G | 1:25 | Flow cytometry |

Material

| Antibody | Source | Manufacturer | Catalog number | Dilution | Application |
|--|--------|---------------------------|---|----------|---|
| Anti-EphB2-PE | rat | R&D Systems | #FAB467P | 1:25 | Flow cytometry |
| Anti-EphB3-APC | mouse | R&D Systems | #FAB56671A | 1:25 | Flow cytometry |
| Anti-EphB4-FITC | rat | R&D Systems | #FAB3038F | 1:25 | Flow cytometry |
| Anti-HSP70 | mouse | BD Biosciences | #610608 | 1:1000 | Western blot |
| Anti-HSP70 capture antibody | mouse | R&D Systems | #DYC1663-2 (DuoSet [®] IC Kit) | 1:180 | ELISA (enzyme-linked immunosorbent assay) |
| Anti-HSP70 detection antibody | rabbit | R&D Systems | #DYC1663-2 (DuoSet [®] IC Kit) | 1:36 | ELISA |
| Anti-HSP70-FITC | mouse | Multimmune | #cmHSP70.1-FITC | 1:100 | Flow cytometry |
| Anti-HSP90 (C45G5) | rabbit | Cell Signaling Technology | #4877 | 1:1000 | Western blot |
| Anti-Integrin $\alpha\beta$ 3-Alexa Fluor [®] 488 | mouse | R&D Systems | #FAB3050G | 1:100 | Flow cytometry |
| Anti-Integrin $\alpha\beta$ 5-PE | mouse | R&D Systems | #FAB2528P | 1:10 | Flow cytometry |
| Anti-MET (25H2) | mouse | Cell Signaling Technology | #3127 | 1:1000 | Western blot |
| Anti-p14 ARF (4C6/4) | mouse | Cell Signaling Technology | #2407 | 1:1000 | Western blot |
| Anti-p21 Waf1/Cip1 (12D1) | rabbit | Cell Signaling Technology | #2947 | 1:1000 | Western blot |
| Anti-p53 (7F5) | rabbit | Cell Signaling Technology | #2527 | 1:1000 | Western blot |
| Anti-PARP (C2-10) | mouse | Trevigen/TACS | #4338-MC-50 | 1:2000 | Western blot |

Material

| Antibody | Source | Manufacturer | Catalog number | Dilution | Application |
|--|--------|---------------------------|----------------|----------|---------------------|
| Anti-Phospho-MET (Tyr1234/1235) (D26) | rabbit | Cell Signaling Technology | #3077 | 1:1000 | Western blot |
| Anti-Tubulin | mouse | Sigma-Aldrich | #T5168 | 1:2000 | Western blot |
| Anti-Tubulin-FITC (TUB 2.1) | mouse | Sigma-Aldrich | #F2043 | 1:400 | Immuno-fluorescence |
| Anti-Vinculin (hVIN-1) | mouse | Sigma-Aldrich | #V9131 | 1:1000 | Western blot |
| Isotype control IgG1-FITC | rat | R&D Systems | #IC005F | 1:25 | Flow cytometry |
| Isotype control IgG1-FITC | mouse | BD Biosciences | #555748 | 1:100 | Flow cytometry |
| Isotype control IgG1-PE | mouse | BD Biosciences | #555749 | 1:10 | Flow cytometry |
| Isotype control IgG2A-Alexa Fluor [®] 488 | mouse | R&D Systems | #IC003G | 1:25 | Flow cytometry |
| Isotype control IgG2A-APC | mouse | R&D Systems | #IC003A | 1:25 | Flow cytometry |
| Isotype control IgG2a-FITC | mouse | BD Biosciences | #555573 | 1:10 | Flow cytometry |
| Isotype control IgG2A-PE | rat | R&D Systems | #IC006P | 1:25 | Flow cytometry |

4.3.2 Secondary antibodies

Table 4. Secondary antibodies

| Antibody | Source | Manufacturer | Catalog number | Dilution | Application |
|---|--------|--------------|----------------|----------|--------------|
| Anti-mouse IgG-IRDye [®] 680LT | goat | LI-COR | #926-68020 | 1:20000 | Western blot |
| Anti-mouse IgG-IRDye [®] 800CW | goat | LI-COR | #926-32210 | 1:20000 | Western blot |

Material

| Antibody | Source | Manufacturer | Catalog number | Dilution | Application |
|------------------------------|--------|--------------|----------------|----------|--------------|
| Anti-rabbit IgG-IRDye® 680LT | goat | LI-COR | #926-68021 | 1:20000 | Western blot |
| Anti-rabbit IgG-IRDye® 800CW | goat | LI-COR | #926-32211 | 1:20000 | Western blot |

4.4 Primers

Table 5. Primers used for quantitative real-time PCR

Primers were synthesized by Sigma-Aldrich. F: forward; R: reverse

| Name | Sequence 5'-3' |
|--------------------|---------------------------|
| 18S-F | CGGCTACCACATCCAAGGAA |
| 18S-R | GCTGGAATTACCGCGGCT |
| ATM-F | CTGGAAGAAGCACAAGTATTCTGGG |
| ATM-R | TGGGATTGTTGCTGCACA |
| ATR-F | GGTCACCACCAGACAGCCTAC |
| ATR-R | GAACATCACCTTGGACCAGA |
| CHK1-F | ATGCCTGAACCAGATGCTCAG |
| CHK1-R | GAGGTTATCCCTTTCATCCAACAG |
| CHK2-F | CTCTTGGAAGTGGTGCCTGTG |
| CHK2-R | GGGTCTGCCTCTCTTGCTGA |
| HGF-F | ACTTCCATTCACTTGCAAGGCT |
| HGF-R | CTCCACTTGACATGCTATTGAAGG |
| HSP70A1A-F | GAAGGACGAGTTTGAGCACAAGA |
| HSP70A1A-R | TGATGATGGGGTTACACACCTG |
| HSP90AA1-F | TTCAAATTCATCAGATGCATTGG |
| HSP90AA1-R | AATATGCAGCTCTTCCCAGAGTC |
| Integrin Alpha V-F | AACTCGCCAGGTGGTATGTGA |
| Integrin Alpha V-R | GACTGCTGGTGCACTGAAA |
| Integrin Beta 3-F | AATGACGGGCAGTGTCATGTT |
| Integrin Beta 3-R | ATCAGCCCCAAAGAGGGATAA |
| Integrin Beta 5-F | AGGCTGGGACGTCATTCAGA |
| Integrin Beta 5-R | GCGAACCTGTAGCTGGAAGGT |

Material

| Name | Sequence 5'-3' |
|-------------|---------------------------|
| MET-F | ATCCACCTTCATTAAAGGAGACCTC |
| MET-R | AAACCACAACCTGCATGAAGC |
| p53-F | CCGCCTGAGGTTGGCTC |
| p53-R | CGCCCATGCAGGAACTGT |

5 Methods

5.1 Cell biology methods

5.1.1 Cell culture

5.1.1.1 Cultivation of cell lines

Detailed information about the utilized cell lines, their origin, and culture conditions is listed in Table 2. Human colorectal carcinoma cell lines were maintained in Mc Coy's 5A medium (Invitrogen Life Sciences) supplemented with 10% heat inactivated fetal calf serum (PAA) in a humidified incubator at 7.5% CO₂ and 37°C. HCT116 BAX- and p53-deficient subclones were reselected with 0.1 mg/ml hygromycin or 0.1 mg/ml hygromycin + 0.4 mg/ml G418 for four weeks prior to using them for experiments. Human glioblastoma cell lines were cultured in DMEM supplemented with 10% heat inactivated fetal calf serum in a humidified incubator at 7.5% CO₂ and 37°C. In order to maintain log phase growth, cells were routinely split at approximately 80% confluence employing accutase (PAA) for detachment. All cell lines were monitored for mycoplasma infection on a regular basis (MycAlert, Lonza), and only mycoplasma negative cell lines were used for experiments. Murine CT26 cells were maintained in RPMI 1640 medium supplemented with 10% heat inactivated fetal calf serum in a humidified incubator at 5.0% CO₂ and 37°C.

For long-term storage, cell lines were frozen in liquid nitrogen. Cells were detached with trypsin or accutase, washed with medium, and resuspended in ice-cold freezing solution containing 90% FCS and 10% DMSO. $1\text{-}5 \times 10^6$ cells were transferred to a 2.0 ml cryo tube, placed into a rack with ice-cold isopropanol, and frozen at -80°C overnight. Afterwards, cells were transferred to liquid nitrogen for long-term storage.

For recultivation, frozen cells were thawed for 60 s at 37°C and carefully resuspended in 20 ml of prewarmed growth medium. After centrifugation (200 g, 5 min), cells were resuspended in medium and seeded into 75 or 175 cm² cell culture flasks. Medium was changed after 24 h to remove residual DMSO.

5.1.1.2 Preparation and maintenance of primary murine hepatocytes

Primary hepatocytes were isolated from adult C57BL/6 mice by liver perfusion and percoll density centrifugation according to the protocol published by Gonçalves et al. (Goncalves et al., 2007). All solutions needed were prepared in advance (Table 6). The preparation was performed with kind support of Kirsten Lauber and Gabriele Zuchtriegel from the Walter Brendel Centre of Experimental Medicine.

Liver perfusion

Liver perfusion was performed *in situ* using a peristaltic pump with adjustable speed. Therefore, the mouse was anaesthetized with isoflurane and immobilized to the preparation desk. The peritoneal cavity was opened and the inner organs were placed aside in order to have free access to the *vena cava inferior* and the *vena porta*. An Abocat needle (20G, 30 mm length) was introduced into the *vena porta*, the *vena cava* was immediately opened, and perfusion was initiated using prewarmed liver perfusion medium (constant flow of 5 ml/min). Perfusion was maintained until the liver was drained off blood and appeared pale (3-4 min). Subsequently, perfusion was continued using liver digestion medium containing 33 µg/ml LiberaseTM collagenase (Roche) and performed until the liver lobe felt very soft (5-6 min).

Cell dissociation

The perfused liver was removed from the peritoneal cavity and transferred into a Petri dish containing 10 ml of William's E complete medium (WCM). The gall bladder was removed and the liver lobe was carefully disrupted using two Q-Tips. At this stage, a fine cloud of cells spread into the medium as a sign of successful dissociation. Afterwards, the cell suspension was forced through a 100 µm cell strainer (BD Biosciences) and diluted with WCM to a final volume of 30 ml. Hepatocytes were sedimented at 35 g for 5 min and the cell pellet was resuspended in 24 ml of WCM.

Hepatocyte isolation

Separation of parenchymal, non-parenchymal, and dead cells was performed using Percoll gradient centrifugation. For each 24 ml suspension of dissociated cells, two Percoll gradient tubes were prepared using three different Percoll density solutions each. 6 ml 1.12 g/ml solution were applied on the bottom of a conical 50 ml tube, and carefully overlaid with 10 ml of 1.08 g/ml solution and 10 ml of 1.06 g/ml solution. 12 ml of liver cell suspension were carefully applied to the Percoll gradient in each tube. The cell suspension was fractionated by centrifugation at 750 g for 20 min at 20°C without brake. Subsequently, the two upper gradient layers containing cell debris and non-parenchymal cells were carefully removed. Then, the lowest layer containing the live hepatocytes was transferred to a fresh 50 ml tube containing 10 ml WCM. The tube was filled up to 40 ml volume using WCM and centrifuged at 355 g for 10 min at 20°C. The cell pellets from the two Percoll gradient tubes were pooled and resuspended in a final volume of 15 ml WCM. After centrifugation at 135 g for 5 min the cell pellet was resuspended in 5 ml William's E supplemented medium (WSM).

Hepatocyte cultivation

Following isolation, cells were seeded in WSM into multiwell plates precoated with 0.2% gelatin solution (Sigma-Aldrich) at a density of 8×10^3 cells per 96-well cavity or 8-well μ -slide (Ibidi), and 4×10^4 cells per 24-well cavity, respectively. Hepatocytes were maintained in a humidified incubator at 5% CO₂ and 37°C and allowed to recover for 24 h before they were used for experiments.

Table 6. Media and solutions used for the isolation and cultivation of primary murine hepatocytes

| Reagent | Composition |
|-----------------------------------|--|
| Liver perfusion medium | 0.9% NaCl 0.05% KCl 0.2% HEPES 0.008% EDTA in aqua dest., pH 7.4 |
| Liver digestion medium | 0.9% NaCl 0.05% KCl 0.2% HEPES 0.008% EDTA 0.07% CaCl ₂ 33 μ g/ml Liberase™ collagenase (Roche) in aqua dest., pH 7.4 |
| 1.124 g/ml Percoll stock solution | Easycoll, isotonic (Biochrom #L6143) |
| 1.12 g/ml Percoll solution | 96.5 ml Easycoll 3.5 ml PBS |
| 1.08 g/ml Percoll solution | 61.5 ml Easycoll 38.5 ml PBS |
| 1.06 g/ml Percoll solution | 43.75 ml Easycoll 56.25 ml PBS |
| Liberase™ collagenase solution | 1 mg Libarase™ collagenase (Roche) dissolved in 1 ml 2% CaCl ₂ |
| William's E Medium | with L-Glutamine (Invitrogen Life Technologies) |
| William's E Complete Medium (WCM) | William's E Medium 4% FCS (PAA) 100 U/ml Penicillin (PAA) 100 U/ml Streptomycin (PAA) |

| Reagent | Composition |
|---------------------------------------|---|
| William's E Supplemented Medium (WSM) | William's E Medium 4% FCS (PAA) 100 U/ml Penicillin (PAA) 100 U/ml Streptomycin (PAA) 50 ng/ml EGF-R (Sigma-Aldrich #E4127) 1 µg/ml Insulin (Sigma-Aldrich #I2643) 10 µg/ml Transferrin (Sigma-Aldrich #T0665) 1.3 µg/ml Hydrocortisone (Sigma-Aldrich #H0888) |

5.1.2 *In vitro* drug treatment and irradiation

The second generation HSP90 inhibitor NW457 (6-hydroxy-pochoxime C) is a synthetic derivative of radicicol and was kindly provided by Nicolas Winssinger (Department of Organic Chemistry, University of Geneva, Switzerland) together with the first generation inhibitor geldanamycin (GA). For *in vitro* studies the drugs were stored as 10 mM and 100 µM stock solutions in DMSO at -20°C and were freshly diluted in the appropriate growth medium immediately before use. Exponentially growing cells were stimulated with the indicated drug concentrations or the respective DMSO concentration as vehicle control for the designated times. Irradiation of tumor cells was carried out at room temperature using a Mueller RT250 X-ray tube (Philips) equipped with a Thoraesus filter at 200 kV and 10 mA at a dose rate of 0.52 Gy/min.

5.1.3 Microscopic quantification of apoptotic cells

Microscopic quantification of apoptotic cells was performed after staining with Hoechst 33342. Briefly, 5×10^5 cells per well were seeded into 24-well plates, stimulated with the respective drug concentrations for 24 h, and irradiated with single fractions of 1, 3, 5, or 10 Gy respectively. Following incubation for the designated times, nuclei were directly stained in the culture dishes with 3 µg/ml Hoechst 33342 for 15 min, and examined by fluorescence microscopy (Axiovert 40 CFL, Zeiss). Cells revealing features of chromatin condensation (patchy Hoechst staining) or nuclear fragmentation were considered apoptotic. For each condition, at least 400 nuclei were counted in randomly selected microscopic fields of two independent wells, and the percentage of apoptotic cells was calculated.

5.1.4 Cell viability assay

Cell viability was determined by using the Alamar Blue reagent (AbD Serotec), an indicator dye for measuring the reducing power of viable cells. In growing cells, the cell-permeable, active ingredient resazurin is continuously reduced to the fluorescent product resorufin, which can be detected with a fluorescence spectrophotometer (excitation 560 nm, emission 590 nm).

Briefly, 1×10^4 cells per well were seeded into 96-well plates and allowed to adhere overnight. Cells were stimulated with the given drug concentrations +/- irradiation and incubated for the indicated times. Subsequently, the medium was removed and the cells were washed once in culture medium (due to strong autofluorescence of the applied HSP90 inhibitors). Alamar Blue reagent was added at $\frac{1}{10}$ vol of culture medium and resazurin reduction was allowed for 4-7 h at 37°C. Resorufin fluorescence was measured directly in the 96-well plate using a microplate reader (Synergy Mx, BioTek) and viability was calculated according to the following formula:

$$\text{Viability [\%]} = \frac{\text{Fluorescence [Unknown Sample]} - \text{Fluorescence [Blank]}}{\text{Fluorescence [Untreated Vehicle Control]} - \text{Fluorescence [Blank]}} \times 100$$

5.1.5 Wound healing assay

To investigate the migratory behavior of glioblastoma cells, wound healing assays were performed. Cells were seeded into specialized culture dishes with a silicone-insert in the middle consisting of two distinct chambers for cell seeding (μ -dishes, Ibidi). Thereby, two rectangular areas of confluent cells with 0.22 cm² each were generated and separated by a well-defined cell-free 'wound' of 8.0 mm x 0.5 mm. After adhesion for 6 h or overnight, cells were exposed to sublethal doses of NW457 +/- irradiation and incubated for further 24 h. Then, the silicone insert was removed and cell migration into the wound was monitored using an inverse epifluorescence microscope (AxioObserver Z1, Zeiss) equipped with a temperature/CO₂ module, a 5x objective lens, and an AxioCam Mr3 camera (Zeiss). Movies were generated by acquiring images every 10 min over a period of 12 h. Individual migration paths of approximately 30 randomly selected cells per treatment were analyzed using the ImageJ manual tracking plugin (ImageJ 1.41o), and the accumulated distances were calculated using the Ibidi Chemotaxis and Migration Tool V2.0 (Ibidi). Additionally, the colonized area was measured using the AxioVision 4.6 software (Zeiss) and calculated according to the following formula:

$$\text{Colonized area after 12 h [mm}^2\text{]} = \frac{\text{free area after 0 h [\mu m}^2\text{]} - \text{free area after 12 h [\mu m}^2\text{]}}{10^6}$$

5.1.6 Transmigration assay

Transmigration of glioblastoma cells was analyzed by using 96-well MultiScreen-MIC plates equipped with tissue-culture-treated polycarbonate membranes of 8 μm pore size (Merck Millipore). Cells were stained with PKH67, a green fluorescent dye for general cell membrane labeling (Sigma-Aldrich). Briefly, cells were washed in serum free medium, pelleted by centrifugation, and stained with 4 μM of PKH67 diluted in Diluent C (Sigma-Aldrich) at room temperature for 5 min. Staining was stopped by adding 1 vol of 100% FCS, and 5 vol of culture medium containing 10% FCS. Afterwards, cells were pelleted, washed twice, and finally resuspended in medium containing 10% FCS. 2×10^4 PKH67 stained cells per well were seeded into 96-well filter plates and allowed to adhere for 3 h. Cells were then exposed to sublethal doses of NW457. After incubation for 24 h, cells were washed with serum free medium, and a final volume of 80 μl medium per well +/- NW457 was added. In order to analyze the impact of a serum gradient on cell migration, assays were performed with 0% FCS in the upper and 10% FCS in the lower chamber, or 10% FCS in the upper and 10% FCS in the lower chamber, respectively. The receiver plate was equipped with 340 μl medium per well +/- NW457, the prewarmed filter and receiver plates were assembled, and migration was allowed for 12 h at 37°C. Finally, the transmigrated cells, which were adherent to the lower side of the membrane, were harvested and quantified. Briefly, the non-migrated cells on the upper side of the filter were removed by washing the filter plate with ice-cold PBS containing 10 mM EDTA, wiping off the cells with a rubber spatula and two additional washing steps. Cells adherent to the lower side of the filter were lysed in 150 μl lysis buffer (Table 12), and PKH fluorescence in the lysates was measured in a microplate reader (Synergy Mx, BioTek). The percentage of transmigrated cells was calculated using a standard curve prepared from a dilution series of PKH stained, lysed cells according to the following formula:

$$\text{Transmigration [\%]} = \frac{\text{Fluorescence [Unknown Sample]} - \text{y Axis Intercept [Standard Curve]}}{\text{Slope [Standard Curve]}}$$

Table 7. Composition of lysis buffer

| Reagent | Composition |
|--------------|---|
| Lysis buffer | 20 mM HEPES-K pH 7.4 84 mM KCl 10 mM MgCl ₂ 0.2 mM EDTA 0.2 mM EGTA 0.5% NP40 |

5.1.7 Immunofluorescence staining and microscopy

The cellular morphology of primary hepatocytes was analyzed by immunofluorescence staining with subsequent microscopic evaluation.

8x10³ primary mouse hepatocytes per well were seeded into Ibidi 8-well μ -slides (Ibidi) coated with 0.2% gelatin. After adherence for 16 h, cells were treated with the indicated concentrations of NW457 or geldanamycin for 48 h. Afterwards, the medium was removed, cells were washed with PBS, and fixed with formaldehyde-containing IF fixation buffer for 10 min at room temperature. The fixation buffer was aspirated, hepatocytes were washed with PBS and permeabilized with 0.5% Triton X-100 in PBS for 5 min. For blocking of unspecific binding sites, cells were incubated with 3% BSA diluted in PBS + 0.1% Triton X-100 for 1 h. Cells were stained with Alexa Fluor 568-labeled phalloidin (Invitrogen) and monoclonal anti- β -tubulin-FITC antibody for 2 h at room temperature. Cells were washed with PBS + 0.1% Triton X-100, and stained with Hoechst 33342 (2 μ g/ml) for 10 min. Finally, hepatocytes were washed twice with PBS + 0.1% Triton X-100, and mounted in Fluoromount medium (Sigma-Aldrich). Microscopy was carried out using an inverse epifluorescence microscope (Zeiss AxioObserver Z1) equipped with a Zeiss Plan-Neofluar 63x/1.3 glycerin objective, AxioVision 4.6 software, and an AxioCam Mr3 camera (Zeiss). Filters used were 01 (BP 365/12) for DAPI, 38HE (BP 470/40) for FITC, and 43HE (BP 550/25) for Alexa Fluor 568 (Zeiss).

Table 8. Buffers used for immunofluorescence staining

| Reagent | Composition |
|----------------------|--|
| IF fixation buffer | 3.7% PFA (Sigma-Aldrich) 0.2% Triton X-100 in PBS |
| IF blocking solution | 3% BSA (Sigma-Aldrich) 0.1% Triton X-100 0.1% NaN ₃ in PBS |

5.1.8 Flow cytometry

All flow cytometric analyses were carried out with a BD LSR II flow cytometer (BD Biosciences). Data were analyzed with the FACSDiva software (BD Biosciences), or FlowJo 7.6.5 (Tree Star Inc.), respectively.

5.1.8.1 Analysis of hypodiploid nuclei

Internucleosomal DNA-fragmentation as a central feature of apoptosis was assessed on the basis of the appearance of hypodiploid nuclei according to Riccardi and Nicoletti (Riccardi and Nicoletti, 2006) using hypotonic propidium iodide staining buffer. $5\text{-}6 \times 10^3$ cells per well were seeded into 96-well plates, allowed to adhere overnight, stimulated with NW457 for 24 h, and irradiated with single fractions of 1, 3, 5, or 10 Gy, respectively. Subsequently, culture plates were spun down and supernatants were removed. Nuclei were released and stained for their DNA content by incubating the cells with hypotonic propidium iodide (PI) staining buffer at 37°C for 5 min (200 µl buffer per 10,000 cells). Forward scatter (FSC), sideward scatter (SSC), and PI fluorescence of the nuclei were analyzed flow cytometrically and all nuclei with less than diploid DNA content were considered apoptotic.

Table 9. Composition of PI staining buffer

| Reagent | Composition |
|--------------------|--|
| PI staining buffer | 50 µg/ml Propidium iodide 0.1% (w/v) Tri-sodium citrate dihydrate 0.1% (v/v) Triton X-100 in aqua dest. |

5.1.8.2 Analysis of cell surface proteins

Flow cytometric analysis of cell surface proteins was performed with the help of fluorescently labeled primary antibodies (see Table 3). Cells were seeded into 6-well (5×10^5 cells per well) or 24-well plates (7×10^4 cells per well), allowed to adhere for 5 h, and stimulated with NW457 +/- irradiation for the indicated times. Afterwards, cells were trypsinized and collected by centrifugation. After washing in FACS staining buffer, cells were distributed for different stainings into a V-bottom 96-well plate and washed again with FACS staining buffer. Appropriate fluorochrome-conjugated primary antibodies and the corresponding isotype control antibodies were diluted in FACS staining buffer and added to the cells (dilutions see Table 3). After incubation for 30 min at 4°C, cells were washed twice, and finally resuspended in 100 µl FACS staining buffer for flow cytometry.

FSC, SSC and the respective fluorescence signals were analyzed. Relative expression of surface proteins was calculated on the basis of the following formula:

$$\text{Relative expression} = \frac{\text{Median FI}}{\text{Median FI (isotype)}}$$

Table 10. Composition of FACS staining buffer

| Reagent | Composition |
|---|-----------------------|
| FACS staining buffer (Pharmingen Stain Buffer, BD Pharmingen) | 0.2% (w/v) BSA in PBS |

5.1.9 Detection of HSP70 release into cell culture supernatants

In order to assess whether HSP90 inhibition by NW457 induces the cellular release of HSP70, cell culture supernatants were monitored for HSP70 using an HSP70-specific ELISA kit (DuoSet[®] IC, R&D Systems) according to the manufacturer's protocol. Briefly, 0.5-1x10⁶ HCT116 cells per well were stimulated in 6-well plates with 0-300 nM NW457 as described before and incubated for 48 or 72 h, respectively. Culture supernatants were harvested and 100 µl of 1:5 dilutions were transferred to 96-well plates precoated with a mouse anti-human HSP70 capture antibody provided by the kit (see Table 3) according to the manufacturer's protocol. After 2 h incubation and washing, a biotinylated rabbit anti-human HSP70 detection antibody (see Table 3) was added and the samples were incubated for 2 h. After washing and 20 min incubation with streptavidin-HRP (horseradish peroxidase), samples were exposed to substrate solution for 20 min and the optical density was measured at 450 nm in a microplate reader (Synergy Mx, BioTek). Concentrations of released HSP70 were calculated using a standard curve prepared from a dilution series of recombinant human HSP70.

5.1.10 Clonogenic survival assay

Clonogenic survival was examined with the help of colony formation assays. Cells were seeded as single cell suspensions into 6-well plates in a range of 150-30,000 cells per well in order to yield 40-80 colonies per well depending on the different stimuli. After adherence for 4 h, cells were subjected to different treatment modalities varying in the time of drug exposure: In the first approach cells were treated with 10 nM NW457 or 0.1% DMSO as vehicle control, concomitantly irradiated with 0-5 Gy, and incubated in drug-containing medium under standard conditions for 14 days. In the second approach cells were prestimulated with 10 nM NW457 or 0.1% DMSO for 24 h and irradiated afterwards. Drug-containing medium was replaced by drug-free medium directly before irradiation and

colony formation was allowed for the following 14 days. Subsequently, cells were fixed and stained with a solution containing 0.3% methylene blue in 80% ethanol, and colonies which consisted of more than 50 cells were quantified. Plating efficiencies and surviving fractions were determined according to the following formulas:

The plating efficiency (PE) represents the percentage of seeded cells giving rise to colonies (without irradiation). The PE was calculated as follows:

$$PE [\%] = \frac{\text{counted colonies} \times 100}{\text{seeded cells}}$$

To determine the clonogenic survival in the presence or absence of NW457, two different plating efficiencies were calculated: PE_{DMSO} of DMSO treated, unirradiated cells, and PE_{NW457} of NW457 treated, unirradiated cells.

The surviving fraction (SF) as a function of the irradiation dose applied, was calculated from the number of counted colonies with regard to the number of seeded cells and was calibrated on the PE_{DMSO} or PE_{NW457} , respectively.

$$SF_{1\text{Gy}} [\%] = \frac{\text{counted colonies} \times 100}{\text{seeded cells}} \times \frac{100}{PE_{\text{DMSO}}}$$

$$SF_{1\text{Gy}+10\text{nM}} [\%] = \frac{\text{counted colonies} \times 100}{\text{seeded cells}} \times \frac{100}{PE_{\text{NW457}}}$$

In order to quantify the radiosensitizing potential of NW457, the radiation dose giving 37% survival (D0) and the survival fraction at 3 Gy (SF3) were determined. Based on these parameters radiation enhancement ratios were calculated as the D0 or SF3 of DMSO treated cells divided by that of NW457 treated cells.

5.2 Biochemical methods

5.2.1 Preparation of whole cell protein lysates

Whole cell protein lysates were prepared for Western blot analyses and caspase activity assays. Briefly, $0.2-1 \times 10^6$ cells per well were stimulated in 6-well plates as described before. Subsequently, cells were detached with a rubber spatula, transferred to a 2 ml tube on ice, and collected by centrifugation (11,000 g, 2 min, 4°C). Cells were washed with ice-cold PBS, and stored as dry pellets at -80°C until lysis. Whole cell protein extracts were prepared by adding approximately 100 µl of Western blot lysis buffer to 1×10^6 cells (for composition see Table 11) and incubating for 20 min on ice with occasional vortexing. Lysates were cleared by centrifugation (11,000 g, 10 min, 4°C), and supernatants were

transferred to fresh 1.5 ml tubes. Protein concentrations were determined by Bradford assay, and lysates were stored at -80°C until further use for a maximum of two months.

5.2.2 Bradford assay

In order to use accurately defined, equal amounts of total protein for Western blotting and caspase activity tests, the protein concentration of whole cell lysates was determined according to Bradford et al. (Bradford, 1976). For quantification, a standard curve of serially diluted bovine serum albumin (BSA, 0-300 µg/ml in PBS) was prepared. Cell lysates were diluted in H₂O at a ratio between 1:41 and 1:101 to yield concentrations in the range of the standard curve. Then, 5 µl of standards and diluted samples were mixed with 250 µl 1x Bradford reagent (BioRad) in a 96-well plate and incubated for 5 min at room temperature. The absorption was measured at 595 nm in a microplate reader (Synergy Mx, BioTek), and sample concentrations were intrapolated from the standard curve.

5.2.3 SDS-PAGE

For Western blot analysis, whole cell protein lysates were separated by denaturing and reducing SDS polyacrylamide gel electrophoresis using 6-15% SDS polyacrylamide gradient gels.

Separation gel solutions containing 6% and 15% acrylamide, respectively, were prepared by premixing separation gel buffer (pH 8.8), aqua dest., and acrylamide/bisacrylamide stock solution (see Table 11). Polymerization was initiated by subsequent addition of TEMED and ammonium peroxodisulfate (APS). Both gel solutions were rapidly transferred into a linear gradient mixer and casted into the gel apparatus. The separation gel was covered with isopropanol and allowed to polymerize for 1 h. Subsequently, isopropanol was removed, and the stacking gel solution was prepared by premixing stacking gel buffer (pH 6.8), aqua dest., and acrylamide/bisacrylamide stock solution (see Table 11). After addition of TEMED and APS the stacking gel was casted, and a comb was inserted to create the sample slots. The polymerized gel was mounted into the SDS-PAGE apparatus, and the electrode buffer reservoirs were filled with running buffer. Depending on the investigated target proteins, 10-200 µg of whole cell protein per lane were mixed with $\frac{1}{9}$ vol 10x Laemmli buffer and heated to 95°C for 5 min. The samples were loaded into the gel pockets with a Hamilton syringe, and electrophoresis was performed for 16 h at 40 Volt until the bromophenol blue front had reached the lower edge of the gel.

Table 11. Reagents used for Western blotting experiments

| Reagent | Composition |
|---|--|
| Acrylamide/bisacrylamide stock solution (37.5 :1) | 30% Acrylamide 0.8% Bisacrylamide in aqua dest. |
| Ammonium peroxodisulfate (APS) | 10% (w/v) APS in aqua dest. |
| Laemmli buffer (10x) | 625 mM Tris-HCl pH 6.8 62.5% (v/v) Glycerol 20% (w/v) SDS 0.1% (w/v) Bromophenol blue 10% (v/v) 2-Mercaptoethanol in aqua dest. |
| SDS-PAGE running buffer (10x) | 250 mM Tris, 1.9 M Glycine 1% SDS in aqua dest. |
| Separation gel | 6-15% (w/v) Acrylamide/Bisacrylamide 390 mM Tris-HCl pH 8.8 0.1% (w/v) SDS 0.05% (w/v) APS |
| Separation gel buffer | 1.5 M Tris-HCl pH 8.8 0.384% SDS in aqua dest. |
| Stacking gel | 5% (w/v) Acrylamide/Bisacrylamide 135 mM Tris-HCl pH 6.8 0.1% (w/v) SDS 0.1% (w/v) APS |
| Stacking gel buffer | 1.0 M Tris-HCl pH 6.8 0.74% SDS in aqua dest. |
| Transfer buffer | 40 mM Glycine 44 mM Tris in 20% MeOH |
| Western blot blocking buffer | 5% Milk powder 0.02% Triton X-100 in 1x TBS |

| Reagent | Composition |
|-----------------------------------|---|
| Western blot lysis buffer | 50 mM Tris pH 7.6 150 mM NaCl 1% Triton X-100 in aqua dest. Supplemented with protease and phosphatase inhibitors directly before use: 3 µg/ml Aprotinin 3 µg/ml Leupeptin 3 µg/ml Pepstatin 2 mM PMSF Phosphatase inhibitor cocktail tablet PhosSTOP (Roche) |
| Western blot washing buffer (10x) | 130 mM Tris pH 7.5 1.5 M NaCl 0.2% Triton X-100 in aqua dest. |

5.2.4 Western blotting and immunodetection

After electrophoresis, proteins were transferred onto a PVDF membrane, which had been activated with 100% methanol for 1 min and equilibrated in transfer buffer. Electrophoretic transfer was performed for 2 h at 0.5 Ampere at 4°C in transfer buffer (Table 11). Membranes were briefly washed in Western blot washing buffer and blocked in 5% skim milk at room temperature for 1 h. Incubation with the primary antibody solutions (diluted in Western blot washing buffer according to Table 3) was performed at 4°C overnight on a shaking device. After washing with Western blot washing buffer (3x 5 min), blots were incubated with IRDye[®]-conjugated secondary antibody solutions (diluted 1:20000 in Western blot blocking buffer, see Table 4) at room temperature for 1 h, washed again with Western blot washing buffer (2x 5 min, 2x 10 min, and 2x 15 min), and dried between Whatman[®] papers. The detection of IRDye[®] fluorescence signals was performed with an Odyssey[®] CLx infrared imaging system (LI-COR Biosciences).

5.2.5 Caspase activity assay

Caspase activity was examined in an enzymatic assay with whole cell protein lysates and fluorogenic peptides. The assay employs Ac-DEVD-AMC, a synthetic tetrapeptide substrate with a consensus sequence that is derived from the poly(ADP-ribose) polymerase cleavage site motif DEVD (Asp-Glu-Val-Asp) and labeled with AMC (7-amino-4-methylcoumarin). Hence, it is preferentially cleaved by the effector caspases -3 and -7.

The release of fluorescent AMC can subsequently be used to quantify the effector caspase activity in apoptotic cells.

Briefly, whole cell protein lysates of stimulated cells were prepared as described for Western blotting (see section 5.2.1) and protein concentrations were determined (see section 5.2.2). 20 µg of total protein were diluted in 100 µl caspase lysis buffer and mixed with equal volume of preheated (37°C) 2x DEVDase reaction buffer completed with Ac-DEVD-AMC peptide (Bachem) and dithiothreitol (DTT) directly before the reaction. AMC-fluorescence was kinetically measured in a microplate reader (Synergy Mx, BioTek, Excitation 360/9 nm, Emmission 460/9 nm) every minute for 1 h at 37°C. Relative caspase activity was calculated from the slope of the linear range of the resulting curves.

Table 12. Buffers used for caspase activity assays

| Reagent | Composition |
|-------------------------------|---|
| DEVDase reaction buffer (10x) | 375 mM HEPES-Na pH 7.4 750 mM NaCl 75% Sucrose 0.75% CHAPS in aqua dest. 10x DEVDase reaction buffer was used to prepare 2x DEVDase reaction mix, which was completed with 20 mM dithiothreitol (DTT) and 100 µM AMC-conjugated peptide directly before reaction |
| Caspase lysis buffer | 20 mM HEPES-K pH 7.4 84 mM KCl 10 mM MgCl ₂ 0.2 mM EDTA 0.2 mM EGTA 0.5% NP40 |

5.3 Molecular biological methods

5.3.1 RNA extraction

Total RNA was isolated by using the NucleoSpin[®] RNA II kit (Macherey-Nagel) according to the manufacturer's protocol. Briefly, 1x10⁶ cells were lysed in a chaotropic buffer, genomic DNA was sheared, isopropanol was added to adjust the binding conditions, and RNA was bound to the silica membrane. Afterwards, the membrane was desalted and contaminating DNA was subjected to DNase digestion. The membrane was extensively washed, and finally RNA was eluted under low ionic strength conditions.

5.3.2 Quantitation of RNA

Total RNA was quantified using a NanoDrop spectrophotometer (NanoDrop 2000c, Thermo Scientific). The absorption at 260 nm was measured in order to calculate the RNA concentration according to the Lambert-Beer law, assuming that the extinction of 1 corresponds to a pure solution of single-stranded RNA with a concentration of 40 µg/ml. To check for contaminations, the absorption at 280 nm was determined, and the ratio of A260/A280 was calculated. For highly pure solutions of nucleic acids the ratio should be in the range between 1.7 and 2.0. Potential contaminations resulting from the extraction procedure would increase the absorption at 280 nm, thus reducing the A260/A280 ratio. RNA was subsequently reversely transcribed into cDNA or frozen at -80°C for long-term storage.

5.3.3 Reverse transcription

1 µg of the isolated RNA was reversely transcribed with 200 u Superscript RevertAid H⁻ reverse transcriptase in the presence of 50 µM random hexamers, 50 µM Oligo dT, 400 µM dNTPs, and 1 u/µl Ribolock RNase inhibitor (all from Thermo Scientific) in a final volume of 20 µl. Mixtures for RNA denaturation and reverse transcription were prepared on ice as follows:

Table 13. Reaction mix for RNA denaturation

| | |
|--|------|
| Random hexamers (Thermo Scientific) | 1 µl |
| Oligo(dT) ₁₈ (Thermo Scientific) | 1 µl |
| dNTP mix, 100 µM (Thermo Scientific) | 1 µl |
| Template RNA (0.5-1.0 µg) diluted in nuclease-free water | 9 µl |

After RNA denaturation at 65°C for 15 min, samples were chilled on ice, and the enzyme containing mixture was added:

Table 14. Reaction mix for reverse transcription

| | |
|---|--------------|
| Nuclease-free water | 2.5 µl |
| 5x Reaction buffer (supplied with reverse transcriptase) | 4 µl |
| RiboLock RNase inhibitor (Thermo Scientific) | 0.5 µl |
| RevertAid H ⁻ reverse transcriptase (200 u/µl) (Thermo Scientific) | 1 µl |
| Total volume | 20 µl |

For reverse transcription samples were incubated for 10 min at 25°C followed by 60 min at 42°C. The reaction was terminated by heating at 70°C for 10 min. Synthesized cDNA was directly used for PCR or stored at -20°C.

5.3.4 Quantitative real-time PCR

In order to analyze the mRNA levels of different genes of interest, quantitative real-time PCR (qPCR) was performed with a LightCycler 480 II platform (Roche) using Maxima SYBR Green I mastermix (Thermo Scientific). Exon-exon boundary spanning, target-specific primers were designed for HSP70, HSP90, the integrins alpha V, beta 3, and beta 5, as well as the matrix metalloproteinases -2, -8, and -9 utilizing Primer Express 2.0.0 software (Invitrogen) and purchased from Sigma-Aldrich (see Table 5). 18S rRNA served as reference for normalization.

5-20 ng of cDNA were subjected to qPCR analyses with 300 nM primers and Maxima SYBR Green mastermix in a final volume of 20 µl (for composition see Table 15, for PCR protocol see Table 16), and for every target gene a relative standard curve of 6 log steps (1:10) was generated. Relative mRNA copy numbers were intrapolated from the respective standard curve and normalized on the values obtained for 18S rRNA. Finally, relative expression values were obtained by calibrating on the untreated control cell population. The following formula summarized the process of relative quantification:

$$\text{Relative expression ratio} \left(\frac{\text{Sample}}{\text{Calibrator}} \right) = \frac{\text{Relative copy number}_{\text{Target gene}} (\text{Sample}) \times \text{Relative copy number}_{\text{Reference gene}} (\text{Calibrator})}{\text{Relative copy number}_{\text{Reference gene}} (\text{Sample}) \times \text{Relative copy number}_{\text{Target gene}} (\text{Calibrator})}$$

Table 15. Reaction mix for quantitative real-time PCR

| | |
|--|--------------|
| 2x Maxima SYBR Green/ROX qPCR Master Mix (Thermo Scientific) | 10 µl |
| Forward primer (0.5-2 µM) | 3 µl |
| Reverse primer (0.5-2 µM) | 3 µl |
| Template cDNA (2.5-10 ng/µl) diluted in nuclease-free water | 2 µl |
| Nuclease-free water | 2 µl |
| Total volume | 20 µl |

Table 16. Program used for qPCR performed on a LightCycler 480 II

| Step | | Temperature [°C] | Time [min:s] | Number of cycles |
|--------------------------------------|--------------|------------------|--------------|------------------|
| Preincubation / Initial denaturation | | 95 | 10:00 | 1 |
| Amplification | Denaturation | 95 | 00:10 | 45 |
| | Annealing | 60 | 00:10 | |
| | Elongation | 72 | 00:10 | |
| Melting Curve | Denaturation | 95 | 00:05 | 1 |
| | Annealing | 65 | 01:00 | |
| | Melting | 97 | | |
| Cooling | | 40 | 00:30 | 1 |

5.4 *In vivo* experiments

In order to investigate the antitumor potency of the novel HSP90 inhibitor NW457 as radiosensitizing therapeutic *in vivo*, a syngenic heterotopic tumor mouse model was used. The experiments were conducted at the Department of Radiation Oncology of the University Hospital Erlangen with kind support of Udo Gaipl and Benjamin Frey.

Throughout these studies, all mice were provided a special diet and water *ad libitum* and were kept individually in well-ventilated cages under standard conditions of humidity ($55 \pm 5\%$), temperature ($22 \pm 2^\circ\text{C}$), and light (12/12 hr light-dark cycles). The animal studies were conducted according to the guidelines of the Federation of European Laboratory Animal Science Associations (FELASA) and the Society of Laboratory Animals (GV-SOLAS).

5.4.1 Tumor implantation

Murine CT26 colon carcinoma cells were routinely cultivated as described above (see section 5.1.1.1). Prior to injection, cells were trypsinized, washed with Ringer's solution (B. Braun), and adjusted to $4.9 \times 10^6/\text{ml}$ in Ringer's solution. Subsequently, 1.28×10^6 CT26 cells were injected into the right flank of 8-week old female Balb/c mice (Janvier Labs) anesthetized with isoflurane (Abbott). Tumors were grown for 9 days consistent with an average tumor volume of approximately 200 mm^3 and the tumor bearing mice were randomized into four experimental groups (NW457 only, vehicle only, 2x 5 Gy + 4x NW457, 2x 5 Gy + 4x vehicle).

5.4.2 *In vivo* drug administration, irradiation, and measurement of tumor volumes

For *in vivo* studies NW457 was dissolved in DMSO as 100 mg/ml stock solution and stored at -20°C. Prior to injection, the stock solution was diluted with a half volume of Tween 20 followed by 8.5 volume of 0.9% NaCl (37°C) to reach a final concentration of 10 mg/ml (10/5/85 DMSO/Tween 20/saline). The vehicle control (DMSO) was prepared in the same way. A fresh preparation was used for each dosing. 100 mg/kg NW457 or vehicle control, respectively, were injected intraperitoneally in a volume of 500 µl on days 9, 12, 18, and 24. Similar to the patient's situation, irradiation was based on computed tomography planning in order to ensure precise and selective irradiation of the tumor tissue and protection of the surrounding normal tissue. Anesthetized mice (inhalation anesthesia with isoflurane) were positioned in a Plexiglas® box and irradiation was carried out on days 10 and 13 using a 6 MV linear accelerator (ONCOR, Siemens) with a total dose of 5 Gy. Tumor dimensions were measured every 2-3 days with an electronic digital caliper, and volumes were calculated using the formula (width x width x length)/2 (Euhus et al., 1986). The tumor growth was monitored to a maximum volume of 1,700 mm³ according to the guidelines of the Federation of European Laboratory Animal Science Associations (FELASA) and the Society of Laboratory Animals (GV-SOLAS).

5.5 Statistical methods

5.5.1 Statistics

Unless otherwise stated, data are presented as means ± SD for *in vitro* and means ± SEM for *in vivo* experiments. Mean values were compared by Student's t-test. The threshold of statistical significance was set at p<0.05.

5.5.2 Combination index

In order to evaluate whether the combined application of irradiation and NW457 treatment results in antagonistic, additive or synergistic effects, the median-drug effect analysis method according to Chou-Talalay (Chou and Talalay, 1981, 1984) was used. This method calculates for each dose pair of irradiation and NW457 treatment a specific combination index (CI), which determines the degree of interaction between the analyzed therapy components, indicating either additivity (CI =1), synergism (CI <1), or antagonism (CI >1). The calculation was kindly carried out by Maximilian Niyazi (Department of Radiation Oncology, LMU Munich) based on the data obtained from FACS analyses of propidium iodide stained hypodiploid nuclei (see sections 6.1.3 and 6.2.1 of the results).

6 Results

6.1 Targeting HSP90 with the novel small-molecule inhibitor NW457 sensitizes colorectal cancer cells to ionizing radiation

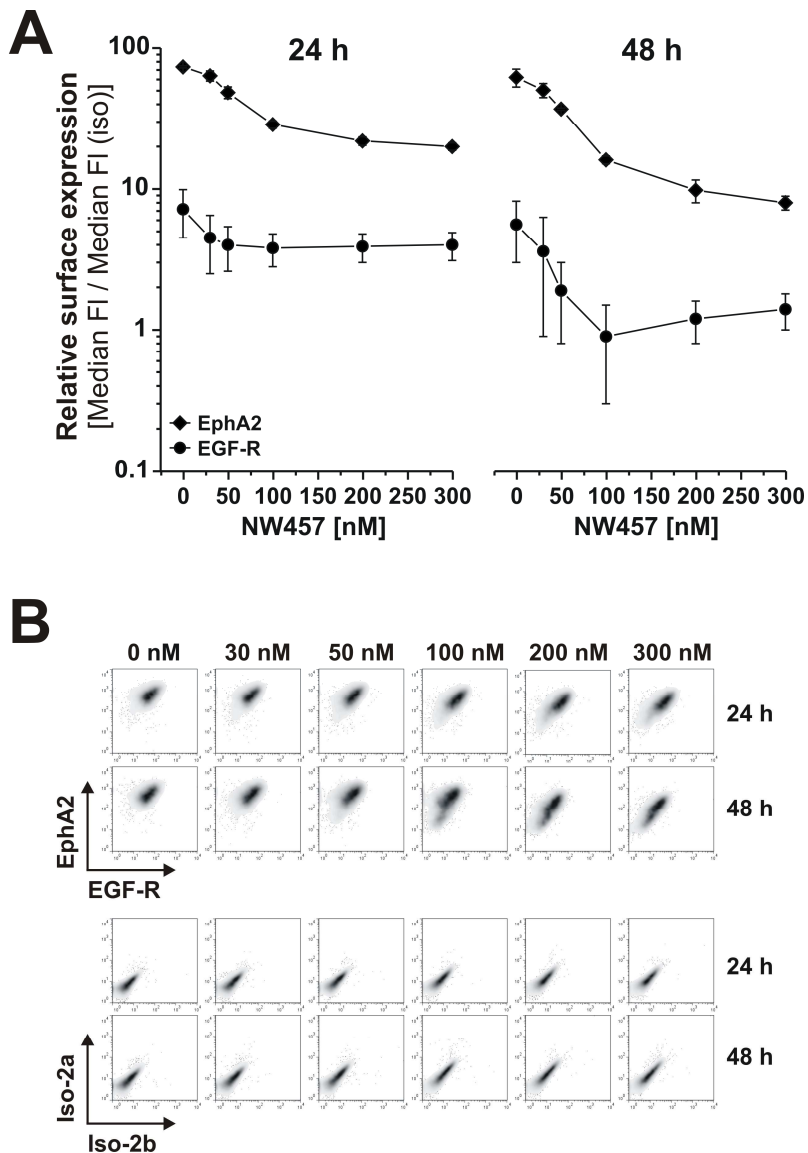
In the first part of this thesis, the impact of the novel pharmacological HSP90 inhibitor NW457 (6-hydroxy-pochoxime C) on tumor cell radiosensitization was investigated in colorectal cancer models with specific regard to the mechanisms of cell death induction and the relevance of the KRAS, p53, and BAX status. In addition, the tolerability of NW457 by primary hepatocytes and its antitumor activity in combination with radiotherapy *in vivo* were analyzed.

6.1.1 Inhibition of HSP90 by NW457 induces the degradation of HSP90 client proteins and mediates the upregulation of HSP70 expression, cell surface exposure, and release

Pharmacological inhibition of HSP90 involves impaired ATPase activity and abrogated chaperone function (Prodromou et al., 1997; Stebbins et al., 1997), which in the cellular context leads to the proteasomal degradation of HSP90 client proteins (Connell et al., 2001; Matts and Manjarrez, 2009). To provide a proof that NW457 acts as a potent inhibitor of HSP90 in tumor cells, the degradation of BRAF, Ephrin receptor A2 (EphA2) and EGF-R, three known client proteins of HSP90 (Ahsan et al., 2012; Annamalai et al., 2009; Chen et al., 2012; Da Rocha Dias et al., 2005; Fukuyo et al., 2008; Gopal et al., 2011; Lavictoire et al., 2003), was monitored. Human HCT116 colorectal cancer cells were treated with 0-300 nM NW457 for 24 h or 48 h, respectively, and the expression levels of EphA2 and EGF-R were measured by FACS surface staining, whereas BRAF protein levels were assessed by Western blot analyses of whole cell lysates (Figure 6A, B, C). Incubation with NW457 clearly induced a dose- and time-dependent decrease in EphA2, EGF-R and BRAF protein levels, thus strongly supporting its function as a potent HSP90 inhibitor. Apart from client protein degradation, upregulation of HSP90 and other heat shock proteins, for instance HSP70, has been described as a central feature of HSP90 inhibition (Jensen et al., 2008; Lundgren et al., 2009; Schilling et al., 2012; Stingl et al., 2010). Therefore, it was next examined, whether this upregulation could also be observed in case of NW457. Quantitative real-time PCR analyses revealed a profound induction of HSP90 and HSP70 mRNA 12 h after NW457 treatment, which was followed by an increase in HSP90 and HSP70 protein levels after 48 h (Figure 6C, D). In case of HSP70, this upregulation was also translated into cell surface exposure and release into culture supernatants as determined by FACS surface staining and ELISA measurements

(Figure 6E, F). Anti-HSP70 FACS surface staining and HSP70 ELISA experiments were performed in cooperation with Daniela Schilling (Department of Radiation Oncology, TU Munich).

These results show convincingly that the key features of HSP90 inhibition, including degradation of prototypical client proteins, upregulation of HSP90 and HSP70 expression, as well as HSP70 externalization and release, which have been described for substances of the first and second generation of HSP90 inhibitors (Annamalai et al., 2009; Da Rocha Dias et al., 2005; Jensen et al., 2008; Schilling et al., 2012; Stingl et al., 2010), can be observed after treatment with NW457. It hence can be concluded that NW457 is a potent HSP90 inhibitor that operates in the nanomolar range. Its antitumor effects alone and in combination with ionizing irradiation will be characterized in the following.



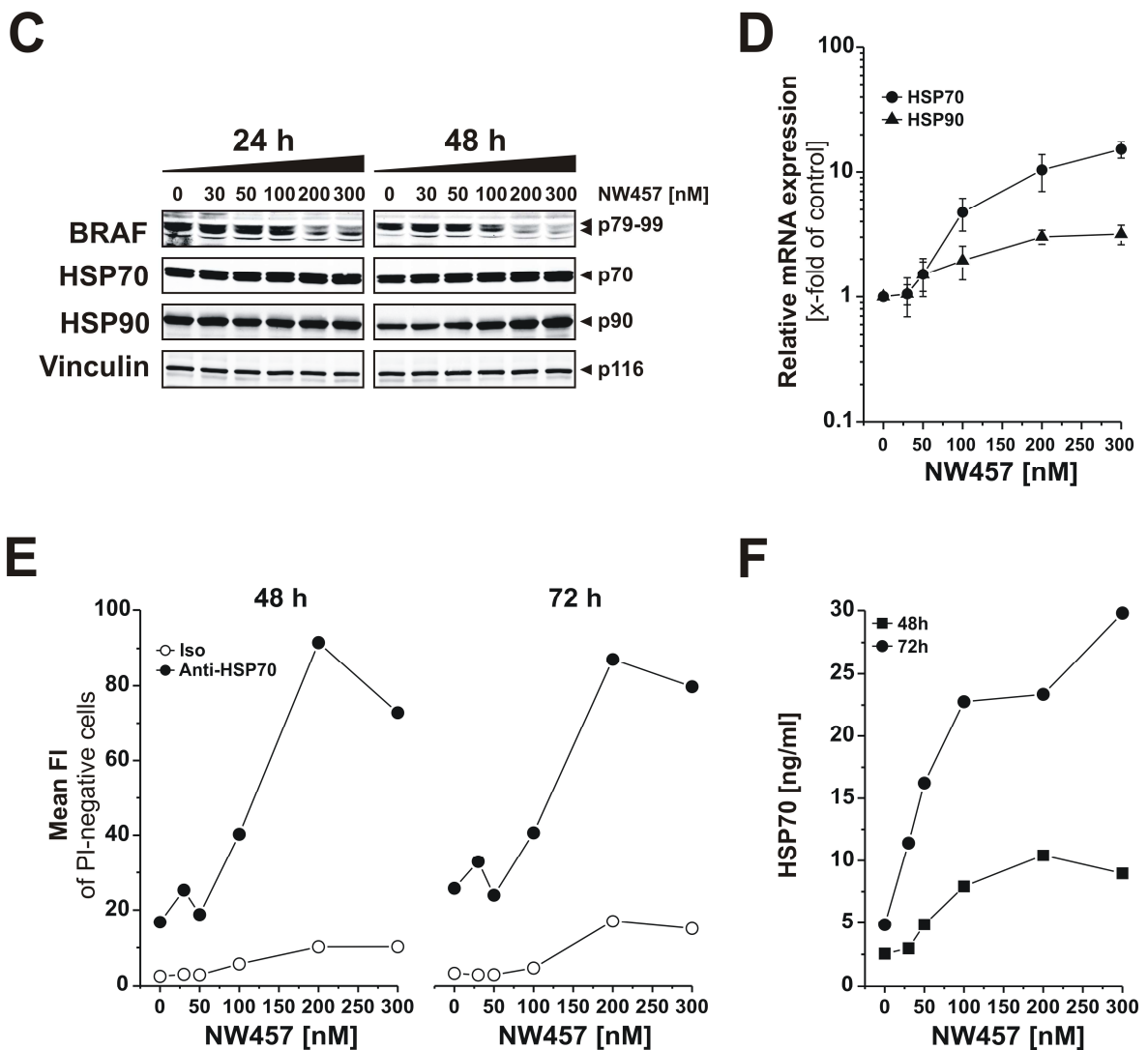


Figure 6. HSP90 inhibition by NW457 treatment of colorectal cancer cells as measured by client protein degradation, upregulation of HSP90 and HSP70 expression, HSP70 cell surface exposure, and HSP70 release.

Human HCT116 colorectal cancer cells were treated with 0-300nM NW457 for the indicated times and subjected to different types of analyses. **(A)** EphA2 and EGF receptor (EGF-R) surface expression was measured 24 h and 48 h after stimulation with NW457 by flow cytometric analysis and is shown as median fluorescence intensity normalized on the median fluorescence of the respective isotype control. Data are means \pm standard deviation (SD) of three independent experiments. **(B)** Representative dot plots of (A) and appropriate isotype controls. **(C)** Protein levels of BRAF, HSP70, and HSP90 were analyzed by Western blot analysis of whole cell lysates (70 μ g protein per lane) 24 h and 48 h after stimulation with NW457. Vinculin served as loading control. Blots of one representative experiment are shown. **(D)** NW457-dependent induction of HSP70 and HSP90 mRNA expression was measured by quantitative real-time PCR 12 h after stimulation. Transcription is depicted as relative expression normalized on 18S mRNA and calibrated on the vehicle control. Data are means \pm SD of three independent experiments. **(E)** Exposure of HSP70 on the cell surface was determined by anti-HSP70 FACS surface staining 48 h and 72 h after treatment with NW457. Mean fluorescence intensity (FI) values of propidium iodide-negative (PI-negative) cells are shown of one experiment performed in duplicates that displayed similar values. This experiment was performed in cooperation with Daniela Schilling (Department of Radiation Oncology, TU Munich). **(F)** NW457-dependent release of HSP70 was quantified by ELISA analysis of HCT116 cell supernatants 48 h and 72 h after stimulation. Data represent means of intra-assay

duplicates of one experiment that displayed similar values. This experiment was performed in cooperation with Daniela Schilling (Department of Radiation Oncology, TU Munich).

6.1.2 NW457 induces apoptosis and sensitizes colorectal cancer cells to ionizing radiation

A number of HSP90 client proteins, such as ERBB2 (HER-2), AKT, BRAF, and EGF-R, have been identified as key players of the cellular response to ionizing radiation in tumor cells (Bull et al., 2004; Machida et al., 2003). Consequently, pharmacological inhibitors of HSP90 were assumed to interfere with the radioresponse via the depletion of proteins associated with relevant pathways. Indeed, various HSP90 inhibitors were demonstrated to induce apoptosis and mediate radiosensitization of cancer cells (Bisht et al., 2003; Bull et al., 2004; Ju et al., 2011; Machida et al., 2005; Russell et al., 2003; Wang et al., 2011). Therefore, both apoptosis-inducing and radiosensitizing effects of the novel HSP90 inhibitor NW457 were characterized in the following – in a first attempt using Hoechst 33342 DNA staining and fluorescence microscopic evaluation. For this purpose, HCT116 cells were treated with NW457 or DMSO as vehicle control for 24 h, irradiated with 5 Gy, and apoptotic nuclei were quantified 24-72 h after irradiation. After treatment with NW457 alone, typical apoptosis-associated morphological changes, including chromatin condensation and nuclear fragmentation, were observed in a time-dependent manner (Figure 7A). Similar results were obtained for irradiation with 5 Gy alone. Notably, the combination of NW457 treatment and irradiation clearly potentiated apoptosis induction and strongly inhibited cell proliferation. Typical apoptosis-associated nuclear phenotypes of early and late apoptotic phases are depicted with higher magnification in Figure 7B. Quantification of the microscopic data revealed a time-dependent, significant enhancement of apoptosis induction upon combined NW457 plus irradiation treatment versus irradiation or NW457 incubation alone (Figure 7C, * $p < 0.01$ for all time points analyzed). In order to compare the potency of NW457 with a first generation HSP90 inhibitor, HCT116 nuclei were alternatively analyzed after stimulation with geldanamycin (GA) in the presence or absence of irradiation. As depicted in Figure 7D, NW457 showed similar potency in apoptosis induction and radiosensitization of HCT116 cells as geldanamycin (GA).

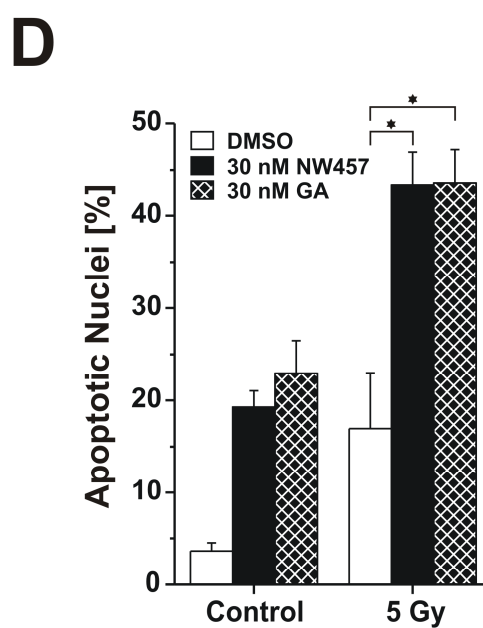
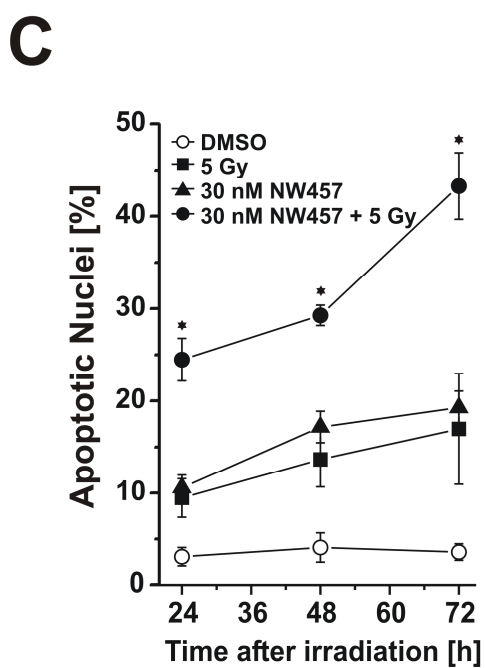
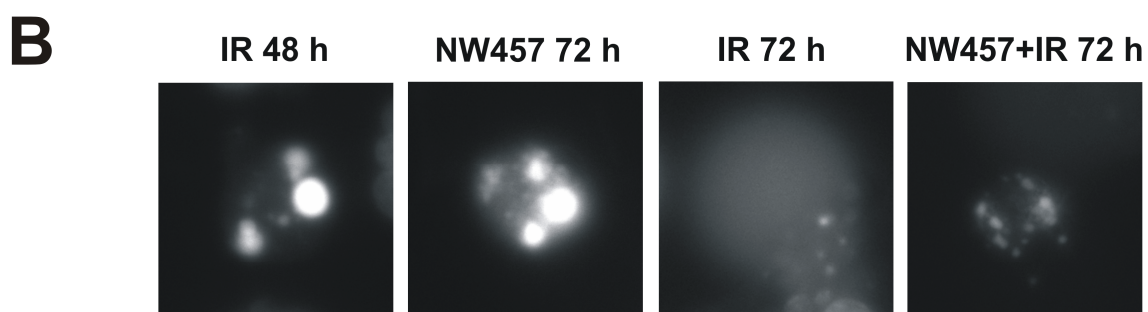
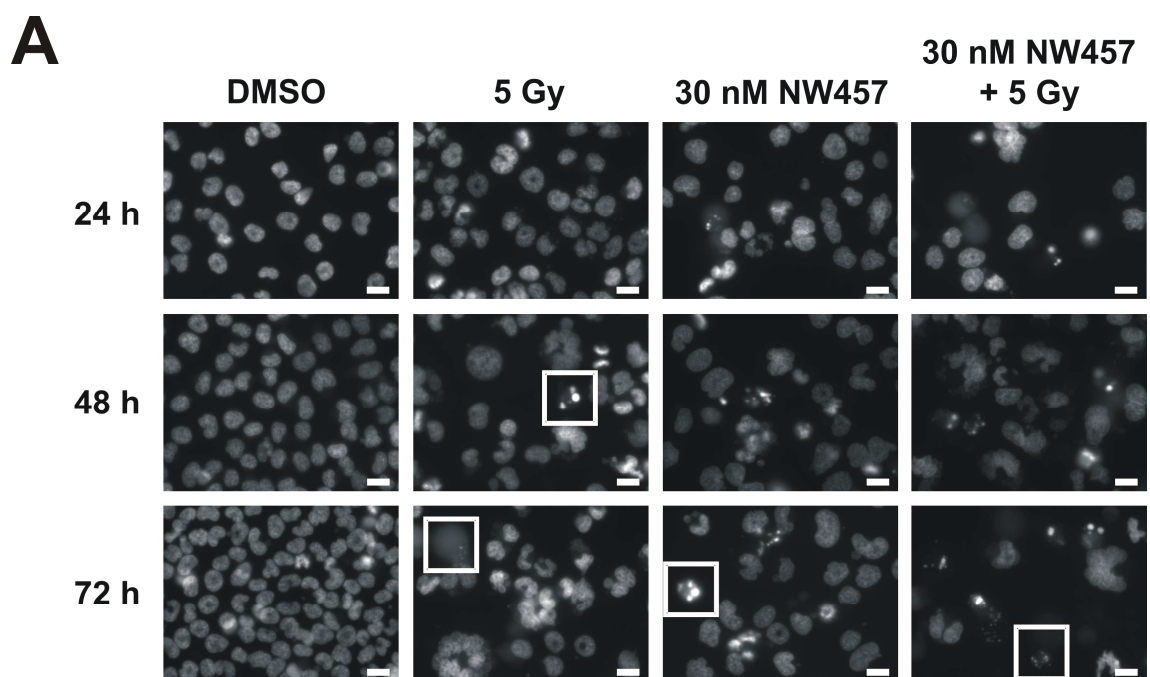


Figure 7. NW457 induces apoptosis and sensitizes colorectal cancer cells to ionizing radiation.

HCT116 cells were treated with 30 nM NW457 or DMSO as vehicle control for 24 h, irradiated with 5 Gy, and subjected to Hoechst 33342 staining after 24-72 h. **(A)** Representative photographs reveal chromatin condensation and nuclear fragmentation as typical apoptosis-associated phenotypes in response to NW457 treatment and irradiation. Scale bars indicate 20 μ m. **(B)** Typical apoptosis-associated changes of the nuclear morphology in early and late apoptotic phases are magnified from photographs in (A). **(C)** Time course analysis of NW457-mediated radiosensitization 24, 48, and 72 h post irradiation. Values represent means \pm SD of three independent experiments. * p <0.01 for combined treatment vs. IR or NW457 only. **(D)** The percentage of cells with apoptotic nuclear phenotype in response to IR, 30 nM NW457 or geldanamycin (GA) treatment was quantified 72 h after irradiation. Values represent means \pm SD of three independent experiments. * p <0.01.

In addition to apoptotic structures, morphological characteristics of mitotic catastrophe, a form of cell death that results from aberrant mitosis, were detected in the form of giant, multi-lobed nuclei and micronuclei in response to irradiation and NW457 treatment (Figure 7A, see pictures of combined treatment).

In summary, these data demonstrate an anti-proliferative and pro-apoptotic effectiveness of the novel HSP90 inhibitor NW457 in HCT116 colorectal cancer cells, which considerably enhances the antitumor effects of ionizing irradiation.

6.1.3 Interaction of NW457 stimulation and ionizing radiation occurs in a synergistic mode

In parallel to microscopic evaluation, the extent of NW457-mediated apoptosis was examined by flow cytometric analysis of propidium iodide (PI) stained nuclei. Here, apoptotic nuclei are identified due to their hypodiploid (subG1) DNA content. HCT116 cells were treated with 0-300 nM NW457 for 24 h, irradiated with 0-5 Gy, and 48 h after irradiation the nuclear DNA content was assessed by hypotonic PI staining and FACS analysis. Figure 8A shows representative nuclear DNA profiles of HCT116 cells treated with 100 nM NW457 or DMSO (vehicle control) +/- irradiation with 5 Gy, and Figure 8B depicts the percentage of hypodiploid nuclei for all combinations tested. Whereas irradiation alone only marginally stimulated the appearance of hypodiploid nuclei, exposure to NW457 resulted in a strong and concentration dependent increase, attaining a maximum at concentrations >100nM (Figure 8B). However, this effect was further elevated when the cells were additionally irradiated - a finding, which again emphasizes the radiosensitizing potency of NW457.

In order to assess the quality of interaction (synergism, additivity, antagonism) between NW457 treatment and ionizing radiation, combination indices (CI) were calculated according to Chou-Talalay (Chou and Talalay, 1981, 1984) for all applied combinatory treatments (Figure 8C).

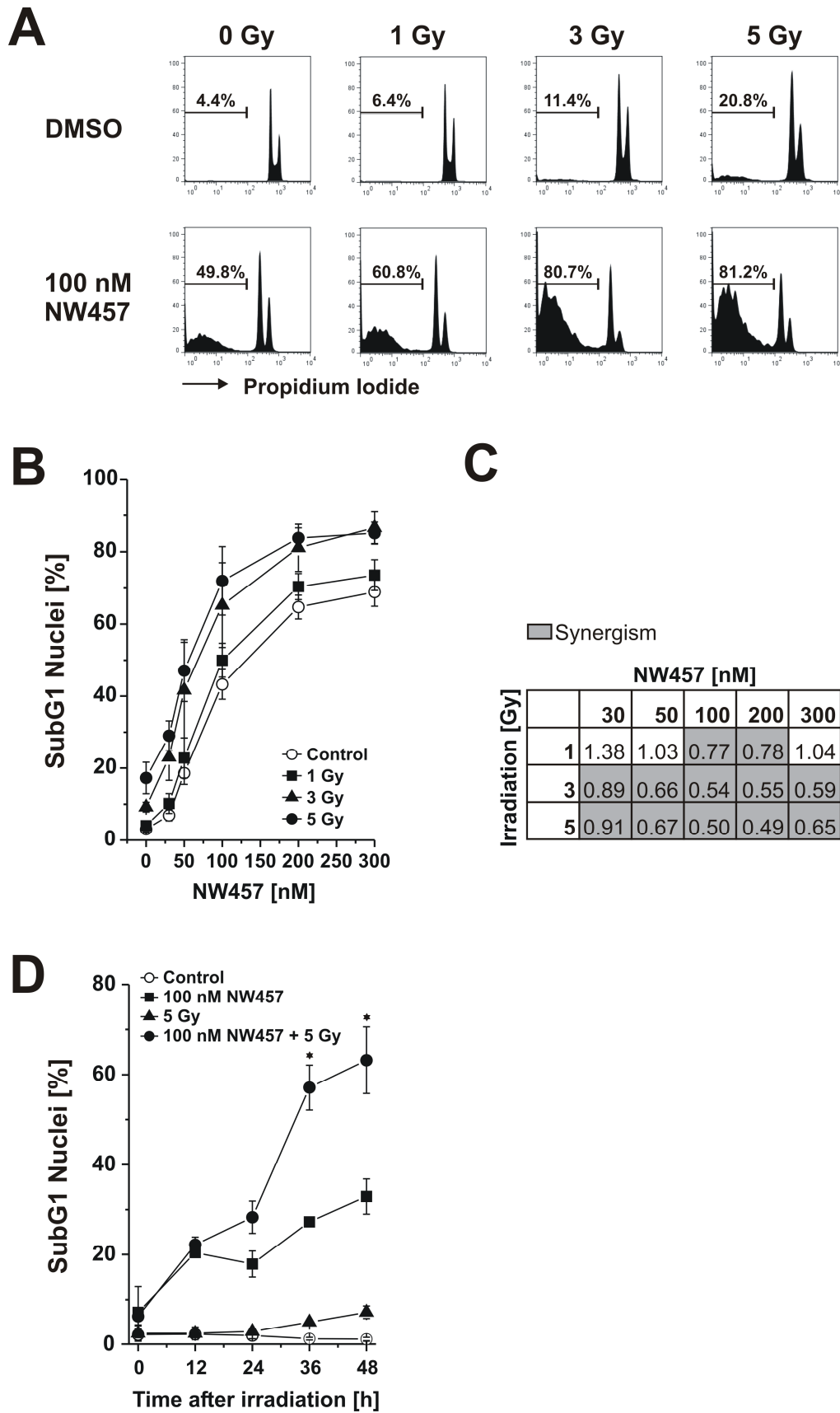


Figure 8. Exposure to NW457 time- and dose-dependently induces the formation of hypodiploid nuclei and shows a synergistic interaction with ionizing radiation. HCT116 cells were treated with 0-300 nM NW457 or DMSO as vehicle control for 24 h, irradiated with 0-5 Gy, and subjected to hypotonic propidium iodide staining for

subsequent FACS analysis of hypodiploid (subG1) nuclei. **(A)** Representative profiles of the nuclear DNA content 48 h after irradiation. Numbers indicate the percentage of hypodiploid nuclei. **(B)** Dose-dependence of hypodiploid nuclei formation in response to treatment with NW457 measured 48 h after irradiation with 0-5 Gy. Means \pm SD of four independent experiments are shown. **(C)** Combination indices (CI) calculated from the data shown in (B). Values highlighted in grey (CI <1) demonstrate a synergistic mode of action between NW457 and irradiation. **(D)** Time course of hypodiploid nuclei formation measured 0-48 h after irradiation with 5 Gy +/- treatment with 100 nM NW457. Data are means \pm SD of three independent experiments. * p <0.01 for combined treatment vs. IR only.

Based on the data from Figure 8B it was tested whether the observed effect - apoptosis induction as measured by the percentage of subG1 nuclei - was due to an additive or synergistic interaction between NW457 and irradiation. Basically, combination indices <1 reveal a synergistic interaction of the two examined modalities, combination indices =1 represent additivity, and combination indices >1 indicate an antagonistic interaction. Interestingly, 80% of the analyzed combinations showed synergistic effects (CI <1, highlighted in grey) and these were predominantly observed for combinations comprising irradiation doses of 3 or 5 Gy, respectively. As the combined treatment with 100 or 200 nM plus 5 Gy irradiation resulted in the greatest synergistic effects (illustrated by combination indices of 0.50 and 0.49, respectively), 100 nM was selected for further investigating the kinetics of NW457-mediated radiosensitization. As shown in Figure 8D, exposure to 100 nM NW457 time-dependently increased the percentage of hypodiploid nuclei, and significantly enhanced irradiation-induced DNA fragmentation, when combined with 5 Gy (* p <0.01 for combination treatment vs. IR alone at 36 and 48 h post irradiation). Taken together, these data strengthen the observations from the microscopic analyses in section 6.1.2 and confirm the potent radiosensitizing capacity of NW457 on colorectal cancer cells.

6.1.4 The radiosensitizing effects of NW457 involve the activation of the caspase cascade with subsequent caspase substrate cleavage

The data presented so far have identified the pochoxime HSP90 inhibitor NW457 as a potent radiosensitizer which significantly enhances the radiosensitivity of colorectal cancer cells by inducing apoptosis. Ionizing irradiation predominantly stimulates the intrinsic apoptotic pathway, which is characterized by mitochondrial release of cytochrome c with subsequent formation of the apoptosome, a complex of cytochrome c and APAF-1 (Apoptotic protease activating factor 1) that in turn provokes the activation of the caspase cascade. Caspases are a family of aspartate-specific cysteine proteases. Upon activation, the initiator caspase-9 proteolytically activates the effector caspases -3, -6, and -7. These in turn mediate the cleavage of caspase substrates, such as the poly(ADP-

ribose)polymerase (PARP), and finally give rise to the full biochemical and morphological outcome of apoptosis (Coultas and Strasser, 2000; Rudner et al., 2001; Strasser et al., 2000). Therefore, the impact of NW457 treatment +/- irradiation on the activation of the caspase cascade and caspase substrate cleavage was analyzed in the next step. To this end, HCT116 cells were stimulated with 0-300 nM NW457 for 24 h, irradiated with 0-5 Gy, and 24 h later whole cell lysates were applied to Western blot analyses of pro-caspases -9 and -3 processing as well as cleavage of the prototypical caspase substrate PARP. As shown in Figure 9A, administration of NW457 dose-dependently stimulated the processing of pro-caspases -9 and -3 with concomitant PARP cleavage. This was further augmented by additional irradiation, most pronounced at 300 nM plus 5 Gy. To complement the proteolytic processing data, caspase activity measurements were performed using the fluorogenic peptide Ac-DEVD-AMC (N-acetyl-Asp-Glu-Val-Asp-7-amino-4-methylcoumarin), which mainly reflects the consensus cleavage motif of caspase-3. Here, a dose-dependent increase in DEVDase activity was detected (particularly in the concentration range >50 nM NW457), which was further amplified by additional irradiation (Figure 9B). Time course analyses of DEVDase activity and PARP cleavage disclosed that the onset of caspase activation occurred later than 12 h after irradiation (Figure 9C, D). Consistent with the subG1 FACS data shown in Figure 8D, DEVDase activity was significantly more pronounced in response to combined treatment than after irradiation or NW457 only approaches (Figure 9C, * $p < 0.05$ for combination treatment vs. IR or NW457 alone, respectively, 36 and 48 h post irradiation).

These data confer first mechanistic insights that the novel HSP90 inhibitor NW457 exerts its radiosensitizing potential in colorectal cancer cells by sensitizing the cells for apoptosis and caspase activation via the mitochondrial pathway.

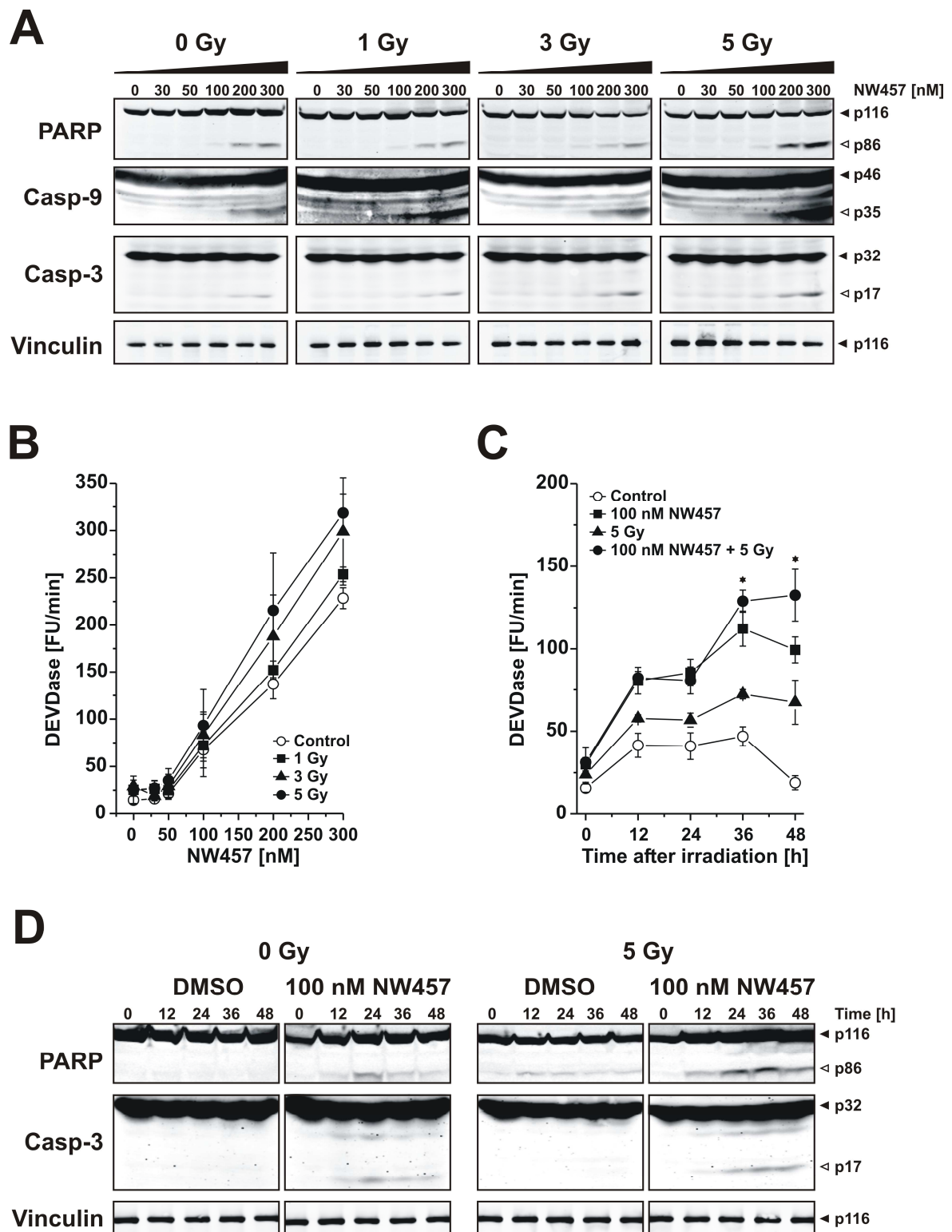


Figure 9. NW457-mediated radiosensitization of colorectal cancer cells involves the activation of caspases and caspase substrate cleavage.

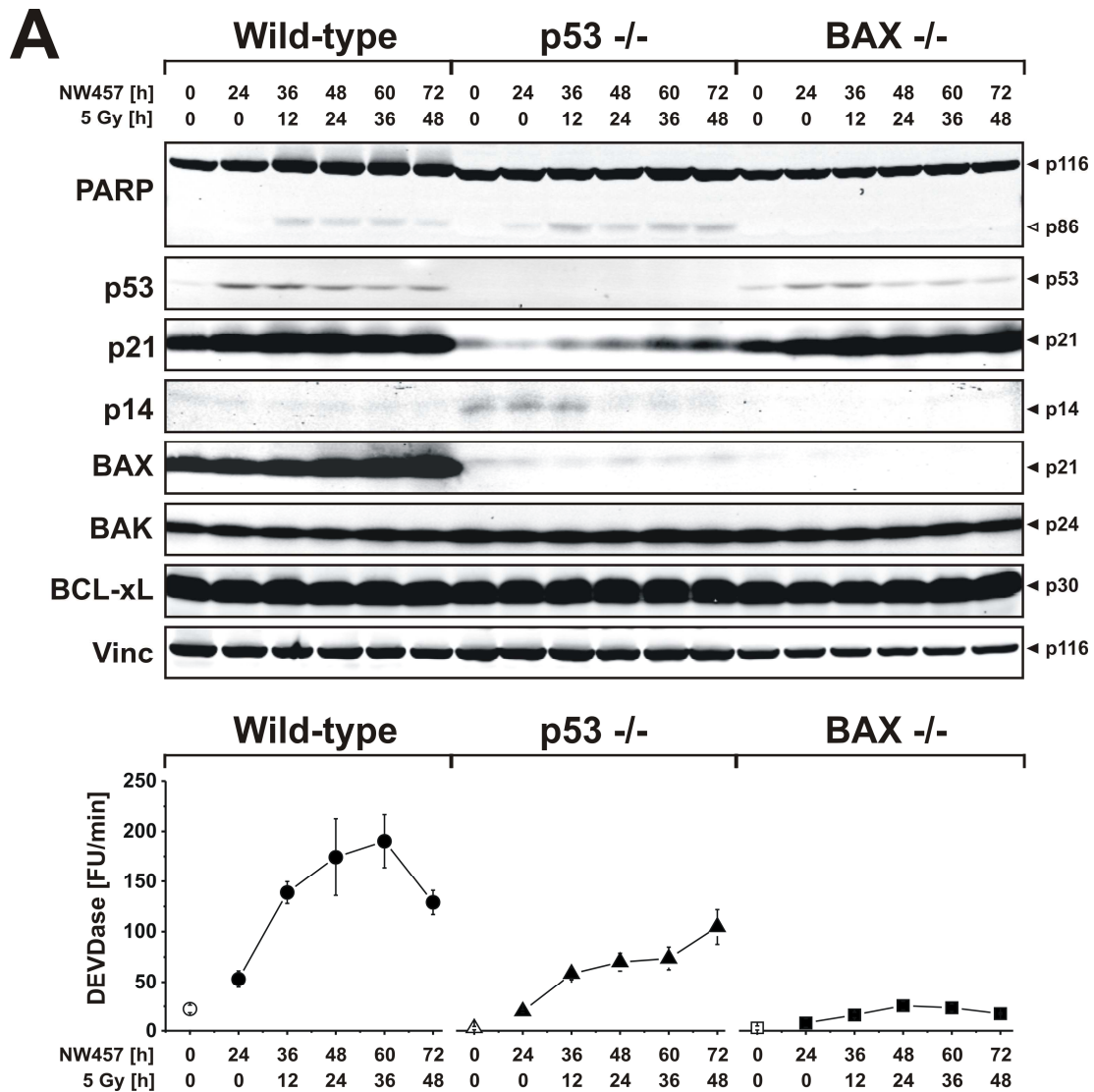
HCT116 cells were stimulated with 0-300 nM NW457 for 24 h, irradiated with 0-5 Gy, and 0-48 h after irradiation whole cell lysates were prepared and then subjected to Western blot analyses of pro-caspases -9 and -3 processing, PARP cleavage, and caspase activity tests with DEVD-AMC peptide. **(A)** Processing of pro-caspases -9, and -3, and cleavage of the caspase substrate PARP were analyzed by Western blotting 24 h after irradiation (150 μ g protein per lane). Vinculin (10 μ g per lane) was used as loading control. Filled arrowheads indicate the full length forms, open arrowheads show the cleavage products.

Each blot is representative for one of three independent experiments. **(B)** Caspase activity was measured by DEVDase assays in protein lysates obtained from cells treated as in (A). 10 µg total protein was used per sample; data are means ± SD of three independent experiments. **(C)** Time course analysis of DEVDase activity 0-48 h after irradiation with 5 Gy +/- 100 nM NW457. 10 µg total protein was used per sample. Data show means ± SD of one representative experiment performed in quadruplicates. Data of further experiments are shown in Appendix 1. * $p < 0.05$ for combined treatment vs. IR only. **(D)** Time dependence of proteolytic pro-caspase-3 processing and PARP cleavage 0-48 h after irradiation. 150 µg protein per lane was used for PARP and caspase-3 detection, 10 µg for vinculin. Filled arrowheads indicate the full length forms and open arrowheads depict the cleavage products. Each blot is representative for one of three independent experiments. Western blot experiments were performed in cooperation with Anne Ernst.

6.1.5 NW457-mediated apoptosis induction and radiosensitization do not require functional p53

Stimulation of the mitochondrial apoptosis pathway by ionizing irradiation has been shown to essentially rely on p53-mediated induction of pro-apoptotic proteins, including the pro-apoptotic BCL-2 family member BAX (Miyashita and Reed, 1995; Yin et al., 1997). To clarify whether this also applies to NW457-mediated apoptosis induction and radiosensitization, two previously described HCT116 subclones were employed which are deficient in p53 or BAX, respectively (Bunz et al., 1998; Zhang et al., 2000). The cells were incubated with 100 nM NW457 for 24 h, irradiated with 5 Gy, and 0-48 h after irradiation whole cell lysates were prepared and subjected to Western blot analyses as well as DEVDase activity tests (Figure 10A). As expected, p53-knockout cells revealed no measurable p53 expression, and irradiation-induced upregulation of p21, a prototypical downstream target of p53, was strongly attenuated. Nevertheless, PARP cleavage and DEVDase activity were clearly detected, even though to a slightly lesser extent than in wild-type cells. Interestingly, the caspase activation occurred virtually in the absence of BAX, since both the basal expression of BAX and the treatment-induced upregulation - which was observed in case of the wild-type cells - were essentially abrogated in the p53 $-/-$ cell line. In strong contrast, genetic ablation of BAX critically interfered with caspase activation in response to NW457 treatment and irradiation, since only marginal DEVDase activity and almost no PARP cleavage were detected in BAX $-/-$ cells. These data suggest that activation of the caspase cascade in response to the combined treatment with NW457 and ionizing irradiation does not require functional p53 but involves BAX-dependent mechanisms. The question that arises at this point is how caspase activation was initiated in p53 $-/-$ cells, which failed to induce BAX expression. Notably, there were no appreciable changes in the protein levels of BAK, a close relative of BAX, which is discussed to be able to compensate for the loss of BAX under certain conditions, or BCL-xL, an anti-apoptotic member of the BCL-2 family, respectively (Kepp et al., 2007; Mondal et al., 2012). However, a constitutive upregulation of the pro-apoptotic cell cycle

regulator p14 ARF was observed in p53 ^{-/-} cells that might account for caspase activation in response to NW457 treatment and irradiation. In this regard it has previously been reported that p14 ARF can mediate apoptosis in a BAX- and p53-independent manner (Hemmati et al., 2002; Hemmati et al., 2006). However, the downstream effectors which couple p14 ARF to the signaling pathways of apoptosis remain elusive and other apoptosis regulators, which have not been investigated here, might also be involved.



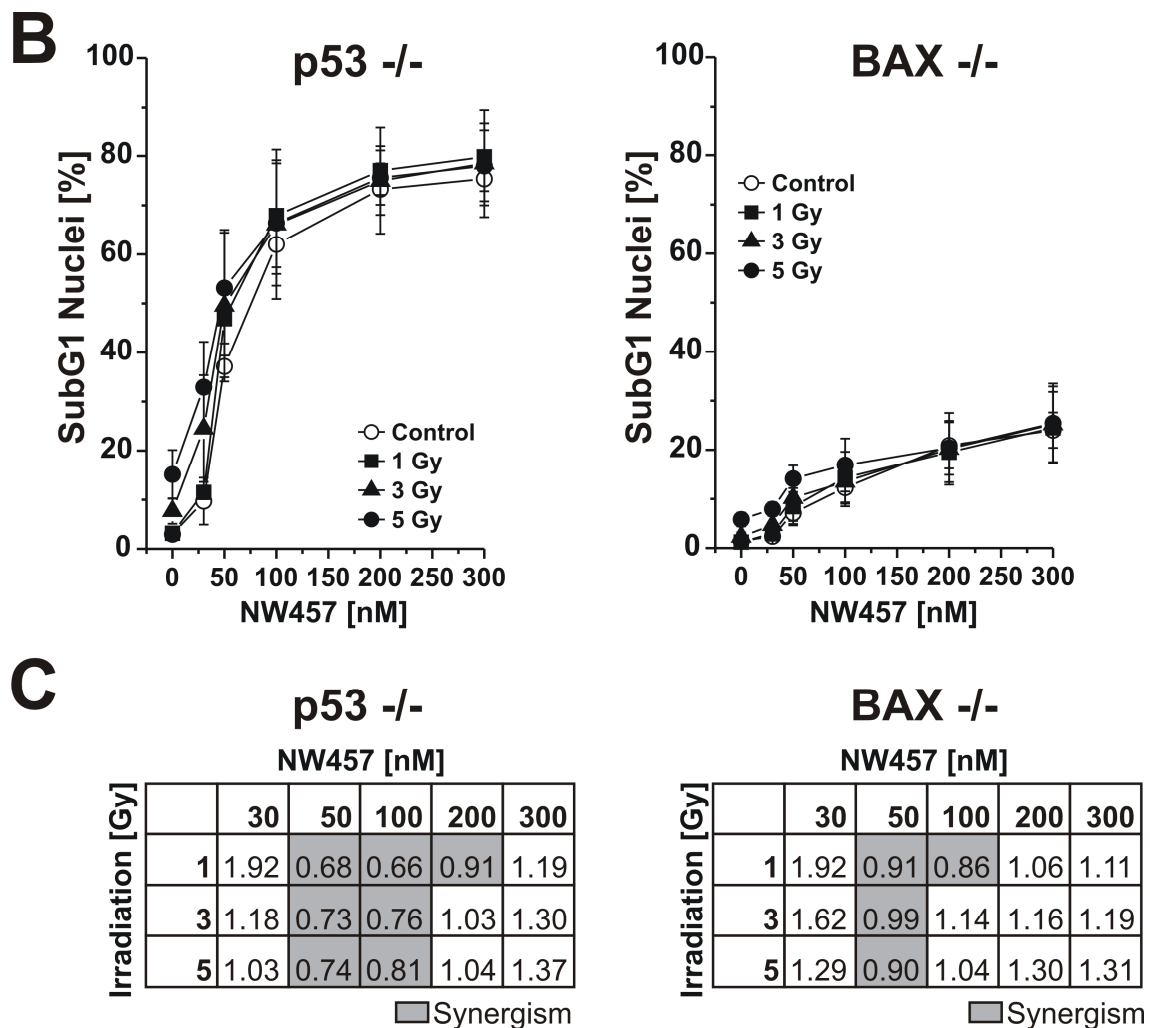


Figure 10. NW457-mediated apoptosis induction and radiosensitization do not require functional p53.

HCT116 wild-type cells and p53-deficient or BAX-deficient subclones were treated with 0-300 nM NW457 for 24 h, irradiated with 0-5 Gy, and subjected to Western blot analyses, DEVDase activity measurements, and FACS analyses of subG1 nuclei. **(A) Upper panel:** Western blot analysis of crucial signaling proteins involved in apoptosis after stimulation with 100 nM NW457 and 5 Gy 0-48 h after irradiation (150 μ g protein per lane). Vinculin was used as loading control (10 μ g protein per lane). Each blot is representative of three independent experiments. **Lower panel:** DEVDase activity measured in whole cell lysates (10 μ g protein per sample). Data are means \pm SD of three experiments. Experiments were performed in cooperation with Anne Ernst. **(B)** FACS analysis of subG1 nuclei of p53 -/- and BAX -/- cells 48 h after irradiation +/- NW457 treatment. Means \pm SD of three independent experiments are shown. See Figure 8B for comparison with HCT116 wild-type cells. **(C)** Combination indices were calculated from the data shown in (B). Values highlighted in grey demonstrate a synergistic mode of action between NW457 treatment and ionizing radiation (CI <1). See Figure 8C for comparison with HCT116 wild-type cells.

In the next step, apoptosis induction was examined in p53- and BAX-deficient HCT116 cells on the basis of subG1 nuclei formation. Cells were treated with 0-300 nM NW457 for 24 h, irradiated with 0-5 Gy, and 48 h after irradiation FACS analyses of hypodiploid nuclei were performed (Figure 10B). p53-knockout cells revealed an NW457 dose-dependent increase in the percentage of subG1 nuclei comparable to the one observed in wild-type

cells (for combinations with 3 or 5 Gy) or even slightly increased (for combinations with 0 or 1 Gy). Notably, enhancement of NW457-mediated apoptosis induction in response to additional irradiation was less pronounced in p53 $-/-$ cells than in the wild-type. Consistently, the degree of synergism between NW457 and irradiation was strongly reduced and the number of synergistic combinations was clearly smaller in these cells than in case of the wild-type (Figure 10C, 7 versus 12 combinations with CI <1; for wild-type cells see Figure 8C).

BAX $-/-$ cells were almost completely resistant to NW457 treatment and irradiation as indicated by only marginal formation of subG1 nuclei. Even treatment with 300 nM NW457 plus 5 Gy irradiation increased the percentage of subG1 nuclei to only 25.4% (Figure 10B) compared to 85.1% in wild-type cells (Figure 8B). Moreover, the degree of synergism between NW457 and irradiation was further reduced in these cells (only 4 combinations with CI <1).

These findings are in line with the data of caspase activation and suggest that both BAX-dependent and -independent mechanisms are involved in NW457-mediated apoptosis induction and radiosensitization, whereas p53 obviously is dispensable. Thus, it can be concluded that NW457 exerts its radiosensitizing effects in colorectal cancer cells via the mitochondrial death pathway even in the absence of functional p53. Given that p53 is mutated or lost in up to 50% of colorectal cancers (Bazan et al., 2005; Lopez et al., 2012; Naccarati et al., 2012), NW457 appears as a highly attractive tool for anticancer therapies also in this regard.

6.1.6 NW457 augments radiation-induced clonogenic cell death of colorectal cancer cells

In order to investigate the long-term effects of NW457 on irradiation-induced cell death, clonogenic survival assays were performed. This endpoint is considered as one of the most relevant *in vitro* endpoints to predict potential radiosensitizing effects *in vivo*.

Depending on inherent plating efficiency and applied stimulus, HCT116 wild-type, BAX-knockout, and p53-knockout cells were seeded in varying densities, irradiated with 0-5 Gy, and cultivated for 14 days in the presence or absence of 10 nM NW457. Afterwards, the surviving fraction was determined on the basis of the number of resulting colonies normalized to the number of seeded cells and the respective plating efficiency. In these experiments, the relatively low drug concentration of 10 nM was selected in order to obtain plating efficiencies of at least 50% of vehicle-treated samples. Permanent incubation with NW457 was deliberately chosen, since conventional chemo- and

molecularly targeted therapeutics are commonly administered over a prolonged time in the clinic.

As can be seen in Figure 11, irradiation dose-dependently reduced the clonogenicity of all three cell lines. p53 $-/-$ cells showed a certain degree of resistance, whereas BAX $-/-$ cells appeared to be slightly more sensitive towards irradiation in comparison to the wild-type controls. Importantly, exposure to the HSP90 inhibitor NW457 enhanced radiation-induced clonogenic cell death in all three cell lines, with a significant reduction of clonogenic survival particularly being observed in the lower dose range of irradiation (1 and 3 Gy for wild-type and BAX $-/-$ cells, 1 Gy for p53 $-/-$ cells; * $p < 0.05$). Hence, NW457 apparently exerts a long-term radiosensitizing effect in HCT116 cells, which is essentially independent of functional p53 and BAX. These findings are to a certain degree contrasting with the data on apoptosis induction as described in chapter 6.1.5 indicating that BAX-deficient HCT116 cells did not undergo apoptosis. However, it has to be considered that apoptosis is only one form of cell death that can be induced by ionizing radiation and HSP90 inhibition, and that clonogenic cell death might also result from necro(pto)sis, mitotic catastrophe, as well as cellular senescence, or irreversible cell cycle arrest (Lauber et al., 2012; Roninson et al., 2001). Signs of mitotic catastrophe, such as giant, multi-lobed nuclei and micronuclei formation, were clearly detected in NW457-treated and irradiated cells (see Figure 7A) and have already been described in context with other HSP90 inhibitors, such as geldanamycin, 17-AAG, or NVP-AUY922 (Moran et al., 2008; Nomura et al., 2004; Stecklein et al., 2012; Zaidi et al., 2012). Moreover, the results here illustrate that the HCT116 subclone with the strongest apoptosis induction in response to NW457 treatment (p53 $-/-$ subclone) reveals the highest percentage of clonogenic survival, and vice versa (BAX $-/-$ subclone displays the weakest apoptosis induction, but the lowest clonogenic survival). This might be explained, at least partially, by recent observations showing that tumor cells undergoing apoptosis can generate proliferation signals, such as prostaglandin E_2 , in a caspase-3 dependent manner for the surviving tumor cells (Huang et al., 2011).

Taken together, these data suggest that NW457-mediated radiosensitization of colorectal cancer cells is not exclusively due to apoptotic cell death, but might involve other cell death forms which reduce the clonogenic survival independently of functional p53 and BAX.

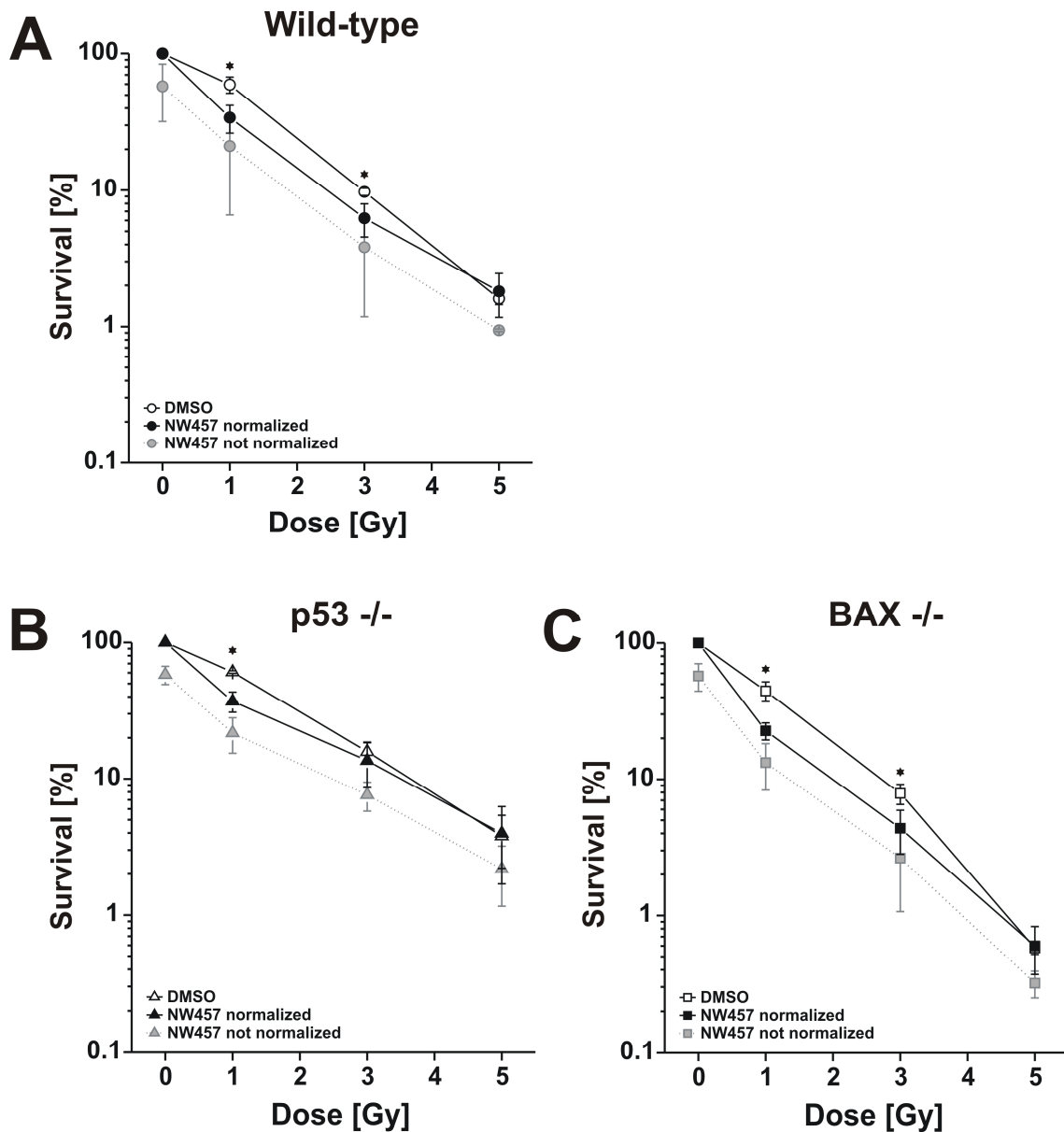


Figure 11. NW457 enhances radiation-induced clonogenic cell death in colorectal cancer cells.

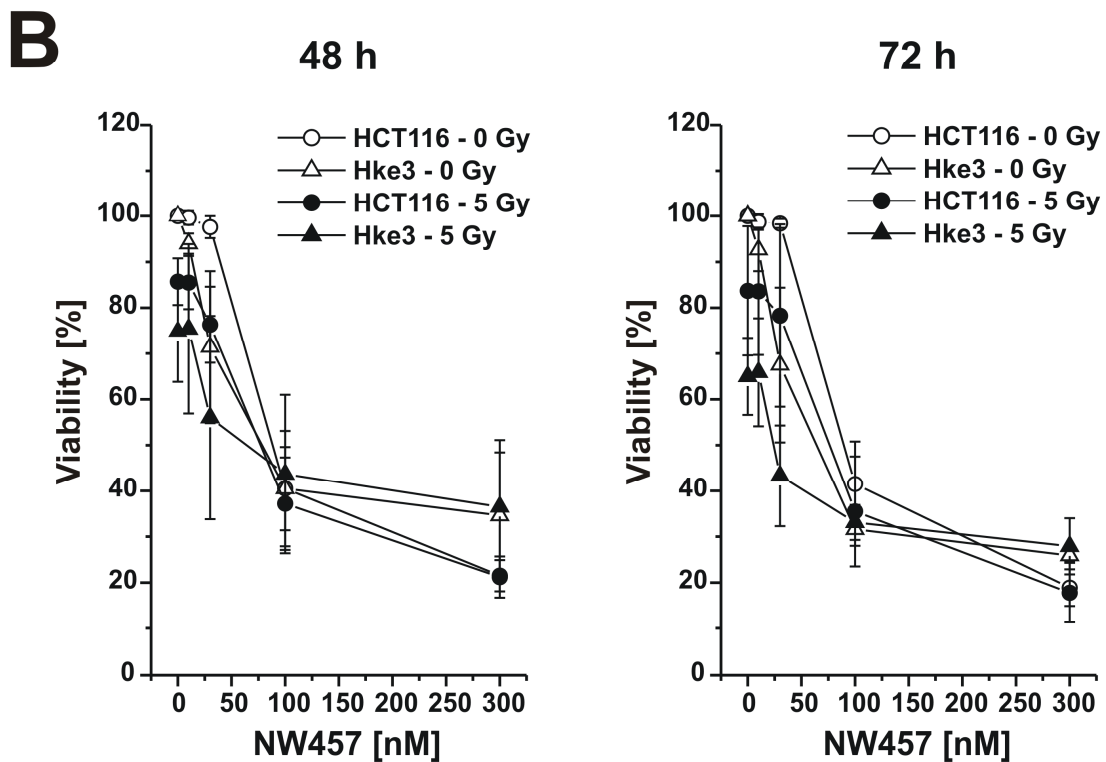
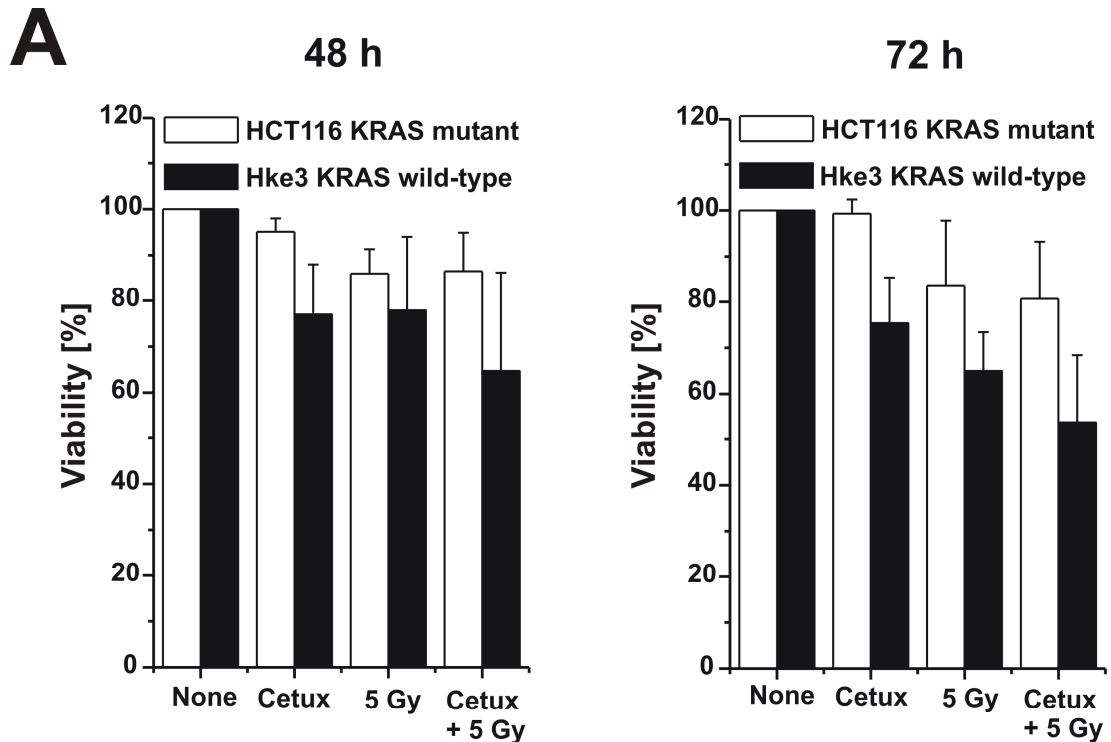
(A) HCT116 wild-type cells, (B) p53-deficient, and (C) BAX-deficient subclones were applied to clonogenic survival assays after irradiation with 0-5 Gy in the absence or presence of 10 nM NW457. After irradiation cells were incubated in drug-free or drug-containing medium for 14 days, and the surviving fraction was calculated on the basis of the resulting colonies with more than 50 cells each. Data represent means \pm SD of at least three independent experiments performed in triplicates. For NW457-treated samples normalized and not normalized data are given with respect to the plating efficiency in the presence or absence of NW457. Student's t-test was performed between normalized samples of identical irradiation dose \pm NW457; * $p < 0.05$.

6.1.7 Colorectal cancer cells are sensitive to HSP90 inhibition irrespective of their KRAS status

KRAS (Kirsten rat sarcoma viral oncogene homolog) is one of the most prominent human proto-oncogenes as it exhibits mutations in approximately 30% of all human cancers. KRAS mutations are predominantly found in cancers of the pancreas, intestine, and biliary tract (Karnoub and Weinberg, 2008). KRAS belongs to the family of RAS proto-oncogenes, which encode small GTPases that play key roles in signal transduction processes downstream of different receptor tyrosine kinases orchestrating survival, cell cycle, and motility (Karnoub and Weinberg, 2008). KRAS mutations occur mainly as activating point mutations in codons 12 and 13 and may be used as suitable biomarkers to predict the responsiveness to therapeutic agents targeting signaling molecules upstream of KRAS, such as EGF-R (Amado et al., 2008; Loupakis et al., 2009). In this regard, targeted EGF-R therapies based on blocking antibodies or tyrosine kinase inhibitors exhibit only limited success if KRAS or other downstream factors are constitutively activated (Amado et al., 2008; Khambata-Ford et al., 2007; Lievre et al., 2008). Consequently, KRAS mutations remain a therapeutic challenge, particularly in colorectal carcinomas, where the oncogene is mutated in up to 50% of all cases (Bazan et al., 2005). Therefore, novel therapeutic approaches that are not sensitive to activating KRAS mutations are urgently needed.

In order to define the impact of mutant KRAS on the responsiveness of colorectal cancer cells to NW457, this work made use of an isogenic pair of colorectal carcinoma cell lines differing only in their KRAS status - the HCT116 cell line, which harbors one wild-type KRAS allele and one KRAS allele with an activating point mutation in codon 13, and the Hke3 subclone, in which the mutant allele was genetically ablated by homologous recombination and which consequently exhibits wild-type KRAS status (Shirasawa et al., 1993). HCT116 and Hke3 cells were treated with NW457 or the EGF-R inhibitor cetuximab (as an indicator of the KRAS status) for 24 h, subsequently irradiated with 0 or 5 Gy, and cellular viability was assessed in Alamar Blue assays 48 or 72 h afterwards. Whereas the viability of heterozygous KRAS mutant HCT116 cells remained basically unaffected after exposure to cetuximab (Figure 12A, $p > 0.05$ for cetuximab vs. none at 48 h and 72 h), the viability of wild-type KRAS expressing Hke3 cells was reduced in response to cetuximab treatment ($p < 0.05$ for cetuximab vs. none at 72 h). The detected inherent radiosensitivity of KRAS wild-type and mutant cells differed, as the KRAS wild-type Hke3 cells revealed a more profound reduction in viability, particularly 72 h after irradiation (Figure 12A, $p < 0.05$ for 5 Gy vs. none at 72 h). Most intriguingly, the novel HSP90 inhibitor NW457 clearly reduced the viability of both cell lines in a dose-dependent

manner (Figure 12B). For cases in which the cells had been pre-stimulated with NW457 concentrations <100 nM, the viability of Hke3 cells was consistently lower compared to HCT116 cells and further decreased by additional irradiation, although this was not statistically significant (Figure 12B, $p > 0.05$).



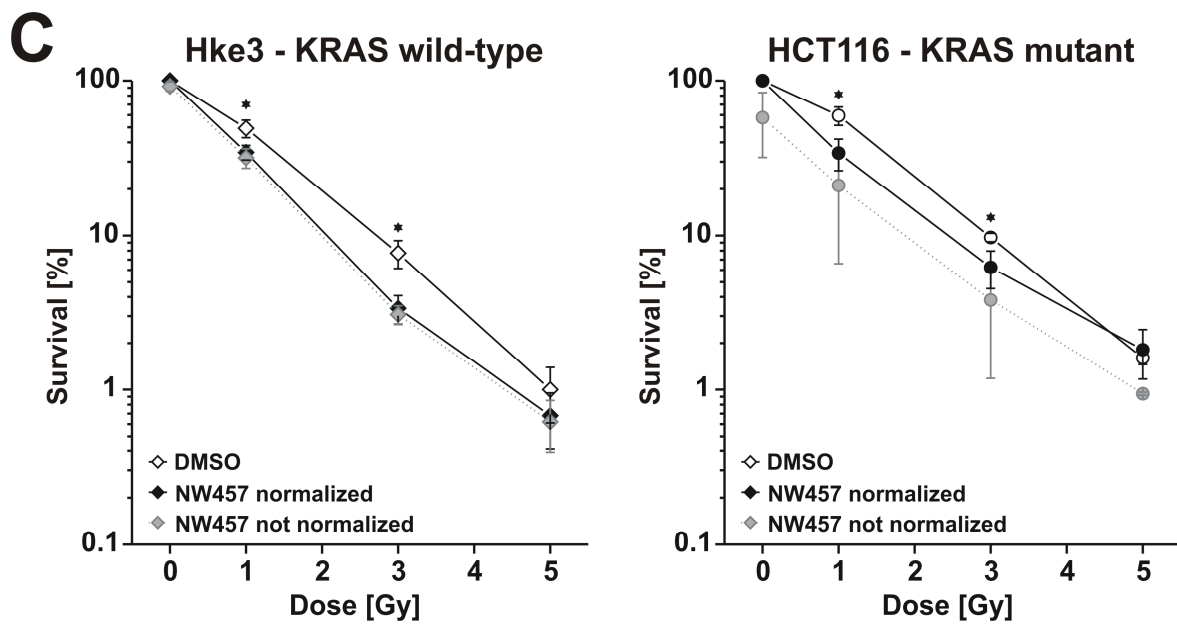


Figure 12. Colorectal cancer cells are sensitive to HSP90 inhibition irrespective of their KRAS status.

(A) Viability of isogenic HCT116 colorectal cancer cell lines differing only in their KRAS status was investigated in response to cetuximab treatment by Alamar Blue assays. HCT116 (KRAS^{wt/mut}) and Hke3 (KRAS^{wt/-}) cells were incubated with 20 µg/ml cetuximab or DMSO (vehicle) for 24 h, irradiated with 0 or 5 Gy, and subjected to Alamar Blue assays 48 and 72 h after irradiation. The cetuximab concentration (20 µg/ml) was selected according to previous publications indicating its potent cytotoxic effects on different colorectal carcinoma cell lines (van Houdt et al., 2010; Xu et al., 2005). Alamar Blue reduction was calibrated on the vehicle-treated controls (100% viability) and is shown as means ± SD of three independent experiments. **(B)** Viability of HCT116 (KRAS^{wt/mut}) and Hke3 (KRAS^{wt/-}) cells was investigated in response to 0-300 nM NW457 +/- irradiation. Cells were stimulated as described in (A). **(C)** Clonogenic survival of Hke3 cells after irradiation was examined in the presence or absence of 10 nM NW457 as described for Figure 11. Data represent means ± SD of three independent experiments. For NW457-treated samples normalized and not normalized data are given. Student's t-test analysis was performed between samples of identical irradiation dose ± NW457; *p<0.05.

In colony formation assays, irradiation dose-dependently reduced the clonogenic survival of both cell lines (Figure 12C). In line with the viability data above, the KRAS wild-type Hke3 cells revealed stronger radiosensitivity than the KRAS mutant HCT116 cells. Exposure to 10 nM NW457 further decreased the clonogenicity of both cell lines and demonstrated significant radiosensitization in cases of irradiation with 1 or 3 Gy (*p<0.05). From these findings it can be concluded that the compromising effects of NW457 on colorectal cancer cell viability and clonogenic survival are in essence independent of the cellular KRAS status. These results confirm very recent observations showing that other HSP90 inhibitors, such as ganetespib (STA-9090), 17-AAG, and PU-H71, also performed potent antitumor activity in tumor cell lines expressing mutant variants of KRAS (Acquaviva et al., 2012; Azoitei et al., 2012).

6.1.8 NW457 reveals very little hepatocytotoxicity

During the preclinical development and characterization of the first generation HSP90 inhibitors, such as geldanamycin (GA) and its derivatives 17-AAG and 17-DMAG, severe limitations were encountered in the form of profound hepatotoxicity (Cysyk et al., 2006; Supko et al., 1995), which confined the dose schedule for *in vivo* studies and finally restricted the success of these compounds in clinical trials. GA-induced liver toxicity is supposed to be associated with the benzoquinone ring as this moiety is metabolized by liver microsomes and generates free radicals that finally induce the hepatotoxic effects (Powis, 1989). Since radicicol and its pochoxime derivatives lack this hydroquinone moiety, they are thought to be considerably less hepatotoxic.

In order to assess this in the case of the novel compound NW457 and to exclude potential hepatotoxic effects prior to its application in *in vivo* studies, primary hepatocytes were isolated from C57BL/6 mice and then exposed to increasing concentrations of NW457 or geldanamycin, respectively. Both drugs were applied in same concentrations as they had demonstrated comparable cytotoxic effects in tumor cells before (Figure 7D). Cellular viability was examined 24-48 h later in Alamar Blue assays and hepatocellular morphology was monitored by immunofluorescence staining.

As expected, geldanamycin dramatically reduced the viability of primary hepatocytes in a time- and dose-dependent manner (Figure 13A). Morphologically, typical hepatocellular features including binucleation due to amitosis and a distinctive cytoskeleton were observed in the DMSO-treated control population (Figure 13B). In clear contrast, geldanamycin-induced cell death was characterized by a complete loss of the typical hepatocellular shape, accompanied by cellular shrinkage, atypical distribution and clustering of tubulin and actin, as well as nuclear flattening. In addition, features of apoptosis, including nuclear fragmentation and formation of apoptotic bodies, as well as autophagic phenotypes with multiple intracellular vesicles were observed. In strong contrast, primary hepatocytes exposed to NW457 did not exhibit any of the mentioned characteristics, and even high inhibitor concentrations did not perturb the typical hepatocellular morphology. Concomitantly, the cellular viability remained virtually unaffected in response to the novel HSP90 inhibitor (Figure 13A).

These results open the perspective for the *in vivo* application of NW457 in order to validate the promising *in vitro* results on the basis of a murine model of colorectal cancer.

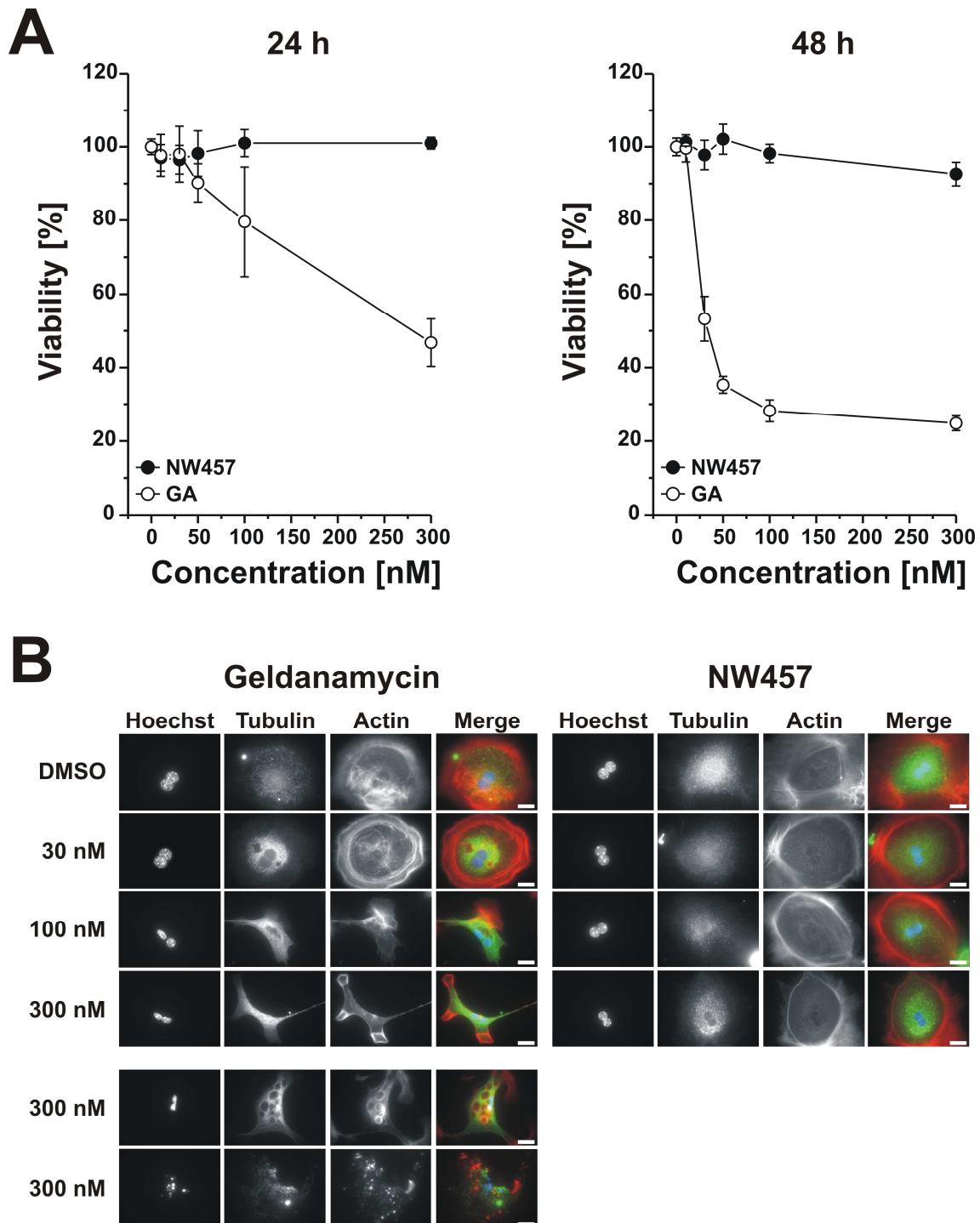


Figure 13. NW457 reveals very little hepatocytotoxicity.

Primary hepatocytes isolated from C57BL/6 mice were exposed to 0-300 nM NW457, geldanamycin, or DMSO as vehicle control for 24-48 h, and cellular viability was assessed by Alamar Blue assays as well as immunofluorescence microscopy. **(A)** Cellular viability was measured 24 and 48 h after stimulation with NW457 or geldanamycin (GA) by Alamar Blue assays. Alamar Blue reduction was calibrated on the vehicle-treated controls (100% viability) and is shown as means \pm SD of intra-assay quadruplicates. 48 h data of one further experiment are shown in Appendix 2. **(B)** Immunofluorescence staining was performed 24 h after inhibitor treatment with anti-tubulin antibody, phalloidin-Alexa Fluor 568 (actin-staining), and Hoechst 33342 (nuclear staining). Scale bars represent 20 μ m. Immunofluorescence experiments were performed in cooperation with Michael Orth.

6.1.9 NW457 shows potent antitumor efficacy in combination with radiotherapy *in vivo*

The antitumor efficacy of HSP90 inhibition in combination with radiotherapy has rarely been examined *in vivo*, and data on HSP90 inhibitor-mediated radiosensitization in colorectal cancer models to the best of my knowledge are currently not available. On the basis of the encouraging *in vitro* results regarding NW457-induced radiosensitization along with its excellent tolerability by primary hepatocytes, it was therefore sought to elucidate the antitumor effects of NW457 in combination with radiotherapy in a heterotopic model of CT26 colorectal cancer cells growing on the flanks of syngeneic, immunocompetent Balb/c mice. These *in vivo* experiments were kindly performed by Benjamin Frey and Udo Gaipl (Department of Radiation Oncology, University Hospital Erlangen).

24 female 8-week old mice were subcutaneously inoculated with murine CT26 cells on day 0, and tumors were allowed to grow for 9 days. At this time, mice with tumors greater than 300 mm³ (n=3) were excluded from the study and the remaining animals with average tumor volumes of 212 ± 9 mm³ (mean ± SEM) were randomly distributed into four groups: NW457 (n=6), DMSO (n=4), 2x 5 Gy + NW457 (n=5), and 2x 5 Gy + DMSO (n=6). NW457 (100 mg/kg) or DMSO (as vehicle control) was administered intraperitoneally on days 9, 12, 18, and 24. Time points for drug administration were determined depending on drug tolerance and weight development. Irradiation was carried out with two fractions of 0 or 5 Gy on days 10 and 13 after tumor implantation, respectively. Tumor volume was monitored every 1-3 days, and mice carrying tumors exceeding 1,700 mm³ were sacrificed due to legal requirements.

Mice in the non-irradiated, vehicle control group exhibited exponential tumor growth (Figure 14A), and until day 21 all animals had to be sacrificed. Treatment with 4x 100 mg/kg NW457 alone resulted in an early delay in tumor growth, which was detected from day 10 to day 20. Later on, tumors resumed exponential growth exceeding a mean volume of 1,700 mm³ until day 24. Radiotherapy plus vehicle induced a potent reduction in tumor growth, with four of six animals carrying tumors of less than 1,700 mm³ on day 27 and the average tumor volume being 1234 ± 246 mm³ (mean ± SEM). Most importantly, the strongest inhibitory effect on tumor growth was observed in the group that had received the combined therapy comprising 2x 5 Gy plus 4x 100 mg/kg NW457. Here, the early delay in tumor growth, which was also observed in the NW457 only group, together with long-term growth inhibitory effects beyond day 20 resulted in an average tumor volume of 546 ± 110 mm³ (mean ± SEM) on day 27. Compared to the radiotherapy plus vehicle group, a significant reduction in tumor growth was detected in the radiotherapy plus NW457 group for the time points indicated (*p<0.05; **p<0.01).

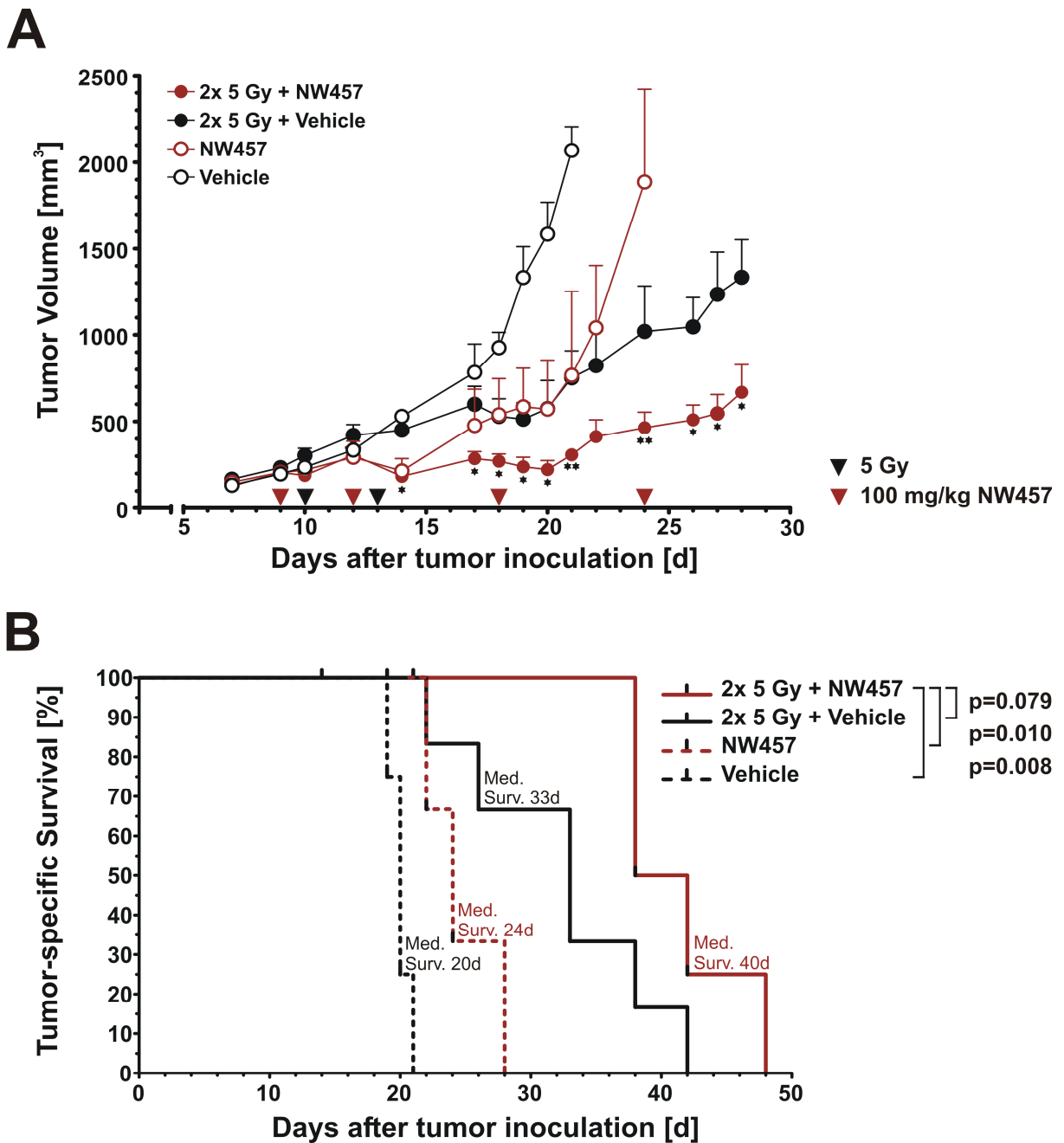


Figure 14: Combined treatment with NW457 and radiotherapy potentially delays tumor growth *in vivo*.

NW457-mediated radiosensitization was assessed *in vivo* in a syngeneic heterotopic Balb/c mouse model of CT26 colorectal tumor cells growing on the right flank. 1.2×10^6 CT26 cells were injected subcutaneously, and tumors were allowed to grow for 9 days. Mice with tumors of less than 300 mm^3 were distributed into four groups and subjected to the following treatments: 4x DMSO only ($n=4$), 4x 100 mg/kg NW457 only ($n=6$), 2x 5 Gy + 4x DMSO ($n=6$), and 2x 5 Gy + 4x 100 mg/kg NW457 ($n=5$). NW457 and DMSO were administered by intraperitoneal injection on days 9, 12, 18, and 24 (red arrowheads). Local irradiation was performed on days 10 and 13 (black arrowheads). *In vivo* experiments were kindly provided by Benjamin Frey and Udo Gaipl (Department of Radiation Oncology, University Hospital Erlangen). **(A)** Tumor dimensions were measured every 1-3 days and tumor volumes were calculated using the formula (width x width x length)/2. Data represent means \pm standard error of the mean (SEM). Mann-Whitney U test was performed between the 2x 5 Gy + vehicle and the 2x 5 Gy + NW457 group. * $p < 0.05$; ** $p < 0.01$. **(B)** Kaplan-Meier curves were generated for the tumor-specific survival

of CT26 tumor bearing Balb/c mice which had been distributed into the following treatment groups: vehicle only (n=4), NW457 only (n=6), 2x 5 Gy + vehicle (n=6), and 2x 5 Gy + NW457 (n=5). The median survival was calculated for each group. Note that one animal of the group receiving 2x 5 Gy + NW457 and three animals of the group receiving NW457 only were censored because they died from other reasons rather than being sacrificed due to tumor volumes $>1,700 \text{ mm}^3$ (day 21 and days 14, 19, and 21, respectively). Log-rank test was carried out for statistical analysis of the tumor-specific survival between the group receiving combined modality therapy of IR plus NW457 and the groups subjected to IR plus vehicle ($p=0.079$), NW457 only ($p=0.010$), and vehicle only ($p=0.008$), respectively.

In addition, Kaplan-Meier curves were established for the tumor-specific survival of the four treatment groups (Figure 14B). The median survival of the vehicle only group was 20 days as all animals succumbed to exceeding tumor volumes within 21 days after tumor inoculation. Mice receiving NW457 alone showed a median tumor-specific survival of 24 days. Interestingly, radiotherapy with two fractions of 5 Gy each prolonged the median survival to 33 days. However, the strongest prolongation in survival was observed in the group which was subjected to combined therapy with 2x 5 Gy irradiation plus 4x 100 mg/kg NW457 as this therapeutic regime resulted in a median survival of 40 days. Statistical analyses revealed that the tumor-specific survival in the radiotherapy plus NW457 group was significantly prolonged compared to the groups receiving NW457 only ($p=0.010$) or vehicle only ($p=0.008$), respectively, but, presumably due to the low number of animals, it was not significant ($p=0.079$) compared to the group receiving irradiation only.

In summary, the findings here identify the novel HSP90 inhibitor NW457 as a highly promising candidate for combined modality approaches together with radiotherapy. It potentially radiosensitizes colorectal cancer cells irrespective of functional p53, BAX, or activated KRAS *in vitro*, reveals very little toxicity on primary hepatocytes, and shows encouraging antitumor efficacy in combination with radiotherapy *in vivo*.

6.2 The novel HSP90 inhibitor NW457 abrogates the radioresistance of human glioblastoma cells and impairs their migratory potential

Glioblastoma multiforme (GBM) is the most common and malignant form of human brain tumors. It displays an aggressively infiltrative phenotype and results in a median survival of less than 15 months (Stupp et al., 2005). One concept to override glioblastoma-associated intrinsic and acquired resistance towards conventional therapies comprises the application of targeted agents that specifically improve the outcome of radiotherapy by interfering with radioresistance-related signaling pathways and suppressing migration and invasion of glioma cells. In this context, different molecular targets have been identified, and some of them have been found to be designated client proteins of HSP90, thus rendering the chaperone itself an attractive target for GBM therapies (Dungey et al., 2009; Kim et al., 2008a; Nomura et al., 2004; Stingl et al., 2010; Zagzag et al., 2003; Zhu et al., 2010). Hence, in the second part of this thesis, the efficacy of NW457 in combination with radiotherapy was investigated in human glioblastoma cell lines.

6.2.1 NW457 abolishes the intrinsic radioresistance of human glioblastoma cells

In order to investigate the radiosensitizing potential of NW457 in glioblastoma cells, human LN229 and T98G cells were used. As an initial characterization of the cellular response to NW457 alone and in combination with ionizing radiation, the nuclear morphology was examined by Hoechst 33342 staining and fluorescence microscopic evaluation. Therefore, LN229 and T98G cells were stimulated with 0-200 nM NW457 or DMSO as vehicle control for 24 h, irradiated with 0-10 Gy, and apoptotic nuclei were quantified at the time points indicated. Representative pictures in Figure 15 reveal that irradiation alone reduced the proliferation, particularly of LN229 cells. However, apoptosis induction was observed to a very limited extent, even 54 h post irradiation. Exposure to NW457 alone impaired proliferation and induced typical apoptosis-associated changes in the nuclear morphology (for typical apoptosis-associated nuclear phenotypes of early and late apoptotic phases compare Figure 7B). Intriguingly, the combination of NW457 treatment plus irradiation time-dependently potentiated nuclear fragmentation and clearly inhibited proliferation, which was more pronounced in LN229 cells compared to T98G cells. These data suggest that NW457 in combination with irradiation exerts anti-proliferative and pro-apoptotic effects not only on colorectal carcinoma cells, but also on glioblastoma cells, and thus might be a promising agent to abrogate glioblastoma-associated radioresistance.

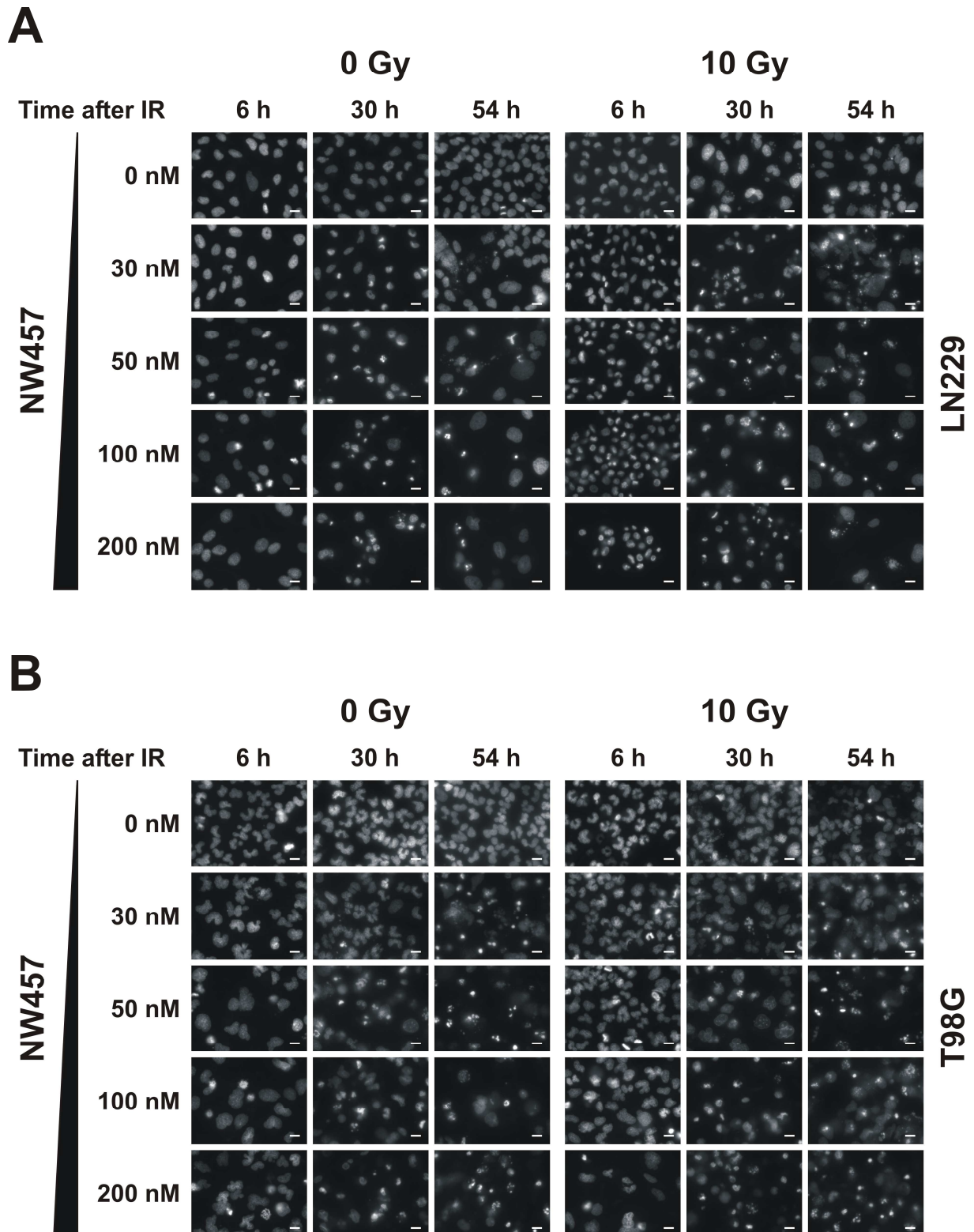


Figure 15. Exposure to NW457 induces typical apoptosis-associated changes of the nuclear morphology and potentiates the effect of ionizing irradiation on human glioblastoma cells.

(A) LN229 and **(B)** T98G cells were treated with 0-200 nM NW457 or DMSO as vehicle control for 24 h, irradiated with 0-10 Gy, and subjected to Hoechst 33342 staining after 6-54 h. Representative photographs demonstrate typical apoptosis-related nuclear phenotypes in response to NW457 and irradiation in LN229 and T98G cells. Scale bars indicate 20 μ m.

To confirm the observations of the microscopic analyses and to define the mode of interaction (synergism, additivity, or antagonism) between NW457 and irradiation in glioblastoma cells, the formation of hypodiploid nuclei was examined in response to NW457 treatment +/- irradiation by flow cytometric analysis of propidium iodide stained nuclei. LN229 and T98G cells were exposed to 0-200 nM NW457 for 24 h, irradiated with 0-10 Gy, and the hypodiploid population (percentage of subG1 nuclei) was quantified 48 h later. Whereas irradiation alone only marginally resulted in the formation of hypodiploid nuclei, NW457 treatment potently stimulated the appearance of hypodiploid nuclei in a concentration-dependent manner both in LN229 and T98G cells (Figure 16A). The combined treatment with additional irradiation further increased the percentage of subG1 nuclei, particularly in LN229 cells when NW457 was applied in a range of <100 nM.

In order to define the quality of interaction between NW457-mediated HSP90 inhibition and ionizing radiation for both glioblastoma cell lines, combination indices (CI) according to Chou-Talalay (Chou and Talalay, 1981, 1984) were assessed for all combinations depicted in Figure 16A. NW457 treatment plus irradiation revealed synergism (CI <1) in LN229 cells mainly in cases when NW457 was administered at 30, 40, 50, or 100 nM (in total 17 synergistic treatment points, Figure 16B) and in T98G cells when NW457 was applied at 40-50 nM (in total 10 synergistic treatment points, Figure 16B).

Taken together, these data indicate a pro-apoptotic effect of NW457 on human glioblastoma cell lines and suggest that the radiosensitizing potential of NW457 might be more pronounced in LN229 cells compared to T98G cells.

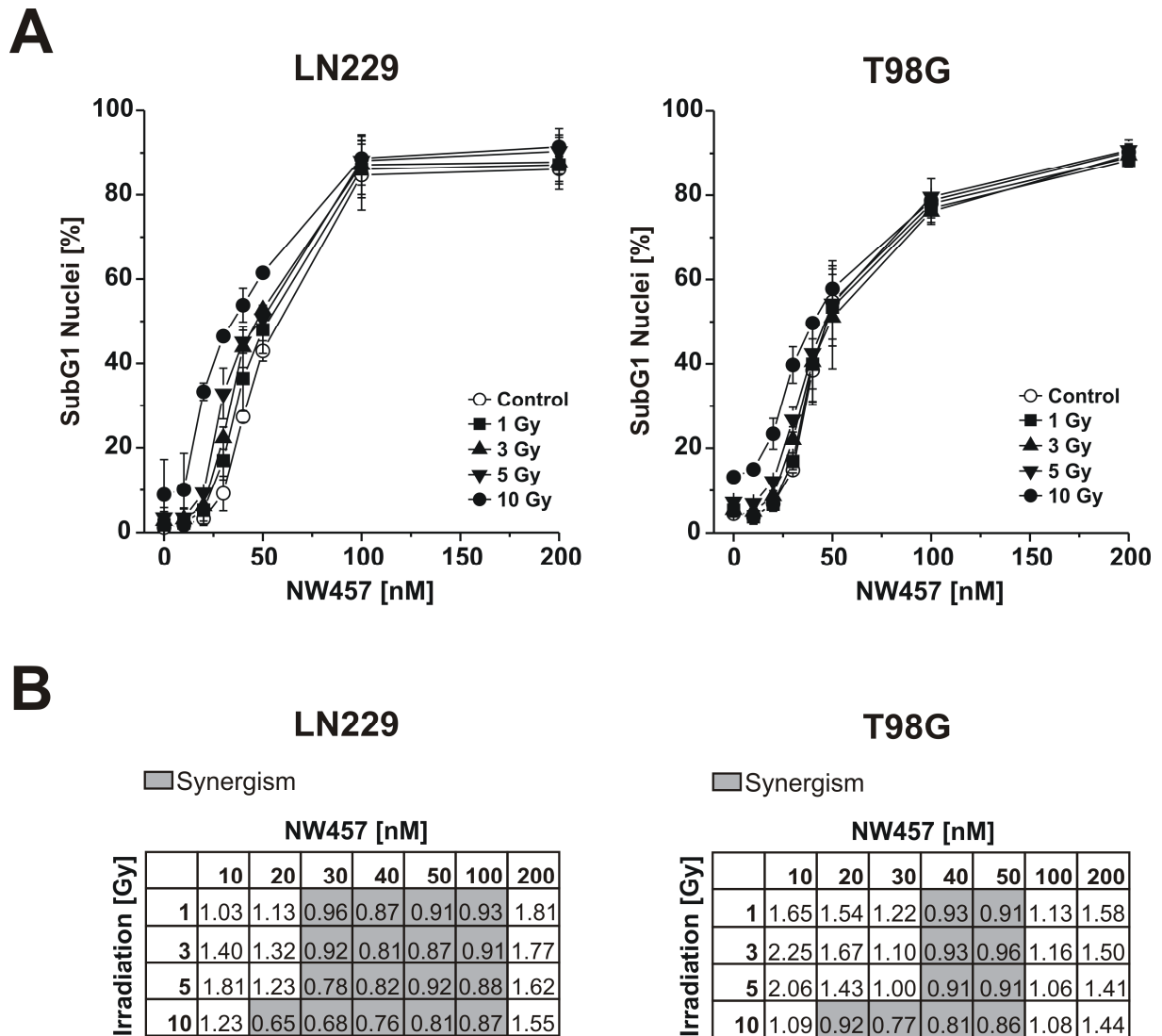


Figure 16. NW457 induces the formation of hypodiploid nuclei and potentiates the effects of ionizing radiation.

LN229 and T98G cells were stimulated with 0-200 nM NW457 for 24 h, irradiated with 0-10 Gy, and stained with propidium iodide for FACS analysis of hypodiploid (subG1) nuclei 48 h after irradiation. **(A)** Dose-dependent induction of hypodiploid nuclei (% subG1) in response to treatment with NW457 and irradiation in LN229 and T98G cells. Data are means \pm SD of six replicates obtained from two independent experiments performed in triplicates each. **(B)** Combination indices calculated from the data shown in (A). Values highlighted in grey demonstrate a synergistic interaction between NW457 and irradiation (CI <1).

6.2.2 NW457 dose-dependently induces apoptosis in glioblastoma cells as characterized by caspase activation and subsequent caspase substrate cleavage

In order to further investigate the molecular mechanisms of NW457-induced apoptosis in glioblastoma cells and considering the findings in colorectal cancer cells (section 6.1.4), activation of the caspase cascade was analyzed in response to NW457 treatment and irradiation. To this end, LN229 and T98G cells were exposed to 0-200 nM NW457 for 24 h, irradiated with 0-10 Gy, and 24 h later whole cell lysates were prepared and subjected to Western blot analyses and caspase activity measurements. In both cell lines, NW457 dose-dependently induced the processing of the pro-caspases -9, and -3 as well as the cleavage of the prototypical caspase substrate PARP (Figure 17A, C). Notably, in LN229 cells additional irradiation of 10 Gy further augmented the levels of cleaved PARP, consistent with an increase in DEVDase activity after combined treatment (Figure 17A, B). Yet, in T98G cells additional irradiation did not result in enhanced PARP cleavage compared to NW457 treatment alone, and DEVDase activity was not further elevated after combined treatment in these cells (Figure 17C, D).

These findings are in accordance with the data presented in Figure 16 indicating that NW457 potently induces apoptosis in both LN229 and T98G cells, but suggesting that LN229 cells are more sensitive towards NW457-based combined radiotherapy treatment than T98G cells.

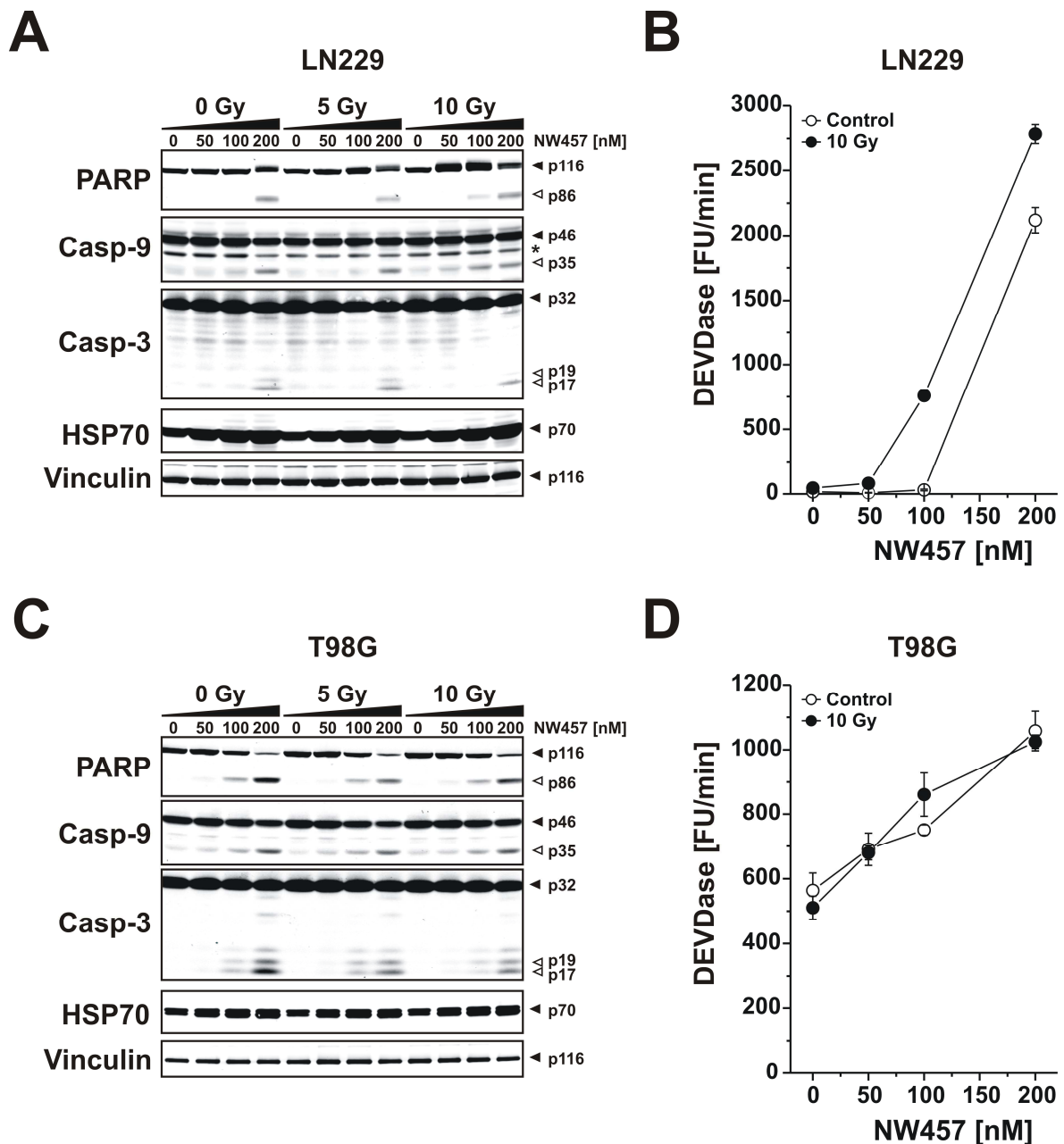


Figure 17. NW457-mediated apoptosis induction in glioblastoma cells involves the activation of the caspase cascade.

LN229 and T98G cells were treated with 0-200 nM NW457 for 24 h, irradiated with 0-10 Gy, and harvested 24 h after irradiation. Whole cell lysates were subjected to Western blot analyses of pro-caspases -9 and -3 processing as well as PARP cleavage. Upregulation of HSP70 expression was used as a marker of HSP90 inhibition. Lysates were also analyzed for caspase activity using the peptide substrate DEVD-AMC. **(A)** Processing of pro-caspases -9 and -3, cleavage of the caspase substrate PARP, and expression of HSP70 were analyzed by Western blotting using protein lysates obtained from LN229 cells treated as described above (150 μ g protein per lane). Vinculin was used as loading control (150 μ g protein per lane). Each blot is representative of one of two independent experiments. *Indicates unspecific antibody binding. **(B)** Caspase activity was measured by DEVDase assays using protein lysates of LN229 cells obtained as in (A). 20 μ g total protein per sample were employed, and means \pm SD of one representative experiment performed in quadruplicates are shown. Results of further experiments are shown in Appendix 3. **(C)** Processing of the pro-caspases -9 and -3, cleavage of the caspase substrate PARP (150 μ g protein per lane), and expression of HSP70 (10 μ g

protein per lane) were analyzed by Western blotting using protein lysates obtained from T98G cells treated as described above. Vinculin was used as loading control (10 µg protein per lane). Each blot is representative of one of two independent experiments. **(D)** Caspase activity was measured by DEVDase assays using protein lysates of T98G cells obtained as in (C). 20 µg total protein per sample were employed, and means ± SD of one representative experiment performed in quadruplicates are shown. Results of further experiments are shown in Appendix 4.

6.2.3 NW457 enhances radiation-induced clonogenic cell death of glioblastoma cell lines and affects critical regulators of the DNA damage response

The efficiency of NW457 to radiosensitize glioblastoma cells *in vitro* was further assessed by clonogenic survival assays. To this end, LN229 and T98G cells were subjected to different treatment approaches varying in the time of NW457 exposure. In the first approach cells were prestimulated with 10 nM NW457 or DMSO as vehicle control for 24 h and irradiated with 0-5 Gy. Drug-containing medium was exchanged for drug-free medium directly before irradiation. Data of the preincubation experiments were kindly provided by Karin Seidl. In the second approach NW457 or DMSO, respectively, was added immediately before irradiation and drug incubation was sustained over the entire assay period of 14 days. Clonogenic survival was determined relative to the respective plating efficiency of non-irradiated cells treated with DMSO or NW457, respectively. Irradiation alone dose-dependently decreased the clonogenic survival of both cell lines, yet LN229 cells revealed higher radiosensitivity compared to T98G cells (Figure 18A, B). Permanent exposure (14 days) to NW457 further reduced the clonogenic survival in response to irradiation, and this effect was more pronounced in LN229 than in T98G cells as illustrated by two treatment points with statistically significant radiosensitization in the case of LN229 cells (3 Gy and 5 Gy) and one treatment point (3 Gy) in the case of T98G cells. Intriguingly, 24 h preincubation with NW457 strongly decreased the clonogenic survival in a manner more pronounced than in the case of permanent drug incubation. Calculation of the radiation enhancement ratio as the D₀ (IR dose resulting in 37% survival) or SF₃ (survival fraction at 3 Gy) of DMSO treated cells divided by that of NW457 treated cells confirmed that 24 h preincubation with NW457 further amplifies the induction of clonogenic cell death compared to simultaneous drug/IR exposure. The question that arises at this point is which molecular mechanisms account for the stronger radiosensitization observed in response to 24 h NW457 preincubation compared to simultaneous drug/IR treatment. Since previous studies have shown that several HSP90 client proteins are functionally associated with the cellular radioresponse and depleted upon pharmacological HSP90 inhibition (Bull et al., 2004; Machida et al., 2003; Dote et al., 2006), I hypothesized that preincubation with NW457 prior to irradiation might affect the stability of crucial regulators of the DNA damage response (DDR), thus preventing

efficient DNA repair upon irradiation 24 h later, and finally accounting for enhanced tumor cell radiosensitization in clonogenic survival assays. Therefore, LN229 and T98G cells were stimulated with 10 nM NW457 - as this concentration was used in clonogenic survival assays - and both RNA transcription and protein expression of ATM (Ataxia telangiectasia mutated protein), ATR (Ataxia telangiectasia and RAD3-related protein), CHK1 (Checkpoint kinase 1), CHK2 (Checkpoint kinase 2), and p53 were analyzed 0-72 h afterwards. These experiments were performed in cooperation with Michael Orth and Karin Seidl. Intriguingly, exposure to NW457 time-dependently induced the depletion of the DNA damage sensor kinase ATM and the signal transducers CHK1 and CHK2 in both cell lines (Figure 18C). Notably, the levels of ATM, CHK1, and CHK2 were already diminished within 12-24 h after drug exposure. These findings indicate that in clonogenic survival assays preincubation with NW457 presumably provoked the degradation of critical DDR-associated proteins before the irradiation was performed and that this might account for enhanced radiosensitivity of LN229 and T98G cells. In contrast, simultaneous exposure to NW457 and IR apparently limited the radiosensitizing efficacy of NW457 in clonogenic survival assays as the DDR was not affected at the time of irradiation, but only 12-72 h later when the majority of IR-induced DNA damage had presumably been repaired. Whereas expression of the DNA damage sensor ATR remained nearly unaffected in T98G cells, ATR levels were slightly decreased in LN229 cells 36-72 h after exposure to NW457. Notably, NW457-mediated depletion of ATM, ATR, CHK1, and CHK2 was limited to the protein level, as mRNA analyses did not reveal transcriptional downregulation (Figure 18D). As a sign of activated DNA damage response, a profound upregulation of p53 was detected in LN229 cells both on the protein and mRNA level. Interestingly, p53 protein expression in T98G cells was initially depleted in response to NW457 (12 h), but was restored at later time points due to increased p53 transcription which was observed 24-48 h after stimulation with NW457. In this respect, it should be noted that LN229 cells exhibit functional wild-type p53 activity despite a p53 mutation in codon 164, whereas T98G cells are homozygously mutated (codon 237) and express non-functional p53 (Van Meir et al., 1994). As mutant p53 is a designated HSP90 client protein (Blagosklonny et al., 1995; Hagn et al., 2011; Muller et al., 2008), suppressed chaperoning activity of HSP90 might account for the rapid depletion of mutant p53 in T98G cells within 12 h after NW457 treatment.

Collectively, these findings strengthen the observations from sections 6.2.1 and 6.2.2, as they confirm the potent radiosensitizing capacity of NW457 also in glioblastoma cell lines. Moreover, the Western blot data here give mechanistic insight of how the novel HSP90 inhibitor mediates tumor cell radiosensitization and indicate that the sequence of

combining pharmacological HSP90 inhibition with radiotherapy should be carefully considered in clinical treatment concepts as it may influence the therapeutic efficacy.

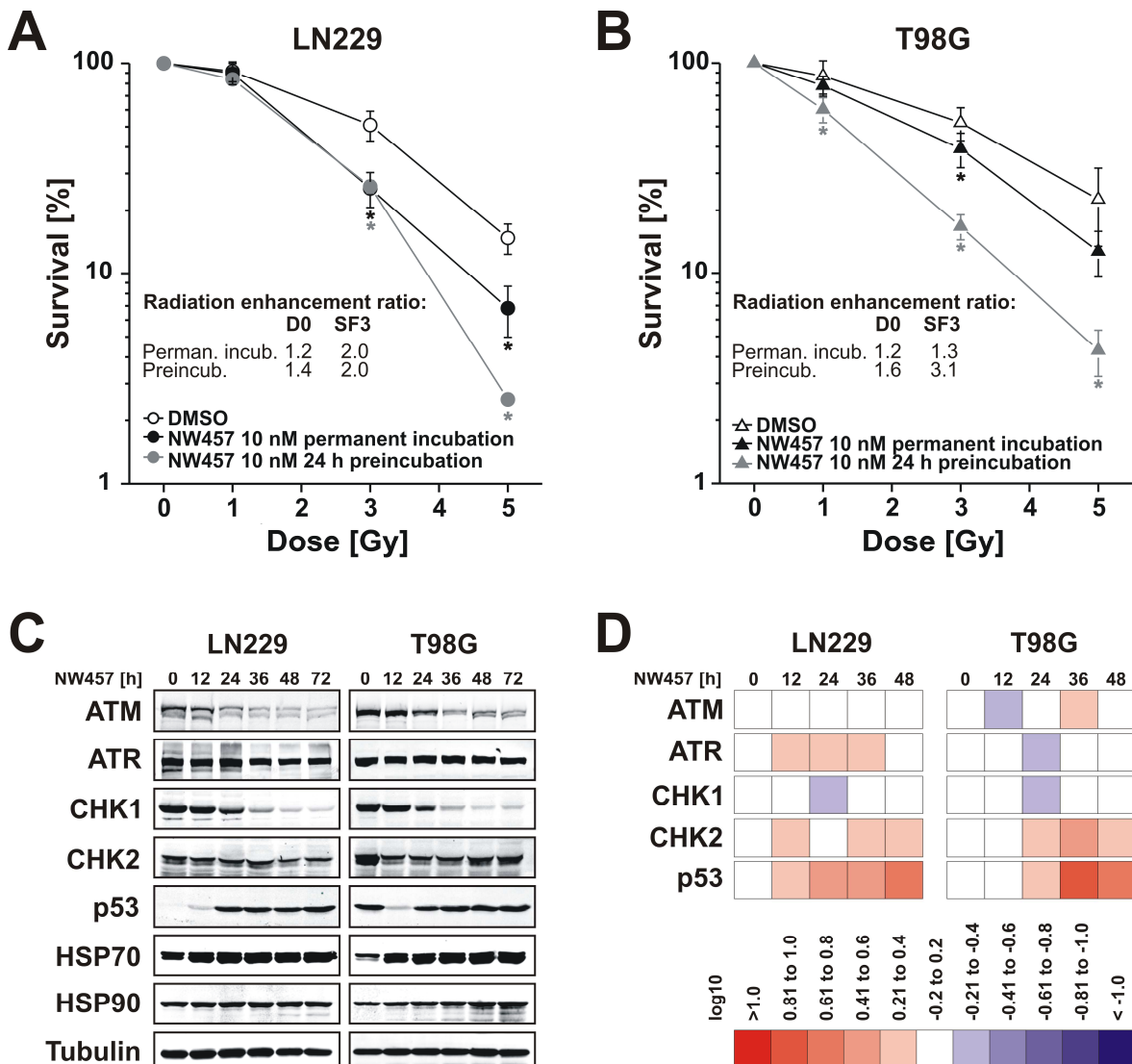


Figure 18. NW457 augments radiation-induced clonogenic cell death of glioblastoma cell lines and compromises regulators of the DNA damage response.

LN229 and T98G cells were exposed to 10 nM NW457 in the presence or absence of irradiation and subjected to clonogenic survival assays, Western blot, and quantitative real-time PCR analyses. **(A)** For clonogenic survival assays LN229 and T98G cells were subjected to different treatment approaches varying in the time of NW457 exposure. In the first approach cells were prestimulated with 10 nM NW457 or DMSO as vehicle control for 24 h and irradiated with 0-5 Gy. Drug-containing medium was exchanged directly before irradiation. In the second approach NW457 or DMSO, respectively, was added directly before irradiation and drug incubation was sustained over the entire assay period. Clonogenic survival [%] was determined after 14 days with respect to the plating efficiencies of DMSO-treated, non-irradiated cells and NW457-treated, non-irradiated cells, respectively. Curves show the clonogenic survival of LN229 cells in response to irradiation only (open symbols), 24 h preincubation with 10 nM NW457 plus irradiation (grey symbols), and permanent exposure to 10 nM NW457 plus irradiation (black symbols). D0 is the radiation dose giving 37% survival and SF3 is the survival fraction in response to irradiation with 3 Gy. The radiation enhancement ratio was calculated as the D0 or SF3, respectively, of DMSO treated cells divided by that of NW457 treated cells.

Data represent means \pm SD of at least three independent experiments. Student's t-test analysis was performed between samples of identical irradiation dose \pm NW457; * $p < 0.05$. Data of the preincubation experiments were kindly provided by Karin Seidl. **(B)** T98G cells were treated as described in (A) and subjected to clonogenic survival assays. Survival curves are shown for T98G cells exposed to irradiation only (open symbols), 24 h preincubation with NW457 plus irradiation (grey symbols), and permanent incubation with NW457 plus irradiation (black symbols). Data represent means \pm SD of at least three independent experiments. Student's t-test analysis was performed between samples of identical irradiation dose \pm NW457; * $p < 0.05$. Data of the preincubation experiments were kindly provided by Karin Seidl. **(C)** For Western blot analyses of proteins associated with the DNA damage response LN229 and T98G cells were exposed to 10 nM NW457 for 0-72 h and the expression of ATM, ATR, CHK1, CHK2, p53, HSP70, and HSP90 was examined. 300 μ g protein per lane was used for detection of ATM, ATR, CHK1, CHK2, and p53; 30 μ g protein was used for analysis of HSP70, HSP90, and tubulin (loading control). Western blots were kindly provided by Michael Orth and Karin Seidl. **(D)** NW457-dependent induction of ATM, ATR, CHK1, CHK2, and p53 mRNA expression was measured by quantitative real-time PCR 0-48 h after stimulation with 10 nM. For each gene, data were normalized on 18S mRNA and calibrated on the 0 h control. Transcriptional regulation is depicted as heat map encoding upregulation in red and downregulation in blue. The fold change is shown as \log_{10} . qPCR analyses were kindly provided by Michael Orth and Karin Seidl.

6.2.4 Inhibition of HSP90 by NW457 decreases the migratory potential of LN229 glioblastoma cells

One major cause for the high malignancy of glioblastomas is their extensively invasive phenotype. Active glioma invasion is initiated by cell detachment from the original tumor site and followed by attachment to extracellular matrix (ECM) proteins which are subsequently degraded by tumor secreted proteases. This creates intracellular space into which invading glioma cells can finally migrate by cytoskeletal contraction. A prerequisite for these processes is the coordination of complex intracellular and extracellular mechanisms. As HSP90 and some of its client proteins are discussed to be involved in regulating tumor cell migration and invasion (Annamalai et al., 2009; Gopal et al., 2011; Zagzag et al., 2003), the migratory potential of glioblastoma cells was investigated in response to NW457 treatment in transwell migration assays.

For this purpose, the LN229 cell line was chosen as microscopic analyses of the colony structure in clonogenic survival assays suggested that these cells might be intrinsically more motile than T98G cells (data not shown). LN229 cells were exposed to 0-50 nM NW457 for 24 h and applied to Boyden chamber transmigration assays with either 0% FCS in the upper and 10% FCS in the lower chamber, or with 10% FCS in the upper and 10% FCS in the lower chamber, respectively. After 12 h the percentage of cells that had migrated through the filter was determined. As shown in Figure 19A, the percentage of migrating LN229 cells was higher in the presence of a serum gradient compared to the setting with 10% FCS in both chambers. Intriguingly, exposure to NW457 clearly decreased the transmigration of LN229 cells in a dose-dependent manner irrespective of

the presence of a serum gradient. Of note, this was not due to toxic effects of NW457, since Alamar Blue viability tests performed in parallel revealed that even in the presence of 50 nM NW457 the viability of LN229 cells was >90%, due to the relatively short exposure of 24 h (Figure 19B).

These data indicate an anti-migratory effect of NW457 on human glioblastoma cells, which - together with its pro-apoptotic and clonogenic survival inhibiting effects - strengthens its perspective as potent antitumor agent.

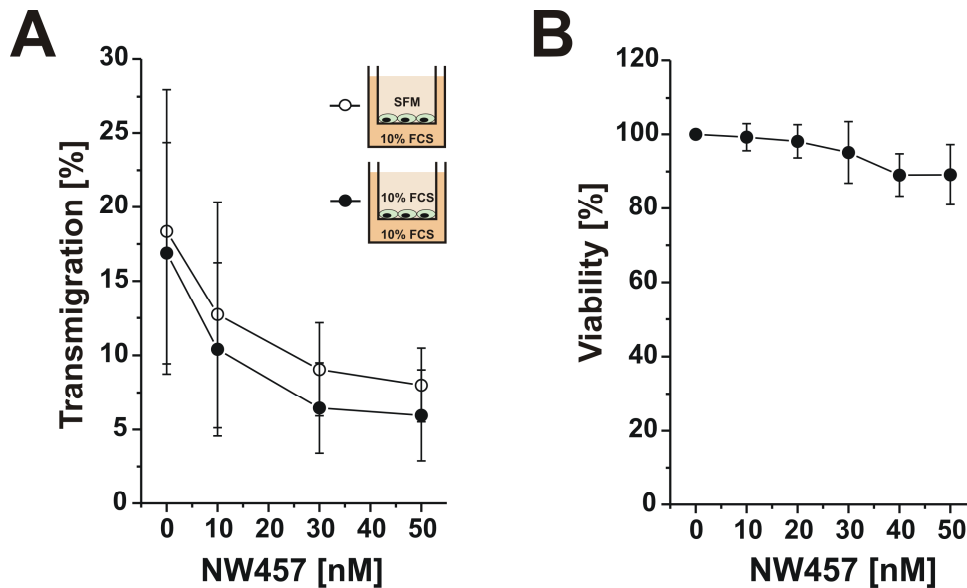


Figure 19. NW457 impairs the trans migratory potential of glioblastoma cells at non-toxic concentrations.

LN229 cells were fluorescently labelled with PKH67, exposed to 0-50 nM NW457 for 24 h, and applied to Boyden chamber transmigration assays. In parallel, viability was assessed by Alamar Blue assays. **(A)** Transmigration assays were performed with either 0% FCS in the upper and 10% FCS in the lower chamber or with 10% FCS in the upper and 10% FCS in the lower chamber, respectively. After 12 h, cells adherent to the lower side of the filter were lysed, and the percentage of transmigrated cells was calculated from the resulting fluorescence intensity using a standard curve. Data represent means \pm SD of four independent experiments. **(B)** Viability of LN229 cells was measured 24 h after stimulation with 0-50 nM NW457. Alamar Blue reduction was calibrated on DMSO-treated control cells (100% viability), and means \pm SD of three independent experiments are shown.

6.2.5 Irradiation-induced hypermigration of glioblastoma cells is inhibited by NW457

Having shown that NW457 dose-dependently reduces the basal migratory potential of LN229 cells, the impact of NW457 on possibly irradiation-induced hypermigration was examined in wound healing assays. Enhanced glioma cell migration has repeatedly been reported in response to photon irradiation *in vitro* (Badiga et al., 2011; De Bacco et al., 2011; Kil et al., 2012; Wild-Bode et al., 2001), thus providing - at least in part - a possible

explanation for the limited therapeutic efficacy of radiotherapy in glioblastoma and the frequently observed tumor recurrence afterwards.

LN229 cells were seeded in special 2D invasion assay devices, irradiated with 0-3 Gy, and exposed to 0-30 nM NW457 for 24 h. Afterwards, the silicon-strip culture dish inserts were removed, thus generating cell-free “wounds” of approximately 500 μm in width, and the wound healing process was microscopically monitored for 12 h. Individual trajectory plots of the cells at the migrating front were generated, and the colonized area as well as the average accumulated distance per cell were calculated. As illustrated in Figure 20A, irradiation with 3 Gy significantly increased the inherent motility of LN229 cells, resulting in pronounced migration into the wound. Intriguingly, concomitant exposure to NW457 potentially abrogated irradiation-induced hypermigration as shown by a significant reduction in the colonized area (Figure 20B). Regarding the average accumulated distance per cell, irradiated LN229 cells revealed approximately 2.5-fold longer distances compared to non-irradiated, DMSO-treated control cells (Figure 20C). Additional NW457 treatment significantly inhibited irradiation-induced hypermigration, although it obviously did not interfere with the basal migratory activity as measured by the colonized area and the average accumulated distance of non-irradiated cells, respectively.

Comparing the results obtained from transmigration assays with those from wound healing assays, astonishingly, 30 nM NW457 induced a decrease in basal migration of LN229 cells only in transmigration assays and not in wound healing assays which might be attributed to the different experimental settings.

Taking together both the data of transmigration and wound healing assays, NW457 seems to interfere with both inherent migration and irradiation-induced hypermigration of human glioblastoma cells, which strengthens its perspective as potent antitumor agent and particularly as novel candidate for anti-invasive glioblastoma therapies.

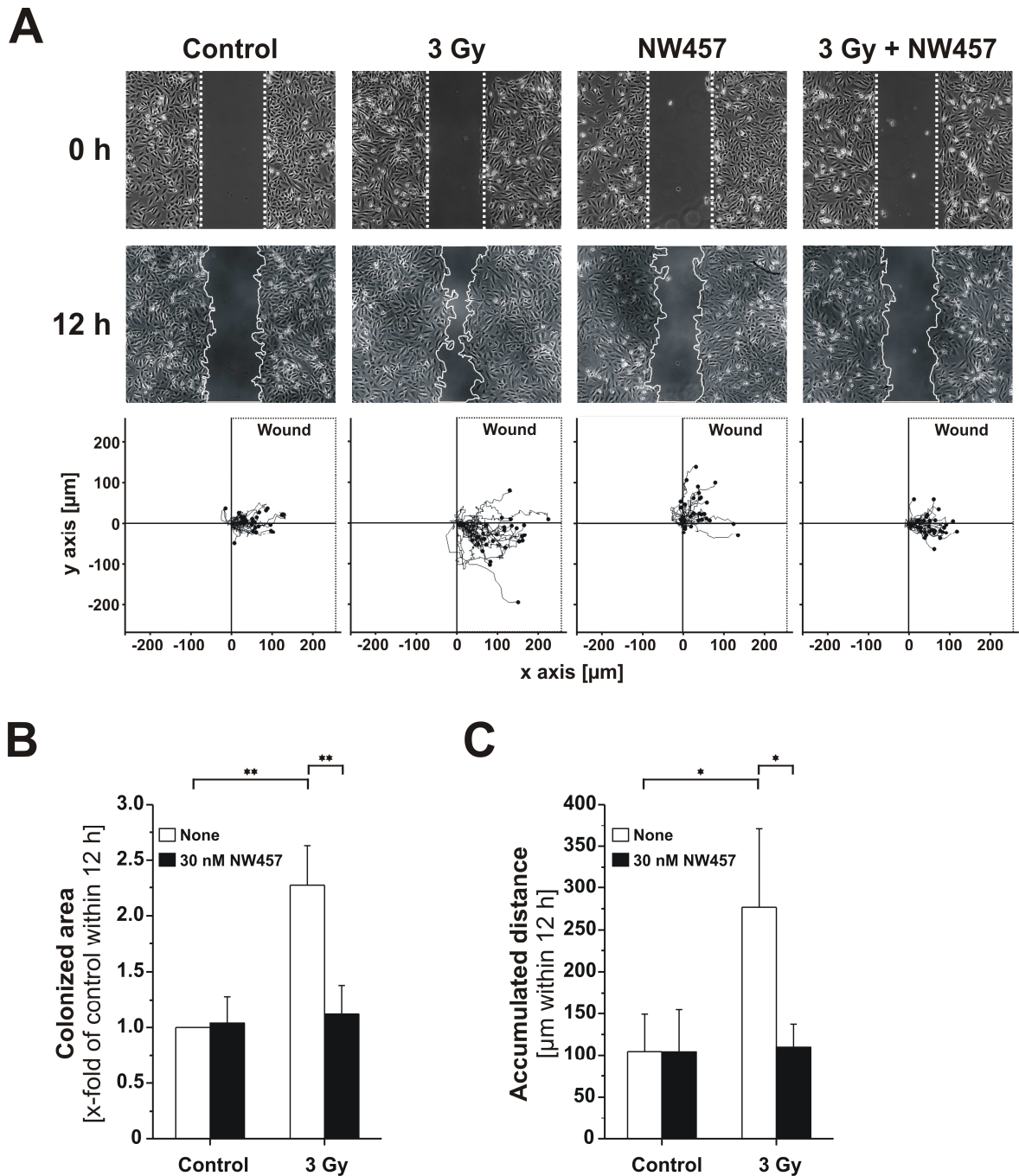


Figure 20. NW457 abrogates irradiation-induced hypermigration of glioblastoma cells.

LN229 cells were simultaneously exposed to 0-30 nM NW457 plus 0-3 Gy irradiation for 24 h, and their migratory potential was studied over a period of 12 h in wound healing assays. **(A)** Upper and middle row: Representative photographs of cell migration into the wounds (cell-free gaps) 0 and 12 h after removing the silicon-strip culture dish inserts. Lower row: Individual trajectory paths of at least 25 randomly selected cells per wound located at the left wound boarder at time point 0 h. **(B)** The area that had been colonized within 12 h in the presence or absence of NW457 +/- IR was quantified by analyzing the photographs at time points 0 and 12 h, respectively. Data represent means \pm SD of three independent experiments. ** $p < 0.05$. **(C)** The accumulated distance per cell in response to NW457 or vehicle +/- IR was determined based on the individual migration paths depicted in (A). Values represent means \pm SD of at least 25 randomly selected cells per treatment condition; * $p < 0.01$.

6.2.6 Analysis of potential mechanisms associated with LN229 migration patterns in response to HSP90 inhibition and irradiation

In a first attempt to illuminate potential mechanisms that might account for the migration patterns of LN229 cells observed in response to NW457 +/- irradiation in transmigration and wound healing assays, the expression of different candidates that had previously been discussed to modulate glioma cell invasion and migration was analyzed. Although numerous proteins are involved in supporting the invasive nature of glioblastomas, much attention has been drawn to members of the integrin family, the MET/HGF (hepatocyte growth factor) axis, as well as the Eph receptor/ephrin ligand system.

Integrins represent an important group of transmembrane adhesion molecules that are organized as dimers of 18 different alpha and 8 beta subunits and predominantly promote the attachment of the cell to the extracellular matrix (ECM). Enhanced expression of different integrins including $\alpha\beta3$ and $\alpha\beta5$ was found to correlate with increased invasiveness and migration of glioma cells and is believed to be associated with irradiation-induced hypermigration (Monferran et al., 2008; Wild-Bode et al., 2001). Enhanced migration in response to ionizing radiation is also supposed to be governed by aberrant expression of the oncogenic MET receptor and its ligand HGF (hepatocyte growth factor) (Buchanan et al., 2011; De Bacco et al., 2011). Notably, expression of the MET/HGF axis has been found to correlate with the grade of malignancy (Athauda et al., 2006; Koochekpour et al., 1997; Rosen et al., 1996). Another receptor/ligand system that is involved in glioblastoma migration is the Eph receptor/ephrin ligand family which represents the largest family of receptor tyrosine kinases with 14 Eph receptors (EphA1-A8, EphA10, EphB1-B4, and EphB6) and 8 ligands (ephrin A1-A5 and ephrin B1-B3) identified (Lemke, 1997; Pasquale, 2010). Upregulation of Eph receptors including EphA2 and EphB2 in glioblastoma cells and their association with migration, invasion, metastatic potential, and adverse outcome has been repeatedly reported (Liu et al., 2006; Nakada et al., 2004; Nakada et al., 2005; Wang et al., 2008; Wykosky et al., 2005).

In order to elucidate whether these candidates are responsible for (i) NW457-mediated decrease in cell migration as was observed in transmigration assays and (ii) irradiation-induced hypermigration and its reversal by NW457 as was observed in wound healing assays, LN229 cells were exposed to 0-50 nM NW457 +/- 0-3 Gy for the indicated time periods and subjected to expression analyses of integrins $\alpha\upsilon$, $\beta3$, and $\beta5$, MET, phospho-MET, and HGF, as well as EphA2, EphB2, and EphB3 by flow cytometry, Western blot, or qPCR. First, the potential involvement of integrins $\alpha\beta3$ and $\alpha\beta5$ in LN229 cell migration was examined. As shown in Figure 21A, the surface expression of $\alpha\beta3$ and $\alpha\beta5$ remained unaffected both after irradiation and NW457 treatment. In addition, mRNA levels of $\alpha\upsilon$, $\beta3$, and $\beta5$ were analyzed 0, 6, 12, and 24 h after stimulation. Neither irradiation nor

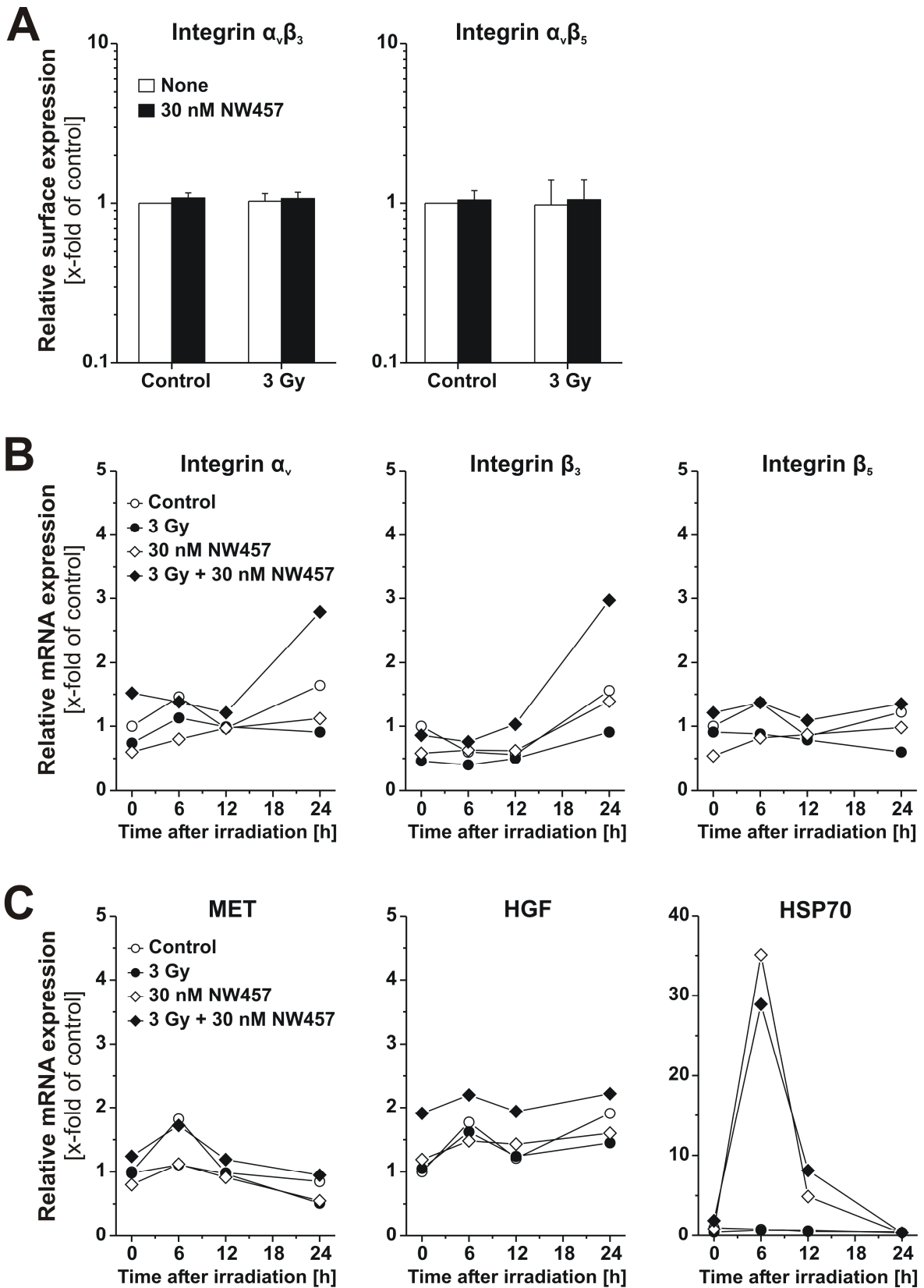
NW457 alone did markedly change integrin transcription. Surprisingly, combined treatment enhanced mRNA expression of integrins αv and $\beta 3$ 24 h after stimulation (Figure 21B), but this cannot explain reduced migration in the combined treatment group as compared to the irradiation only group. This suggests that irradiation-induced hypermigration and NW457-mediated decrease of transmigration are probably mediated by other molecular mechanisms.

Next, the potential involvement of the MET/HGF axis in LN229 cell migration was analyzed in response to irradiation and NW457 treatment. qPCR analyses revealed only marginal induction of MET and HGF transcription (Figure 21C). Since the activation of the MET receptor is largely regulated by HGF stimulation with subsequent receptor phosphorylation, but potentially also by other growth factors that are present in FCS, LN229 cells were grown in the presence or absence of 10% FCS or 10 ng/ml HGF, respectively, and protein levels of total MET and phosphorylated MET were analyzed in Western blots (Figure 21D). It was hypothesized that irradiation might enhance phosphorylation of MET and therefore promote hypermigration of LN229 cells in wound healing assays. In the presence of 10% FCS, irradiation with 3 Gy slightly augmented MET receptor phosphorylation (Figure 21D). Irradiation with a higher dose (8 Gy) clearly increased the expression of total MET and possibly might have involved receptor phosphorylation at later time points. Interestingly, exposure to 30 nM NW457 slightly decreased the level of total MET under serum-free conditions and clearly reduced receptor phosphorylation. Together these data suggest a potential involvement of the MET/HGF axis in LN229 cell migration. However, further investigation is required for precise elucidation.

In order to examine a potential role of different ephrin receptors in LN229 migration, the surface expression of EphA2, EphB2, and EphB3 was analyzed in response to NW457 treatment in the presence and absence of irradiation. Interestingly, exposure to NW457 dose-dependently induced the decline of all three ephrin receptors (Figure 21E), thus providing a possible mechanistic explanation for the observed decrease in LN229 cell migration in transmigration assays. Interestingly, Eph receptor expression was not increased in response to irradiation, although it might have been expected due to the LN229 migration pattern observed in wound healing assays. Instead, combined exposure to NW457 plus IR induced similar effects compared to stimulation with NW457 only, as it dose-dependently reduced the surface expression of all three Eph receptors. However, it is possible that irradiation provokes LN229 hypermigration via ephrin ligand-mediated Eph receptor phosphorylation. In this context, EphB2 stimulation using the high-affinity ligand ephrin B1 was reported to enhance cell migration and invasion of U87 glioma cells,

whereas treatment with a blocking EphB2 antibody inhibited the cellular motility (Nakada et al., 2004).

Collectively, these data hint at an involvement of both MET/HGF and Eph receptor signaling in LN229 cell migration and thus provide a possible explanation - at least in part - for the migration patterns observed in transmigration and Boyden chamber assays in response to NW457 and irradiation. The data suggest that irradiation might promote hypermigration of glioblastoma cells - at least in part - through activation of the MET/HGF axis and that targeting HSP90 via the novel small-molecule inhibitor NW457 might reduce glioblastoma cell motility through downregulation of the ephrin receptors EphA2 and EphB3. In addition, other molecular mechanisms might be involved and further investigations are required for precise elucidation.



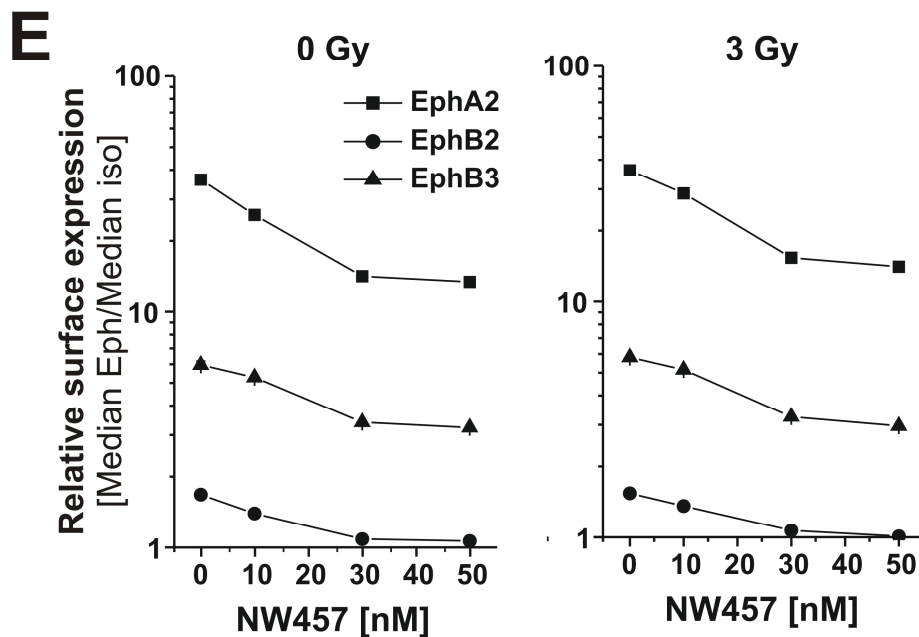
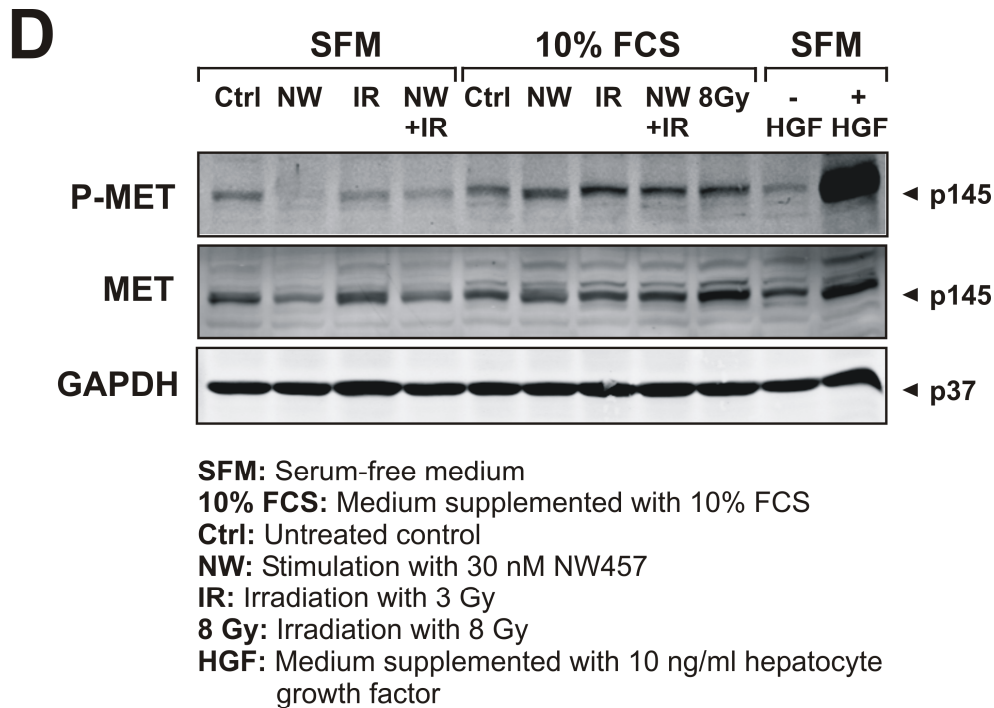


Figure 21. Analysis of potential mechanisms associated with glioma cell migration patterns in response to HSP90 inhibition and irradiation.

LN229 cells were concomitantly exposed to 0-3 Gy irradiation plus 0-50 nM NW457 for the indicated time periods and subjected to mRNA and protein expression analyses of different candidates supposed to be involved in glioma cell migration. **(A)** Relative surface expression of integrins $\alpha\beta 3$ and $\alpha\beta 5$ was analyzed by flow cytometry 24 h after stimulation and is depicted as x-fold increased expression compared to untreated control cells. Means \pm SD of four independent experiments are shown. **(B)** Relative mRNA expression of integrins α_v , β_3 , and β_5 was analyzed by quantitative real-time PCR 0, 6, 12, and 24 h after stimulation and is depicted as x-fold expression of the untreated control. **(C)** Relative mRNA expression of MET, HGF, and HSP70 (positive control for NW457 stimulation) was analyzed by quantitative real-time PCR 0, 6, 12, and 24 h after treatment and is shown as x-fold expression of untreated control cells. **(D)** For Western blot

Results

analyses of MET and phospho-MET, LN229 cells were cultured in serum-free medium (SFM) or medium supplemented with 10% FCS, respectively. Cells were stimulated with 0-3 Gy irradiation plus 0-30 nM NW457 for 24 h or irradiated with 8 Gy only. Stimulation with 10 ng/ml HGF for 2 h was used as positive control for MET receptor phosphorylation. 120 µg protein per lane were utilized for Western blotting. **(E)** Relative surface expression of ephrin receptors EphA2, EphB2, and EphB3 was analyzed by flow cytometry 24 h after stimulation. Data are means \pm SD of three intra-assay replicates.

7 Discussion

7.1 HSP90 - an unlikely but promising drug target for anticancer therapies

HSP90 did at first sight appear to be an unusual and unlikely anticancer drug target when it was introduced in the early 1990s. Targeting a housekeeping protein which is abundantly expressed not only in tumor but also in non-malignant cells and which is indispensable for cell viability was viewed with skepticism. Targeting HSP90 with small-molecule inhibitors was thus suspected to cause unacceptable toxicity in normal tissue and limit the therapeutic benefit.

In the meantime, however, HSP90 has emerged as a promising anticancer drug target with 17 distinct pharmacological inhibitors having entered about 90 clinical trials (<http://clinicaltrials.gov>). The clinical success of HSP90 inhibitors will strongly depend on the therapeutic window which is defined as the range of drug dosage that elicits a therapeutically effective response without inducing unacceptable adverse effects. Thus, the therapeutic window of an HSP90 inhibitor depends on its selectivity for tumor cells over non-malignant cells. Notably, tumor cells were repeatedly shown to be more sensitive to HSP90 inhibitors than non-transformed cells (He et al., 2006; Kamal et al., 2003; Llauger et al., 2005; Plescia et al., 2005; Whitesell et al., 1992) and comparative *in vitro* studies with normal fibroblasts and tumor cells revealed that the radiosensitizing effects of different HSP90 inhibitors were restricted to tumor cells (Bisht et al., 2003; Noguchi et al., 2006; Russell et al., 2003). Furthermore, non-toxic inhibitor concentrations demonstrated potent antitumor activity *in vivo* (Biamonte et al., 2006; Plescia et al., 2005; Vilenchik et al., 2004) and several studies indicated that HSP90 inhibitors preferentially accumulate in the tumor tissue whereas they are rapidly cleared from the plasma and do not concentrate in normal tissues (Eiseman et al., 2005; Sydor et al., 2006; Vilenchik et al., 2004).

Different potential mechanisms are discussed to explain why pharmacological HSP90 inhibitors are preferentially effective in tumor cells compared to non-malignant cells. Firstly, it is assumed that HSP90 is overexpressed in tumor cells due to elevated environmental stresses, such as nutrient stress, proteotoxic stress, hypoxia, and genetic instability, which are associated with the malignant “lifestyle” (Neckers and Workman, 2012). Secondly, it has been proposed that in tumor cells HSP90 exists in an activated form with higher ATPase activity and a 100-fold higher affinity for the inhibitor 17-AAG, whereas HSP90 in normal cells appears in an inactivated, uncomplexed form with lower ATP binding affinity (Kamal et al., 2003). Thirdly, since tumor cell HSP90 was shown to be localized not exclusively in the intracellular milieu, but also on the cell surface and

secreted into the extracellular space, it has been hypothesized that this ectopic expression of HSP90 may promote tumor selectivity of HSP90 inhibitors (Becker et al., 2004; Eustace et al., 2004). Whereas tumor cells constitutively secrete HSP90, normal cells secrete the chaperone only in response to environmental stress (Cheng et al., 2008). Hence, ectopically expressed HSP90 appears to be a tumor-specific drug target.

Taken together, these findings illustrate why HSP90 has emerged as a potent antitumor drug target and may explain - at least in part - the enhanced tumor selectivity of HSP90 inhibitors, even though the entire mechanism has probably not yet been fully elucidated.

7.2 Potential benefits of NW457 in the therapy of colorectal carcinomas and glioblastomas

In the present work, the antitumor potential of the novel pochoxime HSP90 inhibitor NW457 was characterized for the first time in combination with ionizing radiation in preclinical models of colorectal cancer and glioblastoma multiforme. In the following section, the necessity for novel therapy concepts for colorectal carcinomas and glioblastomas is analyzed and the potential benefits of NW457 thereby, are discussed.

Colorectal cancer is the third most common type of cancer in men (664,000 new cases per year, 10.0% of the total) and the second in women (571,000 cases per year, 9.4% of the total) worldwide. Although the development of new treatment options has led to a considerable improvement in the outcome of colorectal cancer in the past years, approximately 609,000 deaths from colorectal cancer per year are estimated worldwide, accounting for 8.1% of all cancer-related deaths and rendering it the fourth most frequent cause of death from cancer (GLOBOCAN 2008, <http://globocan.iarc.fr>).

Surgery is usually the main treatment option for colorectal carcinomas and commonly combined with conventional chemotherapies, such as 5-FU (or the prodrug capecitabine), folinic acid, oxaliplatin, and irinotecan, which are administered in various regimes either as neoadjuvant (before surgical resection) or adjuvant (after surgery) treatment. Radiotherapy is a common treatment modality for cancers of the descending colon (rectal cancer) and implemented either as neoadjuvant or adjuvant therapy (Glimelius, 2002). For cancers of the ascending and transverse colon, however, the delivery of high IR doses is problematic due to the high mobility of these parts and the high sensitivity of the surrounding structures (e.g. small bowel, kidney, and liver) (Moser et al., 2009). However, radiotherapy provides a therapeutic option for certain high-risk subsets of colon cancer patients associated, e.g., with advanced tumor stages, tumor location in immobile sites, local perforation, or residual disease after surgery (Schild et al., 1997; Willett et al., 1993; Willett et al., 1999).

In addition to surgery, conventional chemotherapy, and irradiation, in the last years targeted EGF-R and VEGF-R therapies have emerged and are currently being investigated in combination with conventional chemotherapeutic agents, predominantly in patients with metastatic colorectal carcinomas (Rodriguez et al., 2007). Nevertheless, there is still substantial need for novel treatment options, since therapies targeting the EGF-R are mostly not effective in patients harboring KRAS or BRAF mutations (Cercek and Saltz, 2011). Notably, KRAS is mutated in up to 50% and BRAF in approximately 5-10% of all colorectal carcinomas (Bazan et al., 2005), leading to constitutive activation of these oncoproteins and persistent stimulation of tumor-promoting downstream signaling pathways, including the RAF/MEK/ERK and PI3K/AKT/mTOR cascades. Besides aberrant RAS/RAF signaling, mutations of the tumor suppressor p53 frequently occur in colorectal carcinomas. Approximately 45% of colorectal tumors harbor mutations in the *TP53* gene, and loss of functional p53 is known to be associated with an increased incidence of hepatic metastasis as well as disease progression, thus correlating with worse survival (Bazan et al., 2005; Iacopetta, 2003; Kastrinakis et al., 1995; Russo et al., 2005).

Since HSP90 promotes the stability of a broad range of oncogenic signaling proteins including mutant KRAS, BRAF, and p53 (Acquaviva et al., 2012; Azoitei et al., 2012; Blagosklonny et al., 1996; Blagosklonny et al., 1995; Da Rocha Dias et al., 2005; Fukuyo et al., 2008; Grbovic et al., 2006; Nagata et al., 1999; Sos et al., 2009; Whitesell et al., 1998), colorectal carcinomas are of particular interest with respect to HSP90 inhibitors. Inhibition of the chaperone represents a multifaceted approach and might therefore provide a promising treatment strategy for colorectal carcinomas including KRAS, BRAF, and p53 mutant subtypes.

Glioblastoma multiforme is the most frequent primary brain tumor in adults and represents the most aggressive and lethal glial neoplasm. Glioblastomas are characterized by an extremely infiltrative and highly progressive phenotype which makes them very difficult to control and usually prevents surgical cure. The standard of care therapy involves surgical resection, if possible, radiotherapy, and systemic chemotherapy with DNA-alkylating agents, such as temozolomide (TMZ). However, the outcome remains rather poor as patients frequently suffer from resistance to radiochemotherapy and tumor recurrence. Moreover, the response rate to TMZ therapy is limited since the sensitivity towards TMZ is suggested to depend on the promoter status of the *O*-6-methylguanine-DNA methyltransferase (MGMT) gene and an unmethylated, activated promoter is supposed to be a predictor for a worse therapeutic outcome (Esteller et al., 2000; Hegi et al., 2004; Hegi et al., 2005). The efficacy of radiotherapy plus concomitant and adjuvant TMZ therapy versus radiotherapy only was recently evaluated in a Phase III trial indicating that combined radiochemotherapy increases the median survival time compared to

radiotherapy alone (14.6 months versus 12.1 months) and significantly prolongs the 5-year overall survival (9.8% versus 1.9%) (Stupp et al., 2009; Stupp et al., 2005). However, as the survival times indicate, more effective treatment concepts are strongly needed to overcome the aggressive and lethal nature of glioblastomas.

One promising approach to target treatment resistant and infiltrative phenotypes of glioblastomas might be the involvement of molecularly targeted therapies into current treatment concepts. Since GBMs are driven by a multitude of different genetic aberrations and deregulated oncogenic signaling pathways, it is unlikely that any single agent targeting only one of these critical factors will be efficient in more than a subset of glioblastoma patients. Therefore, a multitarget approach that addresses several GBM pathways simultaneously appears to be a superior strategy. Targeting HSP90 via small-molecule inhibitors of the second generation, such as NW457, represents such a multifaceted approach and the combination with standard radiochemotherapy might provide a promising perspective for glioblastomas. Since multiple HSP90 client proteins are supposed to regulate signaling pathways associated with GBM radioresistance and invasiveness, the involvement of HSP90 inhibitors into novel GBM treatment concepts raises hope to potently attenuate both radioresistant and invasive phenotypes of this disease. Notably, both HSP90 inhibitors and radiotherapy are supposed to selectively induce their cytotoxic effects on tumor cells while sparing non-malignant tissues. Hence, therapeutic approaches in which pharmacological HSP90 inhibition is combined with radiotherapy may result in selective and synergistic tumor radiosensitization.

7.3 HSP90 inhibitor-induced apoptosis and the dispensability of p53

In the present work, HSP90 inhibition by NW457 was shown to induce apoptotic cell death in human colorectal cancer and glioblastoma cells in a concentration- and time-dependent manner. The apoptotic effects were enhanced upon combination with ionizing radiation as demonstrated by increased formation of hypodiploid nuclei and activation of the caspase cascade with subsequent PARP cleavage. Induction of apoptotic cell death as a result of pharmacological HSP90 inhibition has been demonstrated also for other small-molecule inhibitors, such as SNX-2112, geldanamycin, BIIB021, and NVP-AUY922, and shown to be associated with caspase activation and PARP cleavage, mitochondrial release of cytochrome c and AIF (apoptosis inducing factor), as well as downregulation of the anti-apoptotic proteins BCL-2 and BCL-xL (McNamara et al., 2012; Nomura et al., 2004; Stingl et al., 2010; Wang et al., 2011; Yin et al., 2010).

The tumor suppressor p53 functions as a “molecular node” in the DNA damage response and plays an important role in the regulation of cell cycle arrest, DNA repair, and

apoptosis (Sengupta and Harris, 2005). Interestingly, cancer cells deficient in p53 do not necessarily lose their ability to undergo apoptotic cell death as demonstrated in the present work. Functional p53 was not essential for NW457-mediated apoptosis induction, as caspase activation and the formation of hypodiploid nuclei were also observed in p53-deficient colorectal cancer cells and the p53-mutant glioblastoma cell line T98G. Given the fact that p53 is one of the most commonly mutated genes in human cancers and mutated or lost in up to 50% of colorectal cancers (Bazan et al., 2005; Lopez et al., 2012; Naccarati et al., 2012), the present findings are of specific clinical relevance as they suggest that NW457-based therapies may also be efficient in tumor subtypes lacking functional p53.

On the molecular level, there are several potential mechanisms how tumor cells can trigger p53-independent apoptosis in response to DNA damage. One of these involves the pro-apoptotic cell cycle regulator p14 ARF which in this work was shown to be constitutively upregulated in p53-deficient, but not in p53-proficient HCT116 cells, and which was previously discussed to induce mitochondrial apoptosis in a BAK dependent manner (Hemmati et al., 2006). The involvement of BAK in p53-independent apoptosis might also account for NW457-mediated apoptosis induction since the BCL-2 family member is strongly expressed in HCT116 cells and previous studies in gastric cancer cells demonstrated that BAK overexpression triggers activation of caspase-3 and provokes apoptotic cell death independent of functional p53 (Tong et al., 2004).

Another possible mechanism that may be implicated in NW457-mediated, p53-independent apoptosis induction involves the activation of the p53-related proteins p63 and p73. Both exhibit p53-like properties and are able to activate the transcription of typical p53-responsive genes, such as p21, BAX, NOXA, and PUMA, finally leading to cell cycle arrest and/or programmed cell death (Flinterman et al., 2005; Melino et al., 2004; Yang et al., 1998; Zhu et al., 1998). It has been proposed that upon DNA damage in the absence of p53 the checkpoint kinases CHK1 and CHK2 activate the transcription factor E2F1, which in turn activates the transcription of p73, thus giving rise to increased levels of this p53 homologous protein (Marabese et al., 2003; Stiewe and Putzer, 2000; Urist et al., 2004). The involvement of p73 in regulating apoptosis in tumor cells lacking functional p53 was repeatedly described (Cai et al., 2012; Irwin et al., 2000; Oniscu et al., 2004; Rana et al., 2010; Stiewe and Putzer, 2000) and thus may also account for NW457-mediated cell death of HCT116 p53^{-/-} cells.

In addition, Gurley and colleagues proposed another mechanism for p53-independent apoptosis induction as they demonstrated that the apoptotic defect of p53-deficient cells in response to IR-induced DNA damage can be rescued by inactivation of any of the three

subunits (catalytic subunit, Ku80, and Ku70, respectively) of the DNA-PK (DNA-dependent protein kinase) (Gurley et al., 2009). This mechanism might be of particular interest in the context of HSP90 inhibition since NVP-AUY922 and 17-DMAG were shown to reduce the levels of total DNA-PKcs (DNA-PK catalytic subunit) and its phosphorylation, respectively, consequently compromising the repair of DNA double-strand breaks by non-homologous end joining (NHEJ) (Dote et al., 2006; Ha et al., 2011). Hence, inactivation of the DNA-PKcs by HSP90 inhibitors may provide a therapeutic option to drive p53-deficient tumor cells into apoptotic cell death and might account, at least partially, for NW457-mediated apoptosis induction and radiosensitization of HCT116 p53 ^{-/-} cells in the present work.

7.4 Potential mechanisms underlying clonogenic cell death upon HSP90 inhibition

Clonogenic survival is considered as one of the most relevant *in vitro* endpoints to predict the *in vivo* antitumor efficacy of ionizing radiation in the presence or absence of pharmacological agents. The radiosensitizing potential of NW457 was therefore investigated in clonogenic survival assays both in colorectal cancer and glioblastoma cell lines. The experiments revealed that exposure to NW457 enhanced radiation-induced clonogenic cell death of colorectal carcinoma cells and that this was practically independent of the cellular p53 and BAX status. Moreover, studies in LN229 and T98G cells revealed that the radiosensitizing effects of NW457 were more pronounced when the cells were subjected to a treatment regimen with 24 h drug preincubation before irradiation compared to simultaneous NW457/IR treatment. These findings indicate that the sequence of pharmacological HSP90 inhibition and irradiation influences the tumoricidal efficacy of NW457. Therefore, I hypothesized that preincubation with NW457 prior to irradiation might affect the DNA damage response (DDR) and prevent efficient DNA repair upon irradiation, hence culminating in enhanced radiosensitization and clonogenic cell death. Indeed, Western blot analyses revealed that NW457 time-dependently induced the depletion of the DDR-associated kinases ATM, CHK1, and CHK2. Importantly, the protein levels were already diminished within 12-24 h upon NW457 treatment. This suggests that in clonogenic survival assays, preincubation with NW457 presumably provoked the degradation of ATM, CHK1, and CHK2 before the cells were irradiated and that this might account for the enhanced radiosensitivity of LN229 and T98G cells. In contrast to the preincubation setting, concomitant exposure to NW457 and IR limited the radiosensitizing efficacy of the HSP90 inhibitor, presumably because it did not affect the DDR at the time point of irradiation, but at the earliest 12-24 h afterwards

when the majority of IR-induced DNA damage had probably already been repaired. Taken together, the findings indicate that the tumoricidal activity of NW457 is attributed - at least in part - to its compromising effects on the DNA damage response and that the sequence of combining HSP90 inhibitors with irradiation influences the therapeutic efficiency.

According to the findings in the present work, there is accumulated evidence in the literature arguing for an important role of HSP90 in the DNA damage response. A multitude of studies showed that targeting HSP90 with small-molecule inhibitors induces the destabilization of different DDR-regulatory proteins, such as ATM, ATR, CHK1, CHK2, DNA-PK, RAD51, BRCA1, BRCA2, and FANCA (Arlander et al., 2003; Dote et al., 2006; Dungey et al., 2009; Ha et al., 2011; Ko et al., 2012; Koll et al., 2008; Noguchi et al., 2006; Stecklein et al., 2012; Zaidi et al., 2012). Studies by Noguchi and colleagues in prostate carcinoma and lung squamous cell carcinoma cell lines revealed that exposure to 17-AAG diminishes the levels of RAD51 and BRCA2, which are involved in the repair of DSBs by homologous recombination (HR) (Noguchi et al., 2006). These findings are in line with the data of a recent study in NSCLC models demonstrating that 17-AAG mediates the downregulation of RAD51 both on the protein and mRNA level (Ko et al., 2012). In addition to homologous recombination, which is restricted to S and G2 phase, DSBs can be repaired throughout the cell cycle by non-homologous end joining (NHEJ). This pathway might also be affected by pharmacological HSP90 inhibition as studies by Dote and colleagues indicated that the activation of the DNA-PKcs is decreased upon 17-DMAG treatment (Dote et al., 2006). Collectively, these studies suggest that HSP90 is critically involved in the regulation of DSB repair and that inhibition of HSP90 may provide a promising strategy for tumor cell radiosensitization.

Moreover, the base excision repair pathway (BER), which recognizes and removes small base adducts, such as oxidized, reduced, alkylated, or deaminated bases, is suggested to rely on HSP90 function, since exposure to 17-DMAG prior to irradiation was shown to suppress IR-induced activation of two BER key enzymes, the apurinic/apyrimidinic endonuclease 1 (APE1) and the DNA polymerase- β (Pol- β) (Koll et al., 2008).

Collectively with the data of the present work, accumulated evidence argues for an important role of HSP90 in the DNA damage response and together they provide interesting insights of how HSP90 inhibitors exert their radiosensitizing effects on tumor cells.

The colony formation assays in the present work further revealed that HSP90 inhibition by NW457 may be a promising therapeutic option also for tumors driven by activating KRAS mutations. This is in line with previous studies indicating that KRAS mutations may predict sensitivity to the HSP90 inhibitors 17-AAG and ganetespib (STA-9090) in NSCLC models

(Acquaviva et al., 2012; Sos et al., 2009). Moreover, in a recent Phase II monotherapy trial, ganetespib induced tumor shrinkage in 47% of patients with advanced NSCLC harboring KRAS mutations (Acquaviva et al., 2012), thereby suggesting that HSP90 inhibition may offer new promise for this subtype of patients. First mechanistic insight of how HSP90 inhibitors might address KRAS mutant tumors was recently given by Azoitei and colleagues, who investigated the potency of the HSP90 inhibitors 17-AAG and PU-H71 in breast, lung and colon carcinoma cell lines including HCT116 and Caco-2 cells with specific focus on their KRAS status (Azoitei et al., 2012). Drug efficacy studies revealed a higher sensitivity towards HSP90 inhibitors in the case of KRAS mutant cells (e.g. HCT116) compared to KRAS wild-type cells (e.g. Caco-2). The authors attributed the increased sensitivity to a vital dependence of the mutants on STK33, a serine/threonine kinase that was identified as a novel client protein of HSP90 and therefore as a context-dependent therapeutic target in KRAS-driven tumors. However, the precise mechanism underlying the addiction of KRAS mutant tumor cells on STK33 needs further clarification, since different studies yielded conflicting findings in this regard (Babij et al., 2011; Frohling and Scholl, 2011; Luo et al., 2012; Scholl et al., 2009)

In line with my findings on p53-independent induction of clonogenic cell death, also other studies reported that p53 is dispensable for HSP90 inhibitor-induced clonogenic cell death (Koll et al., 2008; Moran et al., 2008; Zaidi et al., 2012). Potential mechanisms through which HSP90 inhibitors, such as geldanamycin, 17-DMAG, and NVP-AUY922, may exert their cytotoxic effects in p53-deficient cells have been discussed in the literature. Moran and colleagues suggested that in p53-deficient cells geldanamycin abrogates irradiation-induced G2 arrest and induces premature mitotic entry (Moran et al., 2008). The authors found that exposure to geldanamycin induced a decrease in the G2 regulatory proteins CHK1 and WEE1 and observed aberrant mitotic phenotypes and micronucleation in these cells. They concluded that p53-negative cells might undergo clonogenic cell death by mitotic catastrophe. This mechanism might also play a role in NW457-mediated radiosensitization of p53-deficient HCT116 cells and p53-mutant T98G cells in the present work and has to be elucidated in further studies.

7.5 Tolerability of HSP90 inhibitors by hepatocytes

As described in section 7.1 the clinical success of NW457 and other HSP90 inhibitors will strongly depend on their therapeutic window. In addition to potential general toxicities on normal tissue, severe hepatotoxicity may also preclude the *in vivo* application of novel small-molecule inhibitors. Therefore, potential cytotoxic effects of NW457 on primary hepatocytes were examined in the present work. In strong contrast to geldanamycin which

clearly perturbed the typical hepatocellular morphology and severely reduced the viability, NW457 did not induce any characteristics of hepatocytotoxicity. These findings are in line with data published for the NW457 relative pochoxime A whose hepatotoxicity was previously investigated *in vivo* (Wang et al., 2009). Whereas high serum levels of the prototypical liver enzymes ALT (alanine transaminase) and AST (aspartate transaminase) were detected in response to 17-AAG treatment, the respective enzyme levels were not elevated upon treatment with pochoxime A. Together with their potent antitumor activities, the absence of hepato(cyto)toxicity represents a second important prerequisite for the successful clinical entry of pochoxime HSP90 inhibitors, such as NW457 and pochoxime A.

7.6 Targeting HSP90 for affecting tumor cell migration

In addition to a general radioresistant phenotype, glioblastomas are characterized by infiltrative growth patterns which also contribute to tumor recurrence and the unfavorable outcome of this disease. It can be assumed that glioblastoma cells which remain after surgical resection and migrate from the primary tumor site into the surrounding brain parenchyma are a putative source of tumor recurrence. Moreover, it has been reported that irradiation itself paradoxically provokes glioma cell migration and invasion in different *in vitro* models (Badiga et al., 2011; De Bacco et al., 2011; Kil et al., 2012; Wild-Bode et al., 2001). Since tumor cells that escape from the target volume of radiotherapy may promote tumor dissemination, radiation-induced migration might account for clinical cases of treatment failure. In the present work, glioma cell migration in response to irradiation was investigated in wound healing assays and it was shown that sublethal doses of IR enhanced the migration of LN229 cells compared to non-irradiated cells.

The molecular mechanisms underlying intrinsic and IR-induced glioblastoma cell motility are complex and involve different classes of molecules, some of which are supposed to rely on HSP90. The involvement of HSP90 in tumor cell migration and invasion has repeatedly been reported (Annamalai et al., 2009; Gopal et al., 2011; Sims et al., 2011; Taiyab and Rao, 2011; Thuringer et al., 2011) and is supported by the present work. Targeting HSP90 via the novel small-molecule inhibitor NW457 was demonstrated to attenuate the basal migration of LN229 cells and to suppress IR-induced hypermigration. Hence, inhibition of HSP90 via the pochoxime NW457 might provide a new approach in order to interfere with the highly infiltrative phenotype of glioblastomas. These data are in line with other reports where different HSP90 inhibitors, including geldanamycin and 17-AAG, were shown to efficiently decrease the migration and invasion of human glioblastoma cell lines (Annamalai et al., 2009; Gopal et al., 2011; Kim et al., 2008a;

Zagzag et al., 2003). Different mechanisms through which HSP90 inhibitors might interfere with tumor cell migration and invasion have been discussed and attention has been drawn, e.g., to the matrix metalloproteinases (MMPs), members of the integrin family, the MET/HGF axis, and the Eph receptor/ephrin ligand system. For instance, Kim and colleagues suggested a critical role for MMP-9 in glioma motility as they revealed that the anti-invasive action of 17-AAG on the human glioblastoma cell lines U251, U373, and U87 was accompanied by decreased activation of the focal adhesion kinase (FAK), which in turn impaired the activation of NF κ B and finally reduced the secretion of MMP-9 (Kim et al., 2008a). In addition, the MMP family member MMP-2, which is also referred to as gelatinase A, has recently been described to be involved in glioma cell motility (Badiga et al., 2011). This study demonstrated that knockdown of MMP-2 by RNA interference potently inhibited irradiation-induced migration and invasion of U251 and U87 cells, thus suggesting a critical role for MMP-2 in glioma cell motility. In the present work, it was hypothesized that MMPs might also be involved in the migration of LN229 cells and thus account for the migration patterns observed in the migration assays upon irradiation and NW457 treatment. Since MMP expression is largely regulated on the transcriptional level, e.g., through NF κ B-mediated promoter activation (Kim et al., 2005; Yan and Boyd, 2007), mRNA expression of MMP-2, -8, and -9 was examined in response to NW457 treatment +/- irradiation. It was hypothesized that MMP transcription in LN229 cells may be enhanced by irradiation and decreased upon NW457 treatment. However, no significant changes of MMP mRNA expression could be observed in my work (data not shown). These discrepancies may result from varying cellular growth conditions and different experimental setups in the present work compared to the studies mentioned above. Importantly, the migration and invasion assays performed by Kim et al. and Badiga et al. employed an artificial extracellular matrix system based on matrigel, a complex gelatinous protein mixture of components found in the extracellular microenvironment of many tissues. In contrast, the transmigration and wound healing assays in the present work were performed on uncoated surfaces providing no specific stimulation for increased MMP activation. Thus, it is not unexpected that in the present context, MMPs were not identified as determinants of altered LN229 migration following IR and NW457 treatment.

Both the MET/HGF axis and members of the integrin family, such as α v, β 3, and β 5, are frequently deregulated in malignant gliomas and suggested to regulate cell migration and invasion in response to irradiation (Buchanan et al., 2011; De Bacco et al., 2011; Monferran et al., 2008; Wild-Bode et al., 2001). It was thus hypothesized in the present work that the expression of one or more of these factors was possibly upregulated in response to irradiation and downregulated upon NW457 treatment. Whereas integrin expression remained virtually unaffected both upon irradiation and NW457 treatment, the

presented results indicated a potential involvement of MET in LN229 motility as irradiation promoted both MET expression and receptor phosphorylation, even though to a moderate extent. A critical role for MET signaling in tumor cell migration and invasion was confirmed by De Bacco and colleagues demonstrating that irradiation dose-dependently induced the expression of MET and increased the wound healing of glioblastoma and breast cancer cell lines which could be prevented by addition of the MET inhibitor PHA665752 (De Bacco et al., 2011). Interestingly, the authors revealed that IR-induced upregulation of MET was a biphasic transcriptional event characterized by an early transcriptional response occurring within 1-2 h after irradiation and a second peak that appeared 6 h after irradiation and diminished after 24 h. Although the present work suggests a potential role of MET signaling in IR-induced hypermigration of LN229 cells, future work has to confirm this and it also remains to be elucidated whether HSP90 is involved in the regulation of MET signaling.

Another receptor/ligand system supposed to promote glioma cell migration is the Eph receptor tyrosine kinase family. Different members have been shown to be overexpressed in malignant gliomas but lowly expressed in adult brain tissue, which makes ephrin receptors a rather tumor-specific therapeutic target (Day et al., 2013; Wykosky et al., 2005). Upregulation of Eph receptors including EphA2, EphB2, and EphA7 in glioblastoma cells has repeatedly been reported to be associated with enhanced migration and invasion, as well as increased metastatic potential and adverse outcome in GBM patients (Liu et al., 2006; Nakada et al., 2004; Nakada et al., 2005; Wang et al., 2008; Wykosky et al., 2005). Interestingly, studies by Annamalai and colleagues revealed an essential role for HSP90 in regulating the stability of nascent EphA2 and maintaining the signaling capacity of the mature receptor (Annamalai et al., 2009). HSP90 inhibition via geldanamycin potently destabilized newly synthesized EphA2 protein and decreased ligand-dependent receptor phosphorylation. In line with these findings, the present work suggests a possible correlation between NW457-mediated decrease of migration and decline of Eph receptors EphA2 and EphB3 in LN229 cells. However, further investigations are necessary to clarify the precise mechanism.

Even though the exact mechanisms of how HSP90 inhibitors, such as NW457, interfere with glioblastoma cell migration have not been fully elucidated so far, the present work provides further evidence that targeting HSP90 may offer a new approach in order to interfere with the highly infiltrative phenotype of glioblastomas. This may be of particular clinical relevance since the aggressively infiltrative phenotype of glioblastomas is one of the main reasons for the poor outcome of this disease.

7.7 *In vivo* potency of HSP90 inhibitors

In addition to *in vitro* studies, the combinatorial benefit of pharmacological HSP90 inhibition and irradiation has also been demonstrated *in vivo*, although the number of studies is still rather limited (Bisht et al., 2003; Bull et al., 2004; Yin et al., 2010; Zaidi et al., 2012). In spite of different pharmacological compounds, dose and radiation schedules, all studies clearly indicated that the therapeutic effect - as measured by tumor growth delay and prolongation of survival - was superior in the case of combined treatment compared to either treatment alone. The data shown in the present work are in line with this, as the *in vivo* application of NW457 plus radiotherapy resulted in a significant tumor growth delay compared to radiotherapy or NW457 administration only. Of note, all previously published *in vivo* data were obtained from xenograft models with tumors derived from human HeLa (cervix carcinoma), JHU12 (HNSCC), DU145 (prostate carcinoma), and HN3 (HNSCC) cells growing in immunocompromised mice. In contrast, the present NW457-based *in vivo* studies were performed in a heterotopic model of murine CT26 colorectal tumor cells growing in syngeneic, immunocompetent Balb/c mice. Employing such an experimental setting with immunocompetent animals might be superior to xenograft experiments as it allows the assessment of the impact that NW457 might have on the immune system and particularly on the antitumor immune response. Having demonstrated that NW457 considerably enhances HSP70 expression, surface exposure, and release *in vitro*, one might expect that NW457 also induces the release of HSP70 *in vivo*. As a well-known immunogenic danger signal HSP70 might trigger the activation and recruitment of macrophages and NK cells to the tumor site (Elsner et al., 2007; Moseley, 2000; Multhoff, 2002; Schmitt et al., 2007; Vega et al., 2008). Interestingly, increased levels of HSP70 were observed in xenograft tumors of human pancreatic cancer cells after application of the HSP90 inhibitor IPI-504 (Song et al., 2008). Immunological functions of secreted or membrane-bound HSP70 have repeatedly been described: For instance, Vega and colleagues demonstrated that HSP70 of heat shocked HepG2 cells translocated into the plasma membrane before it was released in a membrane-associated form and induced the activation of macrophages, as monitored by enhanced levels of TNF- α production (Vega et al., 2008). Another study showed that pancreas and colon carcinoma cell lines released HSP70-containing vesicles (exosomes), which potently stimulated the migratory capacity and cytolytic activity of NK cells (Gastpar et al., 2005). In consideration of these reports, the impact of NW457 on the migratory potential of monocytes and macrophages is currently being investigated in the Department of Radiation Oncology (LMU Munich), and preliminary data indicate increased migration of macrophages towards HSP70 containing supernatants of NW457-treated HCT116 cells (Anne Ernst, personal communication). Furthermore, the *in vivo* impact of

NW457 on tumor cell HSP70 expression and its potential implications for the stimulation of an antitumor immune response will be examined in future studies.

7.8 Conclusion and outlook

The present work was intended as a fundamental characterization of the novel pochoxime HSP90 inhibitor NW457 with regard to its antitumor potential in combination with ionizing radiation. Collectively, the data presented here prove HSP90 as a clinically relevant target for novel therapy concepts for both colorectal carcinomas and glioblastomas and identify NW457 as a promising candidate compound for the entry of pochoxime HSP90 inhibitors into the clinic. Together with the current body of literature, the present work clearly substantiates the strong potential of HSP90 inhibition as an approach for improving the efficacy of anticancer radiotherapy. Notably, no clinical trials have assessed the combinatorial benefit of pharmacological HSP90 inhibition plus radiotherapy so far, but translational clinical studies combining second generation HSP90 inhibitors with irradiation will certainly follow in the near future. Based on the promising *in vitro* and *in vivo* data of the present work and other preclinical studies, it is likely that the clinical combination of small-molecule HSP90 inhibitors and radiotherapy will result in synergistic effects.

Regarding the therapeutic potential of HSP90 inhibitors for the treatment of tumors driven by activating KRAS and EGF-R mutations, a Phase II trial is currently investigating the efficacy of the HSP90 inhibitor NVP-AUY922 in advanced NSCLC with specific focus on the KRAS and EGF-R status and corresponding patient stratification (<http://clinicaltrials.gov>, NCT01124864). In consideration of my findings showing that the antitumor activity of NW457 is virtually independent of the cellular KRAS status and together with previous reports demonstrating potent activity of other HSP90 inhibitors in different KRAS-mutant tumor models (Acquaviva et al., 2012; Azoitei et al., 2012), the clinical results are eagerly awaited.

In summary, targeting HSP90 with novel small-molecule inhibitors will probably have a bright future and the combination with conventional chemotherapeutics and radiotherapy may help to prevent the development of cancer drug resistance.

8 References

URLs

<http://globocan.iarc.fr>

<http://clinicaltrials.gov>

<http://picard.ch/downloads>

Journal articles and book chapters

Acquaviva, J., Smith, D.L., Sang, J., Friedland, J.C., He, S., Sequeira, M., Zhang, C., Wada, Y., and Proia, D.A. (2012). Targeting KRAS Mutant Non-Small Cell Lung Cancer with the Hsp90 Inhibitor Ganetespib. *Mol Cancer Ther* 11, 2633-2643.

Adams, J.M., and Cory, S. (2001). Life-or-death decisions by the Bcl-2 protein family. *Trends Biochem Sci* 26, 61-66.

Agatsuma, T., Ogawa, H., Akasaka, K., Asai, A., Yamashita, Y., Mizukami, T., Akinaga, S., and Saitoh, Y. (2002). Halohydrin and oxime derivatives of radicicol: synthesis and antitumor activities. *Bioorg Med Chem* 10, 3445-3454.

Ahsan, A., Ramanand, S.G., Whitehead, C., Hiniker, S.M., Rehemtulla, A., Pratt, W.B., Jolly, S., Gouveia, C., Truong, K., Van Waes, C., *et al.* (2012). Wild-type EGFR is stabilized by direct interaction with HSP90 in cancer cells and tumors. *Neoplasia* 14, 670-677.

Aligue, R., Akhavan-Niak, H., and Russell, P. (1994). A role for Hsp90 in cell cycle control: Wee1 tyrosine kinase activity requires interaction with Hsp90. *EMBO J* 13, 6099-6106.

Amado, R.G., Wolf, M., Peeters, M., Van Cutsem, E., Siena, S., Freeman, D.J., Juan, T., Sikorski, R., Suggs, S., Radinsky, R., *et al.* (2008). Wild-type KRAS is required for panitumumab efficacy in patients with metastatic colorectal cancer. *J Clin Oncol* 26, 1626-1634.

Anand, P., Kunnumakkara, A.B., Sundaram, C., Harikumar, K.B., Tharakan, S.T., Lai, O.S., Sung, B., and Aggarwal, B.B. (2008). Cancer is a preventable disease that requires major lifestyle changes. *Pharm Res* 25, 2097-2116.

Annamalai, B., Liu, X., Gopal, U., and Isaacs, J.S. (2009). Hsp90 Is an Essential Regulator of EphA2 Receptor Stability and Signaling: Implications for Cancer Cell Migration and Metastasis. *Mol Cancer Res* 7, 1021-1032.

Argon, Y., and Simen, B.B. (1999). GRP94, an ER chaperone with protein and peptide binding properties. *Semin Cell Dev Biol* 10, 495-505.

Argyriou, A.A., and Kalofonos, H.P. (2009). Molecularly targeted therapies for malignant gliomas. *Mol Med* 15, 115-122.

Arlander, S.J., Eapen, A.K., Vroman, B.T., McDonald, R.J., Toft, D.O., and Karnitz, L.M. (2003). Hsp90 inhibition depletes Chk1 and sensitizes tumor cells to replication stress. *J Biol Chem* 278, 52572-52577.

- Athauda, G., Giubellino, A., Coleman, J.A., Horak, C., Steeg, P.S., Lee, M.J., Trepel, J., Wimberly, J., Sun, J., Coxon, A., *et al.* (2006). c-Met ectodomain shedding rate correlates with malignant potential. *Clin Cancer Res* 12, 4154-4162.
- Azoitei, N., Hoffmann, C.M., Ellegast, J.M., Ball, C.R., Obermayer, K., Gossele, U., Koch, B., Faber, K., Genze, F., Schrader, M., *et al.* (2012). Targeting of KRAS mutant tumors by HSP90 inhibitors involves degradation of STK33. *J Exp Med* 209, 697-711.
- Babij, C., Zhang, Y., Kurzeja, R.J., Munzli, A., Shehabeldin, A., Fernando, M., Quon, K., Kassner, P.D., Ruefli-Brasse, A.A., Watson, V.J., *et al.* (2011). STK33 kinase activity is nonessential in KRAS-dependent cancer cells. *Cancer Res* 71, 5818-5826.
- Badiga, A.V., Chetty, C., Kesanakurti, D., Are, D., Gujrati, M., Klopfenstein, J.D., Dinh, D.H., and Rao, J.S. (2011). MMP-2 siRNA inhibits radiation-enhanced invasiveness in glioma cells. *PLoS One* 6, e20614.
- Baeriswyl, V., and Christofori, G. (2009). The angiogenic switch in carcinogenesis. *Semin Cancer Biol* 19, 329-337.
- Barluenga, S., Fontaine, J.G., Wang, C., Aouadi, K., Chen, R., Beebe, K., Neckers, L., and Winssinger, N. (2009). Inhibition of HSP90 with pochoximes: SAR and structure-based insights. *Chembiochem* 10, 2753-2759.
- Barluenga, S., Wang, C., Fontaine, J.G., Aouadi, K., Beebe, K., Tsutsumi, S., Neckers, L., and Winssinger, N. (2008). Divergent synthesis of a pochoxin library targeting HSP90 and in vivo efficacy of an identified inhibitor. *Angew Chem Int Ed Engl* 47, 4432-4435.
- Baselga, J. (2001). The EGFR as a target for anticancer therapy--focus on cetuximab. *Eur J Cancer* 37 Suppl 4, S16-22.
- Basso, A.D., Solit, D.B., Chiosis, G., Giri, B., Tsihchlis, P., and Rosen, N. (2002). Akt forms an intracellular complex with heat shock protein 90 (Hsp90) and Cdc37 and is destabilized by inhibitors of Hsp90 function. *J Biol Chem* 277, 39858-39866.
- Bazan, V., Agnese, V., Corsale, S., Calo, V., Valerio, M.R., Latteri, M.A., Vieni, S., Grassi, N., Cicero, G., Dardanoni, G., *et al.* (2005). Specific TP53 and/or Ki-ras mutations as independent predictors of clinical outcome in sporadic colorectal adenocarcinomas: results of a 5-year Gruppo Oncologico dell'Italia Meridionale (GOIM) prospective study. *Ann Oncol* 16 Suppl 4, iv50-55.
- Becker, B., Multhoff, G., Farkas, B., Wild, P.J., Landthaler, M., Stolz, W., and Vogt, T. (2004). Induction of Hsp90 protein expression in malignant melanomas and melanoma metastases. *Exp Dermatol* 13, 27-32.
- Bergers, G., and Benjamin, L.E. (2003). Tumorigenesis and the angiogenic switch. *Nat Rev Cancer* 3, 401-410.
- Biamonte, M.A., Shi, J., Hong, K., Hurst, D.C., Zhang, L., Fan, J., Busch, D.J., Karjian, P.L., Maldonado, A.A., Sensintaffar, J.L., *et al.* (2006). Orally active purine-based inhibitors of the heat shock protein 90. *J Med Chem* 49, 817-828.
- Bianco, R., Gelardi, T., Damiano, V., Ciardiello, F., and Tortora, G. (2007). Rational bases for the development of EGFR inhibitors for cancer treatment. *Int J Biochem Cell Biol* 39, 1416-1431.

- Bisht, K.S., Bradbury, C.M., Mattson, D., Kaushal, A., Sowers, A., Markovina, S., Ortiz, K.L., Sieck, L.K., Isaacs, J.S., Brechbiel, M.W., *et al.* (2003). Geldanamycin and 17-allylamino-17-demethoxygeldanamycin potentiate the in vitro and in vivo radiation response of cervical tumor cells via the heat shock protein 90-mediated intracellular signaling and cytotoxicity. *Cancer Res* 63, 8984-8995.
- Blagosklonny, M.V., Toretsky, J., Bohlen, S., and Neckers, L. (1996). Mutant conformation of p53 translated in vitro or in vivo requires functional HSP90. *Proc Natl Acad Sci U S A* 93, 8379-8383.
- Blagosklonny, M.V., Toretsky, J., and Neckers, L. (1995). Geldanamycin selectively destabilizes and conformationally alters mutated p53. *Oncogene* 11, 933-939.
- Bonner, J.A., Harari, P.M., Giralt, J., Azarnia, N., Shin, D.M., Cohen, R.B., Jones, C.U., Sur, R., Raben, D., Jassem, J., *et al.* (2006). Radiotherapy plus cetuximab for squamous-cell carcinoma of the head and neck. *N Engl J Med* 354, 567-578.
- Bonner, J.A., Harari, P.M., Giralt, J., Cohen, R.B., Jones, C.U., Sur, R.K., Raben, D., Baselga, J., Spencer, S.A., Zhu, J., *et al.* (2010). Radiotherapy plus cetuximab for locoregionally advanced head and neck cancer: 5-year survival data from a phase 3 randomised trial, and relation between cetuximab-induced rash and survival. *Lancet Oncol* 11, 21-28.
- Bradford, M.M. (1976). A rapid and sensitive method for the quantitation of microgram quantities of protein utilizing the principle of protein-dye binding. *Anal Biochem* 72, 248-254.
- Brunet, A., Bonni, A., Zigmond, M.J., Lin, M.Z., Juo, P., Hu, L.S., Anderson, M.J., Arden, K.C., Blenis, J., and Greenberg, M.E. (1999). Akt promotes cell survival by phosphorylating and inhibiting a Forkhead transcription factor. *Cell* 96, 857-868.
- Buchanan, I.M., Scott, T., Tandle, A.T., Burgan, W.E., Burgess, T.L., Tofilon, P.J., and Camphausen, K. (2011). Radiosensitization of glioma cells by modulation of Met signalling with the hepatocyte growth factor neutralizing antibody, AMG102. *J Cell Mol Med* 15, 1999-2006.
- Bull, E.E., Dote, H., Brady, K.J., Burgan, W.E., Carter, D.J., Cerra, M.A., Oswald, K.A., Hollingshead, M.G., Camphausen, K., and Tofilon, P.J. (2004). Enhanced tumor cell radiosensitivity and abrogation of G2 and S phase arrest by the Hsp90 inhibitor 17-(dimethylaminoethylamino)-17-demethoxygeldanamycin. *Clin Cancer Res* 10, 8077-8084.
- Bunz, F., Dutriaux, A., Lengauer, C., Waldman, T., Zhou, S., Brown, J.P., Sedivy, J.M., Kinzler, K.W., and Vogelstein, B. (1998). Requirement for p53 and p21 to sustain G2 arrest after DNA damage. *Science* 282, 1497-1501.
- Burkhardt, D.L., and Sage, J. (2008). Cellular mechanisms of tumour suppression by the retinoblastoma gene. *Nat Rev Cancer* 8, 671-682.
- Cai, Y., Qiu, S., Gao, X., Gu, S.Z., and Liu, Z.J. (2012). iASPP inhibits p53-independent apoptosis by inhibiting transcriptional activity of p63/p73 on promoters of proapoptotic genes. *Apoptosis* 17, 777-783.
- Carmeliet, P. (2005). VEGF as a key mediator of angiogenesis in cancer. *Oncology* 69 Suppl 3, 4-10.

- Cercek, A., and Saltz, L. (2011). BEYOND KRAS: Other Markers and Potential Treatment Strategies for KRAS Mutant and Wild-type Patients. *Curr Treat Options Oncol* 12, 126-135.
- Chen, W., Sin, S.H., Wen, K.W., Damania, B., and Dittmer, D.P. (2012). Hsp90 inhibitors are efficacious against Kaposi Sarcoma by enhancing the degradation of the essential viral gene LANA, of the viral co-receptor EphA2 as well as other client proteins. *PLoS Pathog* 8, e1003048.
- Cheng, C.F., Fan, J., Fedesco, M., Guan, S., Li, Y., Bandyopadhyay, B., Bright, A.M., Yerushalmi, D., Liang, M., Chen, M., *et al.* (2008). Transforming growth factor alpha (TGFalpha)-stimulated secretion of HSP90alpha: using the receptor LRP-1/CD91 to promote human skin cell migration against a TGFbeta-rich environment during wound healing. *Mol Cell Biol* 28, 3344-3358.
- Chou, T.C., and Talalay, P. (1981). Generalized equations for the analysis of inhibitions of Michaelis-Menten and higher-order kinetic systems with two or more mutually exclusive and nonexclusive inhibitors. *Eur J Biochem* 115, 207-216.
- Chou, T.C., and Talalay, P. (1984). Quantitative analysis of dose-effect relationships: the combined effects of multiple drugs or enzyme inhibitors. *Adv Enzyme Regul* 22, 27-55.
- Connell, P., Ballinger, C.A., Jiang, J., Wu, Y., Thompson, L.J., Hohfeld, J., and Patterson, C. (2001). The co-chaperone CHIP regulates protein triage decisions mediated by heat-shock proteins. *Nat Cell Biol* 3, 93-96.
- Coultas, L., and Strasser, A. (2000). The molecular control of DNA damage-induced cell death. *Apoptosis* 5, 491-507.
- Counter, C.M., Avilion, A.A., LeFeuvre, C.E., Stewart, N.G., Greider, C.W., Harley, C.B., and Bacchetti, S. (1992). Telomere shortening associated with chromosome instability is arrested in immortal cells which express telomerase activity. *EMBO J* 11, 1921-1929.
- Csermely, P., Kajtar, J., Hollosi, M., Jalsovszky, G., Holly, S., Kahn, C.R., Gergely, P., Jr., Soti, C., Mihaly, K., and Somogyi, J. (1993). ATP induces a conformational change of the 90-kDa heat shock protein (hsp90). *J Biol Chem* 268, 1901-1907.
- Csermely, P., Schnaider, T., Soti, C., Prohaszka, Z., and Nardai, G. (1998). The 90-kDa molecular chaperone family: structure, function, and clinical applications. A comprehensive review. *Pharmacol Ther* 79, 129-168.
- Cysyk, R.L., Parker, R.J., Barchi, J.J., Jr., Steeg, P.S., Hartman, N.R., and Strong, J.M. (2006). Reaction of geldanamycin and C17-substituted analogues with glutathione: product identifications and pharmacological implications. *Chem Res Toxicol* 19, 376-381.
- Da Rocha Dias, S., Friedlos, F., Light, Y., Springer, C., Workman, P., and Marais, R. (2005). Activated B-RAF is an Hsp90 client protein that is targeted by the anticancer drug 17-allylamino-17-demethoxygeldanamycin. *Cancer Res* 65, 10686-10691.
- Day, B.W., Stringer, B.W., Al-Ejeh, F., Ting, M.J., Wilson, J., Ensbey, K.S., Jamieson, P.R., Bruce, Z.C., Lim, Y.C., Offenhauser, C., *et al.* (2013). EphA3 maintains tumorigenicity and is a therapeutic target in glioblastoma multiforme. *Cancer Cell* 23, 238-248.

- De Bacco, F., Luraghi, P., Medico, E., Reato, G., Girolami, F., Perera, T., Gabriele, P., Comoglio, P.M., and Boccaccio, C. (2011). Induction of MET by ionizing radiation and its role in radioresistance and invasive growth of cancer. *J Natl Cancer Inst* 103, 645-661.
- De Craene, B., and Berx, G. (2013). Regulatory networks defining EMT during cancer initiation and progression. *Nat Rev Cancer* 13, 97-110.
- de Lange, T., Shiue, L., Myers, R.M., Cox, D.R., Naylor, S.L., Killery, A.M., and Varmus, H.E. (1990). Structure and variability of human chromosome ends. *Mol Cell Biol* 10, 518-527.
- DeBoer, C., Meulman, P.A., Wnuk, R.J., and Peterson, D.H. (1970). Geldanamycin, a new antibiotic. *J Antibiot (Tokyo)* 23, 442-447.
- Delaney, G., Jacob, S., Featherstone, C., and Barton, M. (2005). The role of radiotherapy in cancer treatment: estimating optimal utilization from a review of evidence-based clinical guidelines. *Cancer* 104, 1129-1137.
- Delmotte, P., and Delmotte-Plaque, J. (1953). A new antifungal substance of fungal origin. *Nature* 171, 344.
- Dickson, M.A., Okuno, S.H., Keohan, M.L., Maki, R.G., D'Adamo, D.R., Akhurst, T.J., Antonescu, C.R., and Schwartz, G.K. (2013). Phase II study of the HSP90-inhibitor BIIB021 in gastrointestinal stromal tumors. *Ann Oncol* 24, 252-257.
- Dote, H., Burgan, W.E., Camphausen, K., and Tofilon, P.J. (2006). Inhibition of hsp90 compromises the DNA damage response to radiation. *Cancer Res* 66, 9211-9220.
- Dungey, F.A., Caldecott, K.W., and Chalmers, A.J. (2009). Enhanced radiosensitization of human glioma cells by combining inhibition of poly(ADP-ribose) polymerase with inhibition of heat shock protein 90. *Mol Cancer Ther* 8, 2243-2254.
- Dunne, A.L., Price, M.E., Mothersill, C., McKeown, S.R., Robson, T., and Hirst, D.G. (2003). Relationship between clonogenic radiosensitivity, radiation-induced apoptosis and DNA damage/repair in human colon cancer cells. *Br J Cancer* 89, 2277-2283.
- Eccles, S.A., Massey, A., Raynaud, F.I., Sharp, S.Y., Box, G., Valenti, M., Patterson, L., de Haven Brandon, A., Gowan, S., Boxall, F., *et al.* (2008). NVP-AUY922: a novel heat shock protein 90 inhibitor active against xenograft tumor growth, angiogenesis, and metastasis. *Cancer Res* 68, 2850-2860.
- Eiseman, J.L., Lan, J., Lagattuta, T.F., Hamburger, D.R., Joseph, E., Covey, J.M., and Egorin, M.J. (2005). Pharmacokinetics and pharmacodynamics of 17-demethoxy 17-[[2-dimethylamino)ethyl]amino]geldanamycin (17DMAG, NSC 707545) in C.B-17 SCID mice bearing MDA-MB-231 human breast cancer xenografts. *Cancer Chemother Pharmacol* 55, 21-32.
- Ekstrand, A.J., James, C.D., Cavenee, W.K., Seliger, B., Pettersson, R.F., and Collins, V.P. (1991). Genes for epidermal growth factor receptor, transforming growth factor alpha, and epidermal growth factor and their expression in human gliomas in vivo. *Cancer Res* 51, 2164-2172.
- Elsner, L., Muppala, V., Gehrman, M., Lozano, J., Malzahn, D., Bickeboller, H., Brunner, E., Zientkowska, M., Herrmann, T., Walter, L., *et al.* (2007). The heat shock protein HSP70 promotes mouse NK cell activity against tumors that express inducible NKG2D ligands. *J Immunol* 179, 5523-5533.

- Enggebraaten, O., Bjerkvig, R., Pedersen, P.H., and Laerum, O.D. (1993). Effects of EGF, bFGF, NGF and PDGF(bb) on cell proliferative, migratory and invasive capacities of human brain-tumour biopsies in vitro. *Int J Cancer* 53, 209-214.
- Eriksson, D., and Stigbrand, T. (2010). Radiation-induced cell death mechanisms. *Tumour Biol* 31, 363-372.
- Esteller, M., Garcia-Foncillas, J., Andion, E., Goodman, S.N., Hidalgo, O.F., Vanaclocha, V., Baylin, S.B., and Herman, J.G. (2000). Inactivation of the DNA-repair gene MGMT and the clinical response of gliomas to alkylating agents. *N Engl J Med* 343, 1350-1354.
- Euhus, D.M., Hudd, C., LaRegina, M.C., and Johnson, F.E. (1986). Tumor measurement in the nude mouse. *J Surg Oncol* 31, 229-234.
- Eustace, B.K., Sakurai, T., Stewart, J.K., Yimlamai, D., Unger, C., Zehetmeier, C., Lain, B., Torella, C., Henning, S.W., Beste, G., *et al.* (2004). Functional proteomic screens reveal an essential extracellular role for hsp90 alpha in cancer cell invasiveness. *Nat Cell Biol* 6, 507-514.
- Felts, S.J., Owen, B.A., Nguyen, P., Trepel, J., Donner, D.B., and Toft, D.O. (2000). The hsp90-related protein TRAP1 is a mitochondrial protein with distinct functional properties. *J Biol Chem* 275, 3305-3312.
- Ferrarini, M., Heltai, S., Zocchi, M.R., and Rugarli, C. (1992). Unusual expression and localization of heat-shock proteins in human tumor cells. *Int J Cancer* 51, 613-619.
- Flinterman, M., Guelen, L., Ezzati-Nik, S., Killick, R., Melino, G., Tominaga, K., Mymryk, J.S., Gaken, J., and Tavassoli, M. (2005). E1A activates transcription of p73 and Noxa to induce apoptosis. *J Biol Chem* 280, 5945-5959.
- Folkman, J. (1995). Angiogenesis in cancer, vascular, rheumatoid and other disease. *Nat Med* 1, 27-31.
- Fortugno, P., Beltrami, E., Plescia, J., Fontana, J., Pradhan, D., Marchisio, P.C., Sessa, W.C., and Altieri, D.C. (2003). Regulation of survivin function by Hsp90. *Proc Natl Acad Sci U S A* 100, 13791-13796.
- Freeman, B.C., and Morimoto, R.I. (1996). The human cytosolic molecular chaperones hsp90, hsp70 (hsc70) and hdj-1 have distinct roles in recognition of a non-native protein and protein refolding. *EMBO J* 15, 2969-2979.
- Frohling, S., and Scholl, C. (2011). STK33 kinase is not essential in KRAS-dependent cells--letter. *Cancer Res* 71, 7716; author reply 7717.
- Frydman, J., and Hohfeld, J. (1997). Chaperones get in touch: the Hip-Hop connection. *Trends Biochem Sci* 22, 87-92.
- Fukuyo, Y., Hunt, C.R., and Horikoshi, N. (2010). Geldanamycin and its anti-cancer activities. *Cancer Letters* 290, 24-35.
- Fukuyo, Y., Inoue, M., Nakajima, T., Higashikubo, R., Horikoshi, N.T., Hunt, C., Usheva, A., Freeman, M.L., and Horikoshi, N. (2008). Oxidative stress plays a critical role in inactivating mutant BRAF by geldanamycin derivatives. *Cancer Res* 68, 6324-6330.
- Gallegos Ruiz, M.I., Floor, K., Roepman, P., Rodriguez, J.A., Meijer, G.A., Mooi, W.J., Jassem, E., Niklinski, J., Muley, T., van Zandwijk, N., *et al.* (2008). Integration of gene

dosage and gene expression in non-small cell lung cancer, identification of HSP90 as potential target. *PLoS One* 3, e0001722.

Gaspar, N., Sharp, S.Y., Eccles, S.A., Gowan, S., Popov, S., Jones, C., Pearson, A., Vassal, G., and Workman, P. (2010). Mechanistic evaluation of the novel HSP90 inhibitor NVP-AUY922 in adult and pediatric glioblastoma. *Mol Cancer Ther* 9, 1219-1233.

Gastpar, R., Gehrmann, M., Bausero, M.A., Asea, A., Gross, C., Schroeder, J.A., and Multhoff, G. (2005). Heat shock protein 70 surface-positive tumor exosomes stimulate migratory and cytolytic activity of natural killer cells. *Cancer Res* 65, 5238-5247.

Gewirtz, D.A., Hilliker, M.L., and Wilson, E.N. (2009). Promotion of autophagy as a mechanism for radiation sensitization of breast tumor cells. *Radiother Oncol* 92, 323-328.

Glimelius, B. (2002). Radiotherapy in rectal cancer. *Br Med Bull* 64, 141-157.

Goetz, M.P., Toft, D.O., Ames, M.M., and Erlichman, C. (2003). The Hsp90 chaperone complex as a novel target for cancer therapy. *Ann Oncol* 14, 1169-1176.

Goncalves, L.A., Vigario, A.M., and Penha-Goncalves, C. (2007). Improved isolation of murine hepatocytes for in vitro malaria liver stage studies. *Malar J* 6, 169.

Gopal, U., Bohonowych, J.E., Lema-Tome, C., Liu, A., Garrett-Mayer, E., Wang, B., and Isaacs, J.S. (2011). A novel extracellular Hsp90 mediated co-receptor function for LRP1 regulates EphA2 dependent glioblastoma cell invasion. *PLoS One* 6, e17649.

Grammatikakis, N., Vultur, A., Ramana, C.V., Siganou, A., Schweinfest, C.W., Watson, D.K., and Raptis, L. (2002). The role of Hsp90N, a new member of the Hsp90 family, in signal transduction and neoplastic transformation. *J Biol Chem* 277, 8312-8320.

Grandis, J.R., and Tweardy, D.J. (1993). Elevated levels of transforming growth factor alpha and epidermal growth factor receptor messenger RNA are early markers of carcinogenesis in head and neck cancer. *Cancer Res* 53, 3579-3584.

Grbovic, O.M., Basso, A.D., Sawai, A., Ye, Q., Friedlander, P., Solit, D., and Rosen, N. (2006). V600E B-Raf requires the Hsp90 chaperone for stability and is degraded in response to Hsp90 inhibitors. *Proc Natl Acad Sci U S A* 103, 57-62.

Grenert, J.P., Sullivan, W.P., Fadden, P., Haystead, T.A., Clark, J., Mimnaugh, E., Krutzsch, H., Ochel, H.J., Schulte, T.W., Sausville, E., *et al.* (1997). The amino-terminal domain of heat shock protein 90 (hsp90) that binds geldanamycin is an ATP/ADP switch domain that regulates hsp90 conformation. *J Biol Chem* 272, 23843-23850.

Gurley, K.E., Moser, R., Gu, Y., Hasty, P., and Kemp, C.J. (2009). DNA-PK suppresses a p53-independent apoptotic response to DNA damage. *EMBO Rep* 10, 87-93.

Ha, K., Fiskus, W., Rao, R., Balusu, R., Venkannagari, S., Nalabothula, N.R., and Bhalla, K.N. (2011). Hsp90 Inhibitor-Mediated Disruption of Chaperone Association of ATR with Hsp90 Sensitizes Cancer Cells to DNA Damage. *Mol Cancer Ther* 10, 1194-1206.

Hagn, F., Lagleder, S., Retzlaff, M., Rohrberg, J., Demmer, O., Richter, K., Buchner, J., and Kessler, H. (2011). Structural analysis of the interaction between Hsp90 and the tumor suppressor protein p53. *Nat Struct Mol Biol* 18, 1086-1093.

Hall, E.J., and Giaccia, A.J. (2011). *Radiobiology for the radiologist*. Lippincott Williams & Wilki, 7th edition. ISBN-13: 9781608311934.

- Hanahan, D., and Folkman, J. (1996). Patterns and emerging mechanisms of the angiogenic switch during tumorigenesis. *Cell* 86, 353-364.
- Hanahan, D., and Weinberg, R.A. (2000). The hallmarks of cancer. *Cell* 100, 57-70.
- Hanahan, D., and Weinberg, R.A. (2011). Hallmarks of cancer: the next generation. *Cell* 144, 646-674.
- He, H., Zatorska, D., Kim, J., Aguirre, J., Llauger, L., She, Y., Wu, N., Immormino, R.M., Gewirth, D.T., and Chiosis, G. (2006). Identification of potent water soluble purine-scaffold inhibitors of the heat shock protein 90. *J Med Chem* 49, 381-390.
- Hegi, M.E., Diserens, A.C., Godard, S., Dietrich, P.Y., Regli, L., Ostermann, S., Otten, P., Van Melle, G., de Tribolet, N., and Stupp, R. (2004). Clinical trial substantiates the predictive value of O-6-methylguanine-DNA methyltransferase promoter methylation in glioblastoma patients treated with temozolomide. *Clin Cancer Res* 10, 1871-1874.
- Hegi, M.E., Diserens, A.C., Gorlia, T., Hamou, M.F., de Tribolet, N., Weller, M., Kros, J.M., Hainfellner, J.A., Mason, W., Mariani, L., *et al.* (2005). MGMT gene silencing and benefit from temozolomide in glioblastoma. *N Engl J Med* 352, 997-1003.
- Held, K.D. (1997). Radiation-induced apoptosis and its relationship to loss of clonogenic survival. *Apoptosis* 2, 265-282.
- Hemmati, P.G., Gillissen, B., von Haefen, C., Wendt, J., Starck, L., Guner, D., Dorken, B., and Daniel, P.T. (2002). Adenovirus-mediated overexpression of p14(ARF) induces p53 and Bax-independent apoptosis. *Oncogene* 21, 3149-3161.
- Hemmati, P.G., Guner, D., Gillissen, B., Wendt, J., von Haefen, C., Chinnadurai, G., Dorken, B., and Daniel, P.T. (2006). Bak functionally complements for loss of Bax during p14ARF-induced mitochondrial apoptosis in human cancer cells. *Oncogene* 25, 6582-6594.
- Hernandez, M.P., Sullivan, W.P., and Toft, D.O. (2002). The assembly and intermolecular properties of the hsp70-Hop-hsp90 molecular chaperone complex. *J Biol Chem* 277, 38294-38304.
- Huang, Q., Li, F., Liu, X., Li, W., Shi, W., Liu, F.-F., O'Sullivan, B., He, Z., Peng, Y., Tan, A.-C., *et al.* (2011). Caspase 3-mediated stimulation of tumor cell repopulation during cancer radiotherapy. *Nat Med* 17, 860-866.
- Iacopetta, B. (2003). TP53 mutation in colorectal cancer. *Hum Mutat* 21, 271-276.
- Irwin, M., Marin, M.C., Phillips, A.C., Seelan, R.S., Smith, D.I., Liu, W., Flores, E.R., Tsai, K.Y., Jacks, T., Vousden, K.H., *et al.* (2000). Role for the p53 homologue p73 in E2F-1-induced apoptosis. *Nature* 407, 645-648.
- Isaacs, J.S., Xu, W., and Neckers, L. (2003). Heat shock protein 90 as a molecular target for cancer therapeutics. *Cancer Cell* 3, 213-217.
- Jackson, S.P., and Bartek, J. (2009). The DNA-damage response in human biology and disease. *Nature* 461, 1071-1078.
- Jemal, A., Bray, F., Center, M.M., Ferlay, J., Ward, E., and Forman, D. (2011). Global cancer statistics. *CA Cancer J Clin* 61, 69-90.

- Jensen, M.R., Schoepfer, J., Radimerski, T., Massey, A., Guy, C.T., Brueggen, J., Quadt, C., Buckler, A., Cozens, R., Drysdale, M.J., *et al.* (2008). NVP-AUY922: a small molecule HSP90 inhibitor with potent antitumor activity in preclinical breast cancer models. *Breast Cancer Res* 10, R33.
- Jiang, B.H., and Liu, L.Z. (2009). PI3K/PTEN signaling in angiogenesis and tumorigenesis. *Adv Cancer Res* 102, 19-65.
- Johnson, B.D., Schumacher, R.J., Ross, E.D., and Toft, D.O. (1998). Hop modulates Hsp70/Hsp90 interactions in protein folding. *J Biol Chem* 273, 3679-3686.
- Johnson, J.L., and Toft, D.O. (1994). A novel chaperone complex for steroid receptors involving heat shock proteins, immunophilins, and p23. *J Biol Chem* 269, 24989-24993.
- Johnson, V.A., Singh, E.K., Nazarova, L.A., Alexander, L.D., and McAlpine, S.R. (2010). Macrocytic inhibitors of hsp90. *Curr Top Med Chem* 10, 1380-1402.
- Ju, H.Q., Wang, S.X., Xiang, Y.F., Liu, Z., Liu, J.Y., Chen, Z.P., Zeng, F.L., Xia, M., Liu, Z.H., Xing, G.W., *et al.* (2011). BJ-B11, a novel Hsp90 inhibitor, induces apoptosis in human chronic myeloid leukemia K562 cells through the mitochondria-dependent pathway. *Eur J Pharmacol* 666, 26-34.
- Kamal, A., Thao, L., Sensintaffar, J., Zhang, L., Boehm, M.F., Fritz, L.C., and Burrows, F.J. (2003). A high-affinity conformation of Hsp90 confers tumour selectivity on Hsp90 inhibitors. *Nature* 425, 407-410.
- Karnoub, A.E., and Weinberg, R.A. (2008). Ras oncogenes: split personalities. *Nat Rev Mol Cell Biol* 9, 517-531.
- Kasibhatla, S.R., Hong, K., Biamonte, M.A., Busch, D.J., Karjian, P.L., Sensintaffar, J.L., Kamal, A., Lough, R.E., Brekken, J., Lundgren, K., *et al.* (2007). Rationally designed high-affinity 2-amino-6-halopurine heat shock protein 90 inhibitors that exhibit potent antitumor activity. *J Med Chem* 50, 2767-2778.
- Kastrinakis, W.V., Ramchurren, N., Rieger, K.M., Hess, D.T., Loda, M., Steele, G., and Summerhayes, I.C. (1995). Increased incidence of p53 mutations is associated with hepatic metastasis in colorectal neoplastic progression. *Oncogene* 11, 647-652.
- Kepp, O., Rajalingam, K., Kimmig, S., and Rudel, T. (2007). Bak and Bax are non-redundant during infection- and DNA damage-induced apoptosis. *EMBO J* 26, 825-834.
- Khambata-Ford, S., Garrett, C.R., Meropol, N.J., Basik, M., Harbison, C.T., Wu, S., Wong, T.W., Huang, X., Takimoto, C.H., Godwin, A.K., *et al.* (2007). Expression of epiregulin and amphiregulin and K-ras mutation status predict disease control in metastatic colorectal cancer patients treated with cetuximab. *J Clin Oncol* 25, 3230-3237.
- Kil, W., Tofilon, P.J., and Camphausen, K. (2012). Post-radiation increase in VEGF enhances glioma cell motility in vitro. *Radiat Oncol* 7, 25.
- Kim, M.S., Kwak, H.J., Lee, J.W., Kim, H.J., Park, M.J., Park, J.B., Choi, K.H., Yoo, H., Shin, S.H., Shin, W.S., *et al.* (2008a). 17-Allylamino-17-demethoxygeldanamycin down-regulates hyaluronic acid-induced glioma invasion by blocking matrix metalloproteinase-9 secretion. *Mol Cancer Res* 6, 1657-1665.

- Kim, M.S., Park, M.J., Kim, S.J., Lee, C.H., Yoo, H., Shin, S.H., Song, E.S., and Lee, S.H. (2005). Emodin suppresses hyaluronic acid-induced MMP-9 secretion and invasion of glioma cells. *Int J Oncol* 27, 839-846.
- Kim, R.H., Kim, R., Chen, W., Hu, S., Shin, K.H., Park, N.H., and Kang, M.K. (2008b). Association of hsp90 to the hTERT promoter is necessary for hTERT expression in human oral cancer cells. *Carcinogenesis* 29, 2425-2431.
- Kim, Y.S., Alarcon, S.V., Lee, S., Lee, M.J., Giaccone, G., Neckers, L., and Trepel, J.B. (2009). Update on Hsp90 inhibitors in clinical trial. *Curr Top Med Chem* 9, 1479-1492.
- Klener, P., Jr., and Klener, P. (2012). Molecularly-targeted and biological anti-cancer therapy. *Folia Biol (Praha)* 58, 1-6.
- Ko, J.C., Chen, H.J., Huang, Y.C., Tseng, S.C., Weng, S.H., Wo, T.Y., Huang, Y.J., Chiu, H.C., Tsai, M.S., Chiou, R.Y., *et al.* (2012). HSP90 inhibition induces cytotoxicity via down-regulation of Rad51 expression and DNA repair capacity in non-small cell lung cancer cells. *Regul Toxicol Pharmacol* 64, 415-424.
- Koga, F., Kihara, K., and Neckers, L. (2009). Inhibition of cancer invasion and metastasis by targeting the molecular chaperone heat-shock protein 90. *Anticancer Res* 29, 797-807.
- Koll, T.T., Feis, S.S., Wright, M.H., Teniola, M.M., Richardson, M.M., Robles, A.I., Bradsher, J., Capala, J., and Varticovski, L. (2008). HSP90 inhibitor, DMAG, synergizes with radiation of lung cancer cells by interfering with base excision and ATM-mediated DNA repair. *Mol Cancer Ther* 7, 1985-1992.
- Koochekpour, S., Jeffers, M., Rulong, S., Taylor, G., Klineberg, E., Hudson, E.A., Resau, J.H., and Vande Woude, G.F. (1997). Met and hepatocyte growth factor/scatter factor expression in human gliomas. *Cancer Res* 57, 5391-5398.
- Kwak, E.L., Clark, J.W., and Chabner, B. (2007). Targeted agents: the rules of combination. *Clin Cancer Res* 13, 5232-5237.
- Kwon, H.J., Yoshida, M., Abe, K., Horinouchi, S., and Beppu, T. (1992). Radicol, an agent inducing the reversal of transformed phenotypes of src-transformed fibroblasts. *Biosci Biotechnol Biochem* 56, 538-539.
- Lauber, K., Ernst, A., Orth, M., Herrmann, M., and Belka, C. (2012). Dying cell clearance and its impact on the outcome of tumor radiotherapy. *Front Oncol* 2, 116.
- Lavictoire, S.J., Parolin, D.A., Klimowicz, A.C., Kelly, J.F., and Lorimer, I.A. (2003). Interaction of Hsp90 with the nascent form of the mutant epidermal growth factor receptor EGFRvIII. *J Biol Chem* 278, 5292-5299.
- Lemke, G. (1997). A coherent nomenclature for Eph receptors and their ligands. *Mol Cell Neurosci* 9, 331-332.
- Levine, A.J., Momand, J., and Finlay, C.A. (1991). The p53 tumour suppressor gene. *Nature* 351, 453-456.
- Lievre, A., Bachet, J.B., Boige, V., Cayre, A., Le Corre, D., Buc, E., Ychou, M., Bouche, O., Landi, B., Louvet, C., *et al.* (2008). KRAS mutations as an independent prognostic factor in patients with advanced colorectal cancer treated with cetuximab. *J Clin Oncol* 26, 374-379.

- Lin, T.Y., Bear, M., Du, Z., Foley, K.P., Ying, W., Barsoum, J., and London, C. (2008). The novel HSP90 inhibitor STA-9090 exhibits activity against Kit-dependent and -independent malignant mast cell tumors. *Exp Hematol* 36, 1266-1277.
- Liu, F., Park, P.J., Lai, W., Maher, E., Chakravarti, A., Durso, L., Jiang, X., Yu, Y., Brosius, A., Thomas, M., *et al.* (2006). A genome-wide screen reveals functional gene clusters in the cancer genome and identifies EphA2 as a mitogen in glioblastoma. *Cancer Res* 66, 10815-10823.
- Llauger, L., He, H., Kim, J., Aguirre, J., Rosen, N., Peters, U., Davies, P., and Chiosis, G. (2005). Evaluation of 8-arylsulfanyl, 8-arylsulfoxyl, and 8-arylsulfonyl adenine derivatives as inhibitors of the heat shock protein 90. *J Med Chem* 48, 2892-2905.
- Lopez, I., L, P.O., Tucci, P., Alvarez-Valin, F., R, A.C., and Marin, M. (2012). Different mutation profiles associated to P53 accumulation in colorectal cancer. *Gene* 499, 81-87.
- Loupakis, F., Ruzzo, A., Cremolini, C., Vincenzi, B., Salvatore, L., Santini, D., Masi, G., Stasi, I., Canestrari, E., Rulli, E., *et al.* (2009). KRAS codon 61, 146 and BRAF mutations predict resistance to cetuximab plus irinotecan in KRAS codon 12 and 13 wild-type metastatic colorectal cancer. *Br J Cancer* 101, 715-721.
- Lundgren, K., Zhang, H., Brekken, J., Huser, N., Powell, R.E., Timple, N., Busch, D.J., Neely, L., Sensintaffar, J.L., Yang, Y.C., *et al.* (2009). BIIB021, an orally available, fully synthetic small-molecule inhibitor of the heat shock protein Hsp90. *Mol Cancer Ther* 8, 921-929.
- Luo, T., Masson, K., Jaffe, J.D., Silkworth, W., Ross, N.T., Scherer, C.A., Scholl, C., Frohling, S., Carr, S.A., Stern, A.M., *et al.* (2012). STK33 kinase inhibitor BRD-8899 has no effect on KRAS-dependent cancer cell viability. *Proc Natl Acad Sci U S A* 109, 2860-2865.
- Machida, H., Matsumoto, Y., Shirai, M., and Kubota, N. (2003). Geldanamycin, an inhibitor of Hsp90, sensitizes human tumour cells to radiation. *Int J Radiat Biol* 79, 973-980.
- Machida, H., Nakajima, S., Shikano, N., Nishio, J., Okada, S., Asayama, M., Shirai, M., and Kubota, N. (2005). Heat shock protein 90 inhibitor 17-allylamino-17-demethoxygeldanamycin potentiates the radiation response of tumor cells grown as monolayer cultures and spheroids by inducing apoptosis. *Cancer Sci* 96, 911-917.
- Maloney, A., and Workman, P. (2002). HSP90 as a new therapeutic target for cancer therapy: the story unfolds. *Expert Opin Biol Ther* 2, 3-24.
- Marabese, M., Vikhanskaya, F., Rainelli, C., Sakai, T., and Broggin, M. (2003). DNA damage induces transcriptional activation of p73 by removing C-EBPalpha repression on E2F1. *Nucleic Acids Res* 31, 6624-6632.
- Matts, R.L., and Manjarrez, J.R. (2009). Assays for identification of Hsp90 inhibitors and biochemical methods for discriminating their mechanism of action. *Curr Top Med Chem* 9, 1462-1478.
- McNamara, A.V., Barclay, M., Watson, A.J., and Jenkins, J.R. (2012). Hsp90 inhibitors sensitise human colon cancer cells to topoisomerase I poisons by depletion of key anti-apoptotic and cell cycle checkpoint proteins. *Biochem Pharmacol* 83, 355-367.

- Melino, G., Bernassola, F., Ranalli, M., Yee, K., Zong, W.X., Corazzari, M., Knight, R.A., Green, D.R., Thompson, C., and Vousden, K.H. (2004). p73 Induces apoptosis via PUMA transactivation and Bax mitochondrial translocation. *J Biol Chem* 279, 8076-8083.
- Mendelsohn, J. (2001). The epidermal growth factor receptor as a target for cancer therapy. *Endocr Relat Cancer* 8, 3-9.
- Mirza, A., Wu, Q., Wang, L., McClanahan, T., Bishop, W.R., Gheyas, F., Ding, W., Hutchins, B., Hockenberry, T., Kirschmeier, P., *et al.* (2003). Global transcriptional program of p53 target genes during the process of apoptosis and cell cycle progression. *Oncogene* 22, 3645-3654.
- Miyashita, T., and Reed, J.C. (1995). Tumor suppressor p53 is a direct transcriptional activator of the human bax gene. *Cell* 80, 293-299.
- Mondal, S., Bhattacharya, K., Mallick, A., Sangwan, R., and Mandal, C. (2012). Bak compensated for Bax in p53-null cells to release cytochrome c for the initiation of mitochondrial signaling during Withanolide D-induced apoptosis. *PLoS One* 7, e34277.
- Monferran, S., Skuli, N., Delmas, C., Favre, G., Bonnet, J., Cohen-Jonathan-Moyal, E., and Toulas, C. (2008). Alphasbeta3 and alphasbeta5 integrins control glioma cell response to ionising radiation through ILK and RhoB. *Int J Cancer* 123, 357-364.
- Moran, D.M., Gawlak, G., Jayaprakash, M.S., Mayar, S., and Maki, C.G. (2008). Geldanamycin promotes premature mitotic entry and micronucleation in irradiated p53/p21 deficient colon carcinoma cells. *Oncogene* 27, 5567-5577.
- Moseley, P. (2000). Stress proteins and the immune response. *Immunopharmacology* 48, 299-302.
- Moser, C., Lang, S.A., Hackl, C., Wagner, C., Scheiffert, E., Schlitt, H.J., Geissler, E.K., and Stoeltzing, O. (2012). Targeting HSP90 by the novel inhibitor NVP-AUY922 reduces growth and angiogenesis of pancreatic cancer. *Anticancer Res* 32, 2551-2561.
- Moser, C., Lang, S.A., and Stoeltzing, O. (2009). Heat-shock protein 90 (Hsp90) as a molecular target for therapy of gastrointestinal cancer. *Anticancer Res* 29, 2031-2042.
- Moyzis, R.K., Buckingham, J.M., Cram, L.S., Dani, M., Deaven, L.L., Jones, M.D., Meyne, J., Ratliff, R.L., and Wu, J.R. (1988). A highly conserved repetitive DNA sequence, (TTAGGG)*n*, present at the telomeres of human chromosomes. *Proc Natl Acad Sci U S A* 85, 6622-6626.
- Muller, P., Hrstka, R., Coomber, D., Lane, D.P., and Vojtesek, B. (2008). Chaperone-dependent stabilization and degradation of p53 mutants. *Oncogene* 27, 3371-3383.
- Multhoff, G. (2002). Activation of natural killer cells by heat shock protein 70. *Int J Hyperthermia* 18, 576-585.
- Naccarati, A., Polakova, V., Pardini, B., Vodickova, L., Hemminki, K., Kumar, R., and Vodicka, P. (2012). Mutations and polymorphisms in TP53 gene--an overview on the role in colorectal cancer. *Mutagenesis* 27, 211-218.
- Nagata, Y., Anan, T., Yoshida, T., Mizukami, T., Taya, Y., Fujiwara, T., Kato, H., Saya, H., and Nakao, M. (1999). The stabilization mechanism of mutant-type p53 by impaired ubiquitination: the loss of wild-type p53 function and the hsp90 association. *Oncogene* 18, 6037-6049.

References

- Nakada, M., Nakada, S., Demuth, T., Tran, N.L., Hoelzinger, D.B., and Berens, M.E. (2007). Molecular targets of glioma invasion. *Cell Mol Life Sci* **64**, 458-478.
- Nakada, M., Niska, J.A., Miyamori, H., McDonough, W.S., Wu, J., Sato, H., and Berens, M.E. (2004). The phosphorylation of EphB2 receptor regulates migration and invasion of human glioma cells. *Cancer Res* **64**, 3179-3185.
- Nakada, M., Niska, J.A., Tran, N.L., McDonough, W.S., and Berens, M.E. (2005). EphB2/R-Ras signaling regulates glioma cell adhesion, growth, and invasion. *Am J Pathol* **167**, 565-576.
- Neckers, L., and Ivy, S.P. (2003). Heat shock protein 90. *Curr Opin Oncol* **15**, 419-424.
- Neckers, L., and Neckers, K. (2002). Heat-shock protein 90 inhibitors as novel cancer chemotherapeutic agents. *Expert Opin Emerg Drugs* **7**, 277-288.
- Neckers, L., and Workman, P. (2012). Hsp90 molecular chaperone inhibitors: are we there yet? *Clin Cancer Res* **18**, 64-76.
- Nicholson, R.I., Gee, J.M.W., and Harper, M.E. (2001). EGFR and cancer prognosis. *Eur J Cancer* **37**, 9-15.
- Noguchi, M., Yu, D., Hirayama, R., Ninomiya, Y., Sekine, E., Kubota, N., Ando, K., and Okayasu, R. (2006). Inhibition of homologous recombination repair in irradiated tumor cells pretreated with Hsp90 inhibitor 17-allylamino-17-demethoxygeldanamycin. *Biochem Biophys Res Commun* **351**, 658-663.
- Nomura, M., Nomura, N., Newcomb, E.W., Lukyanov, Y., Tamasdan, C., and Zagzag, D. (2004). Geldanamycin induces mitotic catastrophe and subsequent apoptosis in human glioma cells. *J Cell Physiol* **201**, 374-384.
- Obermann, W.M., Sondermann, H., Russo, A.A., Pavletich, N.P., and Hartl, F.U. (1998). In vivo function of Hsp90 is dependent on ATP binding and ATP hydrolysis. *J Cell Biol* **143**, 901-910.
- Okui, T., Shimo, T., Fukazawa, T., Hassan, N.M., Honami, T., Ibaragi, S., Takaoka, M., Naomoto, Y., and Sasaki, A. (2012). Novel HSP90 Inhibitor NVP-AUY922 enhances the anti-tumor effect of temsirolimus against oral squamous cell carcinoma. *Curr Cancer Drug Targets*, 289-299.
- Oniscu, A., Sphyris, N., Morris, R.G., Bader, S., and Harrison, D.J. (2004). p73alpha is a candidate effector in the p53 independent apoptosis pathway of cisplatin damaged primary murine colonocytes. *J Clin Pathol* **57**, 492-498.
- Panaretou, B., Prodromou, C., Roe, S.M., O'Brien, R., Ladbury, J.E., Piper, P.W., and Pearl, L.H. (1998). ATP binding and hydrolysis are essential to the function of the Hsp90 molecular chaperone in vivo. *EMBO J* **17**, 4829-4836.
- Panaretou, B., Siligardi, G., Meyer, P., Maloney, A., Sullivan, J.K., Singh, S., Millson, S.H., Clarke, P.A., Naaby-Hansen, S., Stein, R., *et al.* (2002). Activation of the ATPase activity of hsp90 by the stress-regulated cochaperone *aha1*. *Mol Cell* **10**, 1307-1318.
- Park, J.H., Kim, S.H., Choi, M.C., Lee, J., Oh, D.Y., Im, S.A., Bang, Y.J., and Kim, T.Y. (2008). Class II histone deacetylases play pivotal roles in heat shock protein 90-mediated proteasomal degradation of vascular endothelial growth factor receptors. *Biochem Biophys Res Commun* **368**, 318-322.

- Pasquale, E.B. (2010). Eph receptors and ephrins in cancer: bidirectional signalling and beyond. *Nat. Rev. Cancer* 10, 165-180.
- Picard, D. (2002). Heat-shock protein 90, a chaperone for folding and regulation. *Cell Mol Life Sci* 59, 1640-1648.
- Pick, E., Kluger, Y., Giltneane, J.M., Moeder, C., Camp, R.L., Rimm, D.L., and Kluger, H.M. (2007). High HSP90 expression is associated with decreased survival in breast cancer. *Cancer Res* 67, 2932-2937.
- Plescia, J., Salz, W., Xia, F., Pennati, M., Zaffaroni, N., Daidone, M.G., Meli, M., Dohi, T., Fortugno, P., Nefedova, Y., *et al.* (2005). Rational design of shepherdin, a novel anticancer agent. *Cancer Cell* 7, 457-468.
- Powers, M.V., and Workman, P. (2007). Inhibitors of the heat shock response: biology and pharmacology. *FEBS Lett* 581, 3758-3769.
- Powis, G. (1989). Free radical formation by antitumor quinones. *Free Radic Biol Med* 6, 63-101.
- Prodromou, C., and Pearl, L.H. (2003). Structure and functional relationships of Hsp90. *Curr Cancer Drug Targets* 3, 301-323.
- Prodromou, C., Roe, S.M., O'Brien, R., Ladbury, J.E., Piper, P.W., and Pearl, L.H. (1997). Identification and structural characterization of the ATP/ADP-binding site in the Hsp90 molecular chaperone. *Cell* 90, 65-75.
- Rana, S., Gupta, K., Gomez, J., Matsuyama, S., Chakrabarti, A., Agarwal, M.L., Agarwal, A., Agarwal, M.K., and Wald, D.N. (2010). Securinine induces p73-dependent apoptosis preferentially in p53-deficient colon cancer cells. *FASEB J* 24, 2126-2134.
- Reed, J.C., Jurgensmeier, J.M., and Matsuyama, S. (1998). Bcl-2 family proteins and mitochondria. *Biochim Biophys Acta* 1366, 127-137.
- Ribatti, D., Nico, B., Crivellato, E., Roccaro, A.M., and Vacca, A. (2007). The history of the angiogenic switch concept. *Leukemia* 21, 44-52.
- Riccardi, C., and Nicoletti, I. (2006). Analysis of apoptosis by propidium iodide staining and flow cytometry. *Nat Protocols* 1, 1458-1461.
- Rodriguez, J., Zarate, R., Bandres, E., Viudez, A., Chopitea, A., Garcia-Foncillas, J., and Gil-Bazo, I. (2007). Combining chemotherapy and targeted therapies in metastatic colorectal cancer. *World J Gastroenterol* 13, 5867-5876.
- Roe, S.M., Prodromou, C., O'Brien, R., Ladbury, J.E., Piper, P.W., and Pearl, L.H. (1999). Structural basis for inhibition of the Hsp90 molecular chaperone by the antitumor antibiotics radicicol and geldanamycin. *J Med Chem* 42, 260-266.
- Romashkova, J.A., and Makarov, S.S. (1999). NF-kappaB is a target of AKT in anti-apoptotic PDGF signalling. *Nature* 401, 86-90.
- Roninson, I.B., Broude, E.V., and Chang, B.D. (2001). If not apoptosis, then what? Treatment-induced senescence and mitotic catastrophe in tumor cells. *Drug Resist Updat* 4, 303-313.

References

- Rosen, E.M., Lattera, J., Joseph, A., Jin, L., Fuchs, A., Way, D., Witte, M., Weinand, M., and Goldberg, I.D. (1996). Scatter factor expression and regulation in human glial tumors. *Int J Cancer* 67, 248-255.
- Rouse, J., and Jackson, S.P. (2002). Interfaces between the detection, signaling, and repair of DNA damage. *Science* 297, 547-551.
- Rudner, J., Belka, C., Marini, P., Wagner, R.J., Faltin, H., Lepple-Wienhues, A., Bamberg, M., and Budach, W. (2001). Radiation sensitivity and apoptosis in human lymphoma cells. *Int J Radiat Biol* 77, 1-11.
- Russell, J.S., Burgan, W., Oswald, K.A., Camphausen, K., and Tofilon, P.J. (2003). Enhanced cell killing induced by the combination of radiation and the heat shock protein 90 inhibitor 17-allylamino-17-demethoxygeldanamycin: a multitarget approach to radiosensitization. *Clin Cancer Res* 9, 3749-3755.
- Russo, A., Bazan, V., Iacopetta, B., Kerr, D., Soussi, T., and Gebbia, N. (2005). The TP53 colorectal cancer international collaborative study on the prognostic and predictive significance of p53 mutation: influence of tumor site, type of mutation, and adjuvant treatment. *J Clin Oncol* 23, 7518-7528.
- Sanchez-Tillo, E., Liu, Y., de Barrios, O., Siles, L., Fanlo, L., Cuatrecasas, M., Darling, D.S., Dean, D.C., Castells, A., and Postigo, A. (2012). EMT-activating transcription factors in cancer: beyond EMT and tumor invasiveness. *Cell Mol Life Sci* 69, 3429-3456.
- Schild, S.E., Gunderson, L.L., Haddock, M.G., Wong, W.W., and Nelson, H. (1997). The treatment of locally advanced colon cancer. *Int J Radiat Oncol Biol Phys* 37, 51-58.
- Schilling, D., Bayer, C., Li, W., Molls, M., Vaupel, P., and Multhoff, G. (2012). Radiosensitization of normoxic and hypoxic h1339 lung tumor cells by heat shock protein 90 inhibition is independent of hypoxia inducible factor-1alpha. *PLoS One* 7, e31110.
- Schmitt, E., Gehrman, M., Brunet, M., Multhoff, G., and Garrido, C. (2007). Intracellular and extracellular functions of heat shock proteins: repercussions in cancer therapy. *J Leukoc Biol* 81, 15-27.
- Scholl, C., Frohling, S., Dunn, I.F., Schinzel, A.C., Barbie, D.A., Kim, S.Y., Silver, S.J., Tamayo, P., Wadlow, R.C., Ramaswamy, S., *et al.* (2009). Synthetic lethal interaction between oncogenic KRAS dependency and STK33 suppression in human cancer cells. *Cell* 137, 821-834.
- Schulte, T.W., Akinaga, S., Soga, S., Sullivan, W., Stensgard, B., Toft, D., and Neckers, L.M. (1998). Antibiotic radicicol binds to the N-terminal domain of Hsp90 and shares important biologic activities with geldanamycin. *Cell Stress Chaperones* 3, 100-108.
- Sengupta, S., and Harris, C.C. (2005). p53: traffic cop at the crossroads of DNA repair and recombination. *Nat Rev Mol Cell Biol* 6, 44-55.
- Shay, J.W., and Bacchetti, S. (1997). A survey of telomerase activity in human cancer. *Eur J Cancer* 33, 787-791.
- Sherr, C.J., and McCormick, F. (2002). The RB and p53 pathways in cancer. *Cancer Cell* 2, 103-112.
- Shimamura, T., Perera, S.A., Foley, K.P., Sang, J., Rodig, S.J., Inoue, T., Chen, L., Li, D., Carretero, J., Li, Y.C., *et al.* (2012). Ganetespib (STA-9090), a Non-Geldanamycin HSP90

Inhibitor, has Potent Antitumor Activity in In Vitro and In Vivo Models of Non-Small Cell Lung Cancer. *Clin Cancer Res*, 4973-4985.

Shirasawa, S., Furuse, M., Yokoyama, N., and Sasazuki, T. (1993). Altered growth of human colon cancer cell lines disrupted at activated Ki-ras. *Science* 260, 85-88.

Sims, J.D., McCreedy, J., and Jay, D.G. (2011). Extracellular heat shock protein (Hsp)70 and Hsp90alpha assist in matrix metalloproteinase-2 activation and breast cancer cell migration and invasion. *PLoS One* 6, e18848.

Song, D., Chaerkady, R., Tan, A.C., Garcia-Garcia, E., Nalli, A., Suarez-Gauthier, A., Lopez-Rios, F., Zhang, X.F., Solomon, A., Tong, J., *et al.* (2008). Antitumor activity and molecular effects of the novel heat shock protein 90 inhibitor, IPI-504, in pancreatic cancer. *Mol Cancer Ther* 7, 3275-3284.

Sos, M.L., Michel, K., Zander, T., Weiss, J., Frommolt, P., Peifer, M., Li, D., Ullrich, R., Koker, M., Fischer, F., *et al.* (2009). Predicting drug susceptibility of non-small cell lung cancers based on genetic lesions. *J Clin Invest* 119, 1727-1740.

Stebbins, C.E., Russo, A.A., Schneider, C., Rosen, N., Hartl, F.U., and Pavletich, N.P. (1997). Crystal structure of an Hsp90-geldanamycin complex: targeting of a protein chaperone by an antitumor agent. *Cell* 89, 239-250.

Stecklein, S.R., Kumaraswamy, E., Behbod, F., Wang, W., Chaguturu, V., Harlan-Williams, L.M., and Jensen, R.A. (2012). BRCA1 and HSP90 cooperate in homologous and non-homologous DNA double-strand-break repair and G2/M checkpoint activation. *Proc Natl Acad Sci U S A* 109, 13650-13655.

Stepanova, L., Leng, X., Parker, S.B., and Harper, J.W. (1996). Mammalian p50Cdc37 is a protein kinase-targeting subunit of Hsp90 that binds and stabilizes Cdk4. *Genes Dev* 10, 1491-1502.

Stiewe, T., and Putzer, B.M. (2000). Role of the p53-homologue p73 in E2F1-induced apoptosis. *Nat Genet* 26, 464-469.

Stingl, L., Stuhmer, T., Chatterjee, M., Jensen, M.R., Flentje, M., and Djuzenova, C.S. (2010). Novel HSP90 inhibitors, NVP-AUY922 and NVP-BEP800, radiosensitize tumour cells through cell-cycle impairment, increased DNA damage and repair protraction. *Br J Cancer* 102, 1578-1591.

Strasser, A., O'Connor, L., and Dixit, V.M. (2000). Apoptosis signaling. *Annu Rev Biochem* 69, 217-245.

Stupp, R., Hegi, M.E., Mason, W.P., van den Bent, M.J., Taphoorn, M.J., Janzer, R.C., Ludwin, S.K., Allgeier, A., Fisher, B., Belanger, K., *et al.* (2009). Effects of radiotherapy with concomitant and adjuvant temozolomide versus radiotherapy alone on survival in glioblastoma in a randomised phase III study: 5-year analysis of the EORTC-NCIC trial. *Lancet Oncol* 10, 459-466.

Stupp, R., Mason, W.P., van den Bent, M.J., Weller, M., Fisher, B., Taphoorn, M.J., Belanger, K., Brandes, A.A., Marosi, C., Bogdahn, U., *et al.* (2005). Radiotherapy plus concomitant and adjuvant temozolomide for glioblastoma. *N Engl J Med* 352, 987-996.

Sugimoto, K., Sasaki, M., Isobe, Y., Tsutsui, M., Suto, H., Ando, J., Tamayose, K., Ando, M., and Oshimi, K. (2008). Hsp90-inhibitor geldanamycin abrogates G2 arrest in p53-negative leukemia cell lines through the depletion of Chk1. *Oncogene* 27, 3091-3101.

- Supko, J.G., Hickman, R.L., Grever, M.R., and Malspeis, L. (1995). Preclinical pharmacologic evaluation of geldanamycin as an antitumor agent. *Cancer Chemother Pharmacol* 36, 305-315.
- Sydor, J.R., Normant, E., Pien, C.S., Porter, J.R., Ge, J., Grenier, L., Pak, R.H., Ali, J.A., Dembski, M.S., Hudak, J., *et al.* (2006). Development of 17-allylamino-17-demethoxygeldanamycin hydroquinone hydrochloride (IPI-504), an anti-cancer agent directed against Hsp90. *Proc Natl Acad Sci U S A* 103, 17408-17413.
- Taipale, M., Jarosz, D.F., and Lindquist, S. (2010). HSP90 at the hub of protein homeostasis: emerging mechanistic insights. *Nat Rev Mol Cell Biol* 11, 515-528.
- Taiyab, A., and Rao Ch, M. (2011). HSP90 modulates actin dynamics: inhibition of HSP90 leads to decreased cell motility and impairs invasion. *Biochim Biophys Acta* 1813, 213-221.
- Teodorczyk, M., and Martin-Villalba, A. (2010). Sensing invasion: cell surface receptors driving spreading of glioblastoma. *J Cell Physiol* 222, 1-10.
- Thaker, N.G., and Pollack, I.F. (2009). Molecularly targeted therapies for malignant glioma: rationale for combinatorial strategies. *Expert Rev Neurother* 9, 1815-1836.
- Thuringer, D., Hammann, A., Benikhlef, N., Fourmaux, E., Bouchot, A., Wettstein, G., Solary, E., and Garrido, C. (2011). Transactivation of the epidermal growth factor receptor by heat shock protein 90 via Toll-like receptor 4 contributes to the migration of glioblastoma cells. *J Biol Chem* 286, 3418-3428.
- Tong, Q.S., Zheng, L.D., Wang, L., Liu, J., and Qian, W. (2004). BAK overexpression mediates p53-independent apoptosis inducing effects on human gastric cancer cells. *BMC Cancer* 4, 33.
- Trepel, J., Mollapour, M., Giaccone, G., and Neckers, L. (2010). Targeting the dynamic HSP90 complex in cancer. *Nat Rev Cancer* 10, 537-549.
- Urist, M., Tanaka, T., Poyurovsky, M.V., and Prives, C. (2004). p73 induction after DNA damage is regulated by checkpoint kinases Chk1 and Chk2. *Genes Dev* 18, 3041-3054.
- van Houdt, W.J., Hoogwater, F.J., de Bruijn, M.T., Emmink, B.L., Nijkamp, M.W., Raats, D.A., van der Groep, P., van Diest, P., Borel Rinkes, I.H., and Kranenburg, O. (2010). Oncogenic KRAS desensitizes colorectal tumor cells to epidermal growth factor receptor inhibition and activation. *Neoplasia* 12, 443-452.
- Van Meir, E.G., Kikuchi, T., Tada, M., Li, H., Diserens, A.C., Wojcik, B.E., Huang, H.J., Friedmann, T., de Tribolet, N., and Cavenee, W.K. (1994). Analysis of the p53 gene and its expression in human glioblastoma cells. *Cancer Res* 54, 649-652.
- Vega, V.L., Rodriguez-Silva, M., Frey, T., Gehrman, M., Diaz, J.C., Steinem, C., Multhoff, G., Arispe, N., and De Maio, A. (2008). Hsp70 translocates into the plasma membrane after stress and is released into the extracellular environment in a membrane-associated form that activates macrophages. *J Immunol* 180, 4299-4307.
- Vilenchik, M., Solit, D., Basso, A., Huez, H., Lucas, B., He, H., Rosen, N., Spampinato, C., Modrich, P., and Chiosis, G. (2004). Targeting wide-range oncogenic transformation via PU24FCI, a specific inhibitor of tumor Hsp90. *Chem Biol* 11, 787-797.

- Vogelstein, B., Lane, D., and Levine, A.J. (2000). Surfing the p53 network. *Nature* 408, 307-310.
- Wang, C., Barluenga, S., Koripelly, G.K., Fontaine, J.G., Chen, R., Yu, J.C., Shen, X., Chabala, J.C., Heck, J.V., Rubenstein, A., *et al.* (2009). Synthesis of pochoxime prodrugs as potent HSP90 inhibitors. *Bioorg Med Chem Lett* 19, 3836-3840.
- Wang, J., Cui, S., Zhang, X., Wu, Y., and Tang, H. (2013). High expression of heat shock protein 90 is associated with tumor aggressiveness and poor prognosis in patients with advanced gastric cancer. *PLoS One* 8, e62876.
- Wang, L.F., Fokas, E., Bieker, M., Rose, F., Rexin, P., Zhu, Y., Pagenstecher, A., Engenhart-Cabillic, R., and An, H.X. (2008). Increased expression of EphA2 correlates with adverse outcome in primary and recurrent glioblastoma multiforme patients. *Oncol Rep* 19, 151-156.
- Wang, S.X., Ju, H.Q., Liu, K.S., Zhang, J.X., Wang, X., Xiang, Y.F., Wang, R., Liu, J.Y., Liu, Q.Y., Xia, M., *et al.* (2011). SNX-2112, a novel Hsp90 inhibitor, induces G2/M cell cycle arrest and apoptosis in MCF-7 cells. *Biosci Biotechnol Biochem* 75, 1540-1545.
- Weinberg, R.A. (2007). *The Biology of cancer*. Garland Science, Taylor & Francis Group New York. ISBN-13: 9780815340768.
- Welch, W.J., and Feramisco, J.R. (1982). Purification of the major mammalian heat shock proteins. *J Biol Chem* 257, 14949-14959.
- Whitesell, L., Bagatell, R., and Falsey, R. (2003). The stress response: implications for the clinical development of hsp90 inhibitors. *Curr Cancer Drug Targets* 3, 349-358.
- Whitesell, L., and Lindquist, S.L. (2005). HSP90 and the chaperoning of cancer. *Nat Rev Cancer* 5, 761-772.
- Whitesell, L., Mimnaugh, E.G., De Costa, B., Myers, C.E., and Neckers, L.M. (1994). Inhibition of heat shock protein HSP90-pp60v-src heteroprotein complex formation by benzoquinone ansamycins: essential role for stress proteins in oncogenic transformation. *Proc Natl Acad Sci U S A* 91, 8324-8328.
- Whitesell, L., Shifrin, S.D., Schwab, G., and Neckers, L.M. (1992). Benzoquinonoid ansamycins possess selective tumoricidal activity unrelated to src kinase inhibition. *Cancer Res* 52, 1721-1728.
- Whitesell, L., Sutphin, P.D., Pulcini, E.J., Martinez, J.D., and Cook, P.H. (1998). The physical association of multiple molecular chaperone proteins with mutant p53 is altered by geldanamycin, an hsp90-binding agent. *Mol Cell Biol* 18, 1517-1524.
- Wild-Bode, C., Weller, M., Rimner, A., Dichgans, J., and Wick, W. (2001). Sublethal irradiation promotes migration and invasiveness of glioma cells: implications for radiotherapy of human glioblastoma. *Cancer Res* 61, 2744-2750.
- Willett, C.G., Fung, C.Y., Kaufman, D.S., Efrid, J., and Shellito, P.C. (1993). Postoperative radiation therapy for high-risk colon carcinoma. *J Clin Oncol* 11, 1112-1117.
- Willett, C.G., Goldberg, S., Shellito, P.C., Grossbard, M., Clark, J., Fung, C., Proulx, G., Daly, M., and Kaufman, D.S. (1999). Does postoperative irradiation play a role in the adjuvant therapy of stage T4 colon cancer? *Cancer J Sci Am* 5, 242-247.

References

- Williams, J.R., Zhang, Y., Zhou, H., Russell, J., Gridley, D.S., Koch, C.J., and Little, J.B. (2008). Genotype-dependent radiosensitivity: clonogenic survival, apoptosis and cell-cycle redistribution. *Int J Radiat Biol* 84, 151-164.
- Willis, S.N., and Adams, J.M. (2005). Life in the balance: how BH3-only proteins induce apoptosis. *Curr Opin Cell Biol* 17, 617-625.
- Winssinger, N., Fontaine, J.G., and Barluenga, S. (2009). Hsp90 inhibition with resorcyclic acid lactones (RALs). *Curr Top Med Chem* 9, 1419-1435.
- World Health Organization (2008). The global burden of disease: 2004 update. ISBN-13: 9789241563710.
- Wykosky, J., Gibo, D.M., Stanton, C., and Debinski, W. (2005). EphA2 as a novel molecular marker and target in glioblastoma multiforme. *Mol Cancer Res* 3, 541-551.
- Xu, H., Yu, Y., Marciniak, D., Rishi, A.K., Sarkar, F.H., Kucuk, O., and Majumdar, A.P. (2005). Epidermal growth factor receptor (EGFR)-related protein inhibits multiple members of the EGFR family in colon and breast cancer cells. *Mol Cancer Ther* 4, 435-442.
- Xu, W., Marcu, M., Yuan, X., Mimnaugh, E., Patterson, C., and Neckers, L. (2002). Chaperone-dependent E3 ubiquitin ligase CHIP mediates a degradative pathway for c-ErbB2/Neu. *Proc Natl Acad Sci U S A* 99, 12847-12852.
- Yan, C., and Boyd, D.D. (2007). Regulation of matrix metalloproteinase gene expression. *J Cell Physiol* 211, 19-26.
- Yang, A., Kaghad, M., Wang, Y., Gillett, E., Fleming, M.D., Dotsch, V., Andrews, N.C., Caput, D., and McKeon, F. (1998). p63, a p53 homolog at 3q27-29, encodes multiple products with transactivating, death-inducing, and dominant-negative activities. *Mol Cell* 2, 305-316.
- Yang, Z.Q., Geng, X., Solit, D., Pratilas, C.A., Rosen, N., and Danishefsky, S.J. (2004). New efficient synthesis of resorcinylic macrolides via ynolides: establishment of cycloproparadicicol as synthetically feasible preclinical anticancer agent based on Hsp90 as the target. *J Am Chem Soc* 126, 7881-7889.
- Yin, C., Knudson, C.M., Korsmeyer, S.J., and Van Dyke, T. (1997). Bax suppresses tumorigenesis and stimulates apoptosis in vivo. *Nature* 385, 637-640.
- Yin, X., Zhang, H., Lundgren, K., Wilson, L., Burrows, F., and Shores, C.G. (2010). BIIB021, a novel Hsp90 inhibitor, sensitizes head and neck squamous cell carcinoma to radiotherapy. *Int J Cancer* 126, 1216-1225.
- Young, J.C., Agashe, V.R., Siegers, K., and Hartl, F.U. (2004). Pathways of chaperone-mediated protein folding in the cytosol. *Nat Rev Mol Cell Biol* 5, 781-791.
- Yuan, T.L., and Cantley, L.C. (2008). PI3K pathway alterations in cancer: variations on a theme. *Oncogene* 27, 5497-5510.
- Zagzag, D., Nomura, M., Friedlander, D.R., Blanco, C.Y., Gagner, J.P., Nomura, N., and Newcomb, E.W. (2003). Geldanamycin inhibits migration of glioma cells in vitro: a potential role for hypoxia-inducible factor (HIF-1 α) in glioma cell invasion. *J Cell Physiol* 196, 394-402.

References

Zaidi, S., McLaughlin, M., Bhide, S.A., Eccles, S.A., Workman, P., Nutting, C.M., Huddart, R.A., and Harrington, K.J. (2012). The HSP90 inhibitor NVP-AUY922 radiosensitizes by abrogation of homologous recombination resulting in mitotic entry with unresolved DNA damage. *PLoS One* 7, e35436.

Zhang, L., Yu, J., Park, B.H., Kinzler, K.W., and Vogelstein, B. (2000). Role of BAX in the apoptotic response to anticancer agents. *Science* 290, 989-992.

Zhou, B.B., and Elledge, S.J. (2000). The DNA damage response: putting checkpoints in perspective. *Nature* 408, 433-439.

Zhu, H., Woolfenden, S., Bronson, R.T., Jaffer, Z.M., Barluenga, S., Winssinger, N., Rubenstein, A.E., Chen, R., and Charest, A. (2010). The Novel Hsp90 Inhibitor NXD30001 Induces Tumor Regression in a Genetically Engineered Mouse Model of Glioblastoma Multiforme. *Mol Cancer Ther* 9, 2618-2626.

Zhu, J., Jiang, J., Zhou, W., and Chen, X. (1998). The potential tumor suppressor p73 differentially regulates cellular p53 target genes. *Cancer Res* 58, 5061-5065.

9 List of figures and tables

Figures

| | |
|--|----|
| Figure 1. The hallmarks of cancer..... | 16 |
| Figure 2. Schematic model of the HSP90—client protein cycle..... | 22 |
| Figure 3. Association of crucial HSP90 client proteins with the hallmarks of cancer..... | 23 |
| Figure 4. Modulation of the HSP90—client protein cycle in the presence of the pharmacological HSP90 inhibitor NW457 (schematic model)..... | 25 |
| Figure 5. Chemical and cocrystal structures of pochoxime HSP90 inhibitors and their interference with the N-terminal ATP-binding pocket of HSP90. | 28 |
| Figure 6. HSP90 inhibition by NW457 treatment of colorectal cancer cells as measured by client protein degradation, upregulation of HSP90 and HSP70 expression, HSP70 cell surface exposure, and HSP70 release. | 58 |
| Figure 7. NW457 induces apoptosis and sensitizes colorectal cancer cells to ionizing radiation..... | 60 |
| Figure 8. Exposure to NW457 time- and dose-dependently induces the formation of hypodiploid nuclei and shows a synergistic interaction with ionizing radiation..... | 62 |
| Figure 9. NW457-mediated radiosensitization of colorectal cancer cells involves the activation of caspases and caspase substrate cleavage. | 65 |
| Figure 10. NW457-mediated apoptosis induction and radiosensitization do not require functional p53. | 68 |
| Figure 11. NW457 enhances radiation-induced clonogenic cell death in colorectal cancer cells..... | 71 |
| Figure 12. Colorectal cancer cells are sensitive to HSP90 inhibition irrespective of their KRAS status. | 74 |
| Figure 13. NW457 reveals very little hepatocytotoxicity. | 76 |
| Figure 14: Combined treatment with NW457 and radiotherapy potentially delays tumor growth <i>in vivo</i> | 78 |
| Figure 15. Exposure to NW457 induces typical apoptosis-associated changes of the nuclear morphology and potentiates the effect of ionizing irradiation on human glioblastoma cells. | 81 |
| Figure 16. NW457 induces the formation of hypodiploid nuclei and potentiates the effects of ionizing radiation..... | 83 |
| Figure 17. NW457-mediated apoptosis induction in glioblastoma cells involves the activation of the caspase cascade. | 85 |

Figure 18. NW457 augments radiation-induced clonogenic cell death of glioblastoma cell lines and compromises regulators of the DNA damage response.....88

Figure 19. NW457 impairs the transmigratory potential of glioblastoma cells at non-toxic concentrations.....90

Figure 20. NW457 abrogates irradiation-induced hypermigration of glioblastoma cells. ...92

Figure 21. Analysis of potential mechanisms associated with glioma cell migration patterns in response to HSP90 inhibition and irradiation.97

Tables

Table 1. Manufacturers and suppliers 31

Table 2. Cell lines 32

Table 3. Primary antibodies 33

Table 4. Secondary antibodies..... 35

Table 5. Primers used for quantitative real-time PCR..... 36

Table 6. Media and solutions used for the isolation and cultivation of primary murine hepatocytes 40

Table 7. Composition of lysis buffer 44

Table 8. Buffers used for immunofluorescence staining 44

Table 9. Composition of PI staining buffer..... 45

Table 10. Composition of FACS staining buffer..... 46

Table 11. Reagents used for Western blotting experiments 48

Table 12. Buffers used for caspase activity assays..... 51

Table 13. Reaction mix for RNA denaturation 52

Table 14. Reaction mix for reverse transcription 52

Table 15. Reaction mix for quantitative real-time PCR..... 53

Table 16. Program used for qPCR performed on a LightCycler 480 II..... 53

10 Appendix

Appendix 1: Supplementary to Figure 9C. NW457-mediated radiosensitization of colorectal cancer cells involves caspase substrate cleavage. HCT116 cells were stimulated with 0-300 nM NW457 for 24 h, irradiated with 0-5 Gy, and 0-48 h after irradiation whole cell lysates were prepared and then subjected to caspase activity tests with DEVD-AMC peptide. Time course analyses of DEVDase activity 0-48 h after irradiation with 5 Gy +/- 100 nM NW457. 10 µg total protein was used per data point. Tables show data (means ± SD) of two independent experiments each performed in quadruplicates.

| Time after irradiation [h] | 0 | | 12 | | 24 | | 36 | | 48 | |
|----------------------------|-------|------|-------|-------|-------|------|--------|------|--------|-------|
| | Mean | SD | Mean | SD | Mean | SD | Mean | SD | Mean | SD |
| DEVDase [FU/min] | | | | | | | | | | |
| Control | 28,00 | 2,82 | 36,16 | 4,44 | 26,02 | 5,71 | 56,48 | 6,30 | 40,15 | 6,04 |
| 100 nM NW457 | 26,21 | 7,52 | 77,00 | 11,09 | 59,29 | 3,32 | 85,39 | 7,73 | 88,66 | 9,08 |
| 5 Gy | 19,31 | 2,13 | 45,31 | 6,83 | 44,66 | 9,90 | 52,39 | 7,35 | 83,25 | 9,81 |
| 100 nM NW457 + 5 Gy | 31,56 | 2,41 | 81,96 | 2,40 | 91,38 | 7,51 | 103,39 | 6,61 | 114,11 | 15,26 |

| Time after irradiation [h] | 0 | | 12 | | 24 | | 36 | | 48 | |
|----------------------------|-------|-------|-------|------|-------|------|-------|-------|-------|------|
| | Mean | SD | Mean | SD | Mean | SD | Mean | SD | Mean | SD |
| DEVDase [FU/min] | | | | | | | | | | |
| Control | 23,35 | 17,96 | 46,58 | 2,93 | 27,98 | 0,31 | 28,38 | 4,96 | 45,16 | 3,14 |
| 100 nM NW457 | 31,40 | 3,68 | 50,30 | 1,50 | 53,90 | 3,16 | 52,26 | 1,84 | 85,82 | 2,84 |
| 5 Gy | 34,52 | 5,77 | 47,36 | 3,47 | 46,57 | 2,98 | 50,97 | 7,38 | 76,49 | 2,12 |
| 100 nM NW457 + 5 Gy | 33,87 | 3,27 | 59,02 | 7,44 | 65,02 | 2,96 | 90,69 | 15,03 | 95,69 | 1,07 |

Appendix 2: Supplementary to Figure 13A. NW457 reveals very little hepatocytotoxicity. Primary hepatocytes isolated from C57BL/6 mice were exposed to 0-300 nM NW457 or geldanamycin (GA) for 48 h and cellular viability was measured by Alamar Blue assays. Alamar Blue reduction was calibrated on untreated controls (100% viability) and is shown as means ± SD of intra-assay quadruplicates.

| Concentration [nM] | NW457 | | GA | |
|--------------------|-------|-----|-------|-----|
| | Mean | SD | Mean | SD |
| 0 | 100,0 | 3,6 | 100,0 | 3,6 |
| 10 | 98,8 | 3,1 | 97,7 | 1,9 |
| 30 | 99,1 | 0,5 | 80,2 | 5,8 |
| 50 | 97,1 | 6,2 | 48,4 | 4,7 |
| 100 | 96,4 | 3,4 | 29,7 | 4,2 |
| 300 | 99,3 | 6,7 | 30,0 | 5,8 |

Appendix 3: Supplementary to Figure 17B. NW457-mediated apoptosis induction in glioblastoma cells involves caspase substrate cleavage. LN229 cells were treated with 0-200 nM NW457 for 24 h, irradiated with 0-10 Gy, and harvested 24 h afterwards. Caspase activity was analyzed in whole cell lysates (20 µg total protein per data point) by DEVDase assays. Each table shows data (means ± SD) of an independent experiment each performed in quadruplicates.

| LN229 NW457 [nM] | 0 Gy | | 10 Gy | |
|------------------------|---------|-------|---------|-------|
| | Mean | SD | Mean | SD |
| 0 | 2,36 | 3,63 | 2,27 | 11,68 |
| 50 | -2,94 | 2,85 | 29,74 | 6,88 |
| 100 | 22,44 | 5,17 | 444,23 | 9,43 |
| 200 | 1229,50 | 56,28 | 2077,31 | 85,42 |

| LN229 NW457 [nM] | 0 Gy | | 10 Gy | |
|------------------------|---------|-------|---------|-------|
| | Mean | SD | Mean | SD |
| 0 | 2,27 | 5,64 | 6,08 | 4,90 |
| 50 | -6,49 | 2,87 | 22,45 | 7,72 |
| 100 | 11,48 | 6,74 | 329,61 | 43,98 |
| 200 | 1017,94 | 46,45 | 1171,56 | 45,66 |

Appendix 4: Supplementary to Figure 17D. NW457-mediated apoptosis induction in glioblastoma cells involves caspase substrate cleavage. T98G cells were treated with 0-200 nM NW457 for 24 h, irradiated with 0-10 Gy, and harvested 24 h afterwards. Caspase activity was analyzed in whole cell lysates (20 µg total protein per data point) by DEVDase assays. Each table shows data (means ± SD) of an independent experiment each performed in quadruplicates.

| T98G NW457 [nM] | 0 Gy | | 10 Gy | |
|-----------------------|---------|-------|---------|-------|
| | Mean | SD | Mean | SD |
| 0 | 327,62 | 27,81 | 241,71 | 14,67 |
| 50 | 319,68 | 12,18 | 344,98 | 24,00 |
| 100 | 417,07 | 47,09 | 433,21 | 12,77 |
| 200 | 1214,70 | 77,89 | 1124,35 | 40,70 |

| T98G NW457 [nM] | 0 Gy | | 10 Gy | |
|-----------------------|--------|-------|---------|-------|
| | Mean | SD | Mean | SD |
| 0 | 329,14 | 13,98 | 305,69 | 25,35 |
| 50 | 285,10 | 18,16 | 357,71 | 27,62 |
| 100 | 352,55 | 27,18 | 390,35 | 45,32 |
| 200 | 812,77 | 29,72 | 1249,52 | 93,31 |

Eidesstattliche Erklärung

Hiermit versichere ich an Eides statt, dass die vorliegende Dissertation von mir selbstständig und ohne unerlaubte Hilfe angefertigt wurde.

Martinsried, den 19.09.2013

Unterschrift

Acknowledgments

First of all, I would like to thank PD Dr. Anna A. Friedl who gave me the opportunity to work on my PhD thesis in her lab. Thank you for your great support, ideas, motivation, and encouragement at any time!

Furthermore, I would like to thank Prof. Dr. Heinrich Leonhardt for his second opinion on my thesis.

I would like to thank the BMBF for providing the funding of this project (02NUK004D).

Moreover, I would like to thank Prof. Dr. Claus Belka for the opportunity to work on such an interesting and clinically relevant project, his confidence, and support during the past years.

I would like to thank Prof. Dr. Kirsten Lauber for her great support and ideas. Thank you for your confidence, encouragement, and your patience at any time!

Many thanks go to Prof. Dr. Nicolas Winssinger who kindly supplied me with the HSP90 inhibitor NW457 and thus provided the basis for the present work.

I would also like to thank Dr. Minglun Li for his support and ideas during the initial phase of my PhD thesis.

Furthermore, I would like to thank all my colleagues of the “Schillerstraße Lab” and the “Großhadern Lab” for the great time together, their support and assistance with experiments, and the nice lunch breaks we had together! Special thanks go to Anne, Michael, Karin, Jenny, Viola, and Iris - thank you for your great support and experimental assistance in the lab! Many thanks go also to Belinda, Cornelius, Doris, Frauke, Guido, Heike, Lars, Markus, Roman, Seyd, Sophie, and Susanne for the great time we had together!

Special thanks go also to Dr. Benjamin Frey and Dr. Udo Gaipl for performing the *in vivo* experiments, Gabi Zuchtriegel for her assistance with the preparation of the primary hepatocytes, Dr. Daniela Schilling for her assistance with the HSP70 FACS and ELISA experiments, and Dr. Maximilian Niyazi for the calculation of the combination indices.

Finally, I would like to thank my family and friends, especially Matthias and my parents, for their great support and patience at any time! Thank you so much!

